

## ABSTRACT

Title of Document: AN IMPROVED PSEUDO-  
DETERMINISTIC RECEPTOR  
MODEL (iPDRM) TO APPORTION  
AMBIENT PM CONSTITUENTS TO  
SOURCES IN TAMPA, FL

Gregory Marcus Beachley, Ph.D. 2009

Directed By: John M. Ondov, Ph.D  
Department of Chemistry and  
Biochemistry

In 2005, Park et al., developed a new Pseudo-Deterministic Receptor Model (PDRM) to apportion SO<sub>2</sub> and ambient particulate matter (PM) constituents to local sources near Tampa Bay. Ambient pollutant measurements were fit to products of emission rates and dispersion factors constrained with a Gaussian plume model for individual sources. In our study, the original samples were reanalyzed by ICPMS for 10 additional elements to improve the resolving power. Chemical mass balance (CMB) terms were added to PDRM to allow fitting of background aerosol sources. More accurate curvilinear plume trajectories were computed to predict arrival times in both surface and aloft layers. This allowed application of the PDRM to complicated meteorological conditions, e.g. wind shifts. Predicted emission rates for particle-bound elements were constrained using chemical compositional information obtained from published source profiles for generic

source types. Constraints applied to emissions of known tracer species allowed the “conditioning” of dispersion factor temporal profiles to tracer species concentration profiles. This enabled the model to apportion pollutants to individual sources with intermittent emissions, the omission of which in Park et al. lead to significant residuals. Excellent fits were obtained for all modeled pollutants: 14 of 22 species have Normalized Mean Square Errors (NMSE) < 2.5%, and 21 of 22 have values < 8%. These were improved for SO<sub>2</sub> and 8 of 10 elements (by 7-35% for Al, Cu, Ni, Pb, and Zn) modeled by Park et al. Our predicted emission rates are in much better agreement with chemical compositions for generic source types. Key results include: (1) predicted SO<sub>2</sub> contributions to ambient levels from a small, lead battery recycling plant were reduced from 50-59% at its peak influence to a more reasonable 2-4%, (2) Pb/Zn ratios from that plant increased from 1.0 to 734 and better agree with published ratios of 67-440, (3) predicted Ni emission rates for one of the oil-fired power plants (OFPP) was increased by 100-fold (larger than Park’s), and now better agrees with its published National Emissions Inventory (NEI) emission rate and with X/Ni ratios for generic OFPP emissions derived from EPA’s SPECIATE database, and (4) our predicted emission rates for hazardous air pollutants and toxics from power plants agree within a factor of 5 for ~75% of the annual emission rates reported in the NEI and Toxic Release Inventories (TRI). This suggests that NEI and TRI data provide good qualitative emission estimates, but should not be treated as accurate in a predictive model to quantify source emissions. It was also observed that the TRI values for As emission rates from coal-fired power plants are more accurate than their NEI values.

AN IMPROVED PSEUDO-DETERMINISTIC RECEPTOR MODEL  
(iPDRM) TO APPORTION AMBIENT PM CONSTITUENTS TO  
SOURCES IN TAMPA, FL

By

Gregory Marcus Beachley

Dissertation submitted to the Faculty of the Graduate School of the  
University of Maryland, College Park, in partial fulfillment  
of the requirements for the degree of  
Doctor of Philosophy  
2009

Advisory Committee:

John M. Ondov, Ph.D.  
Alice Mignerey, Ph.D.  
Robert Hudson, Ph.D.  
Neil Blough, Ph.D.  
William B. Walters, Ph.D.

© Copyright by  
Gregory Marcus Beachley  
2009

## **Acknowledgements**

I would like to thank my advisor, Professor John M. Ondov for his guidance and help with this work. This work would not be possible without the funding provided by the United States Department of Energy Award no. DE-FG26-06NT42738.

I would also like to thank my family, especially my parents, Ralph and Carol, for their tremendous support and encouragement throughout my time at the University. I thank all of my friends for their continued and necessary comic relief, and especially Natalie, who has shown extraordinary patience as I completed this project.

# Table of Contents

Acknowledgements.....	ii
Table of Contents.....	iii
List of Tables.....	iv
List of Figures.....	vi
1. Introduction.....	1
1.1 Park's PDRM.....	6
1.1.1. Inputs.....	9
1.1.2. Results.....	11
2. Dataset and Methods.....	18
2.1. Reanalysis of Tampa Sources.....	18
2.2. Meteorological Data.....	23
2.3. Ambient Pollutant Measurements.....	24
2.4 Modeling Methods.....	33
2.4.1. Trajectory Construction and Trajectory-Related Parameters.....	33
2.4.2. Estimation of the Background Sources.....	39
2.4.3. The iPDRM Configuration.....	46
2.4.3.1. Emission Rate constraints.....	49
2.4.3.2. $\chi/Q$ constraints.....	50
2.4.3.3. Scaling of Input Concentrations.....	51
2.4.3.4. Hierarchical Approach.....	51
3. Results and Discussion.....	59
3.1. Analytical Results.....	59
3.2. Discussion of Modeling Results.....	64
3.2.1. Source $\chi/Q$ profiles and Discussion.....	65
3.2.2. Predicted vs. Observed Fits.....	78
3.2.3. Emission Rates.....	84
3.2.4. Comparison to NEI and TRI reported emission rates.....	96
4. Summary and Conclusions.....	100
Appendices.....	104
Appendix A.....	104
Appendix B.....	110
Appendix C.....	114
Glossary.....	132
Bibliography.....	135

## List of Tables

**Table 1.** Source abundance profiles (relative to Pb) as derived from EPA SPECIATE for Pb recycling plants and for Gulf Coast, as predicted by Park and this work.

**Table 2.** Source abundance profiles (relative to Ni) as derived from EPA SPECIATE for oil-fired power plants and for Manatee and Bartow, as predicted by Park and this work.

**Table 3.** Sources, source-receptor distances, and station angles (measured from due North at Sydney), fuel type, emission control devices, and emissions data compiled from CEM, NEI, and TRI.

**Table 4.** Stack information compiled from the National Emissions Inventory database.

**Table 5.** ICPMS operating conditions.

**Table 6.** Detection limits elements in SEAS samples using ICPMS and GFAAZ compared with reported detection limits from US EPA Speciation Trends Network Protocols.

**Table 7.** Experimental results for ICPMS determination of total dissolution of the yet-to-be-released NIST atmospheric fine SRM.

**Table 8.** Yields for determinations of elements in slurry samples by ICPMS.

**Table 9.** Background concentrations ( $\text{ng}/\text{m}^3$ ) as predicted by Park and the iPDRM. Concentration profiles for iPDRM predicted soil and sea salt varied over the course of the study period and are listed as average values.

**Table 10.** Chemical Mass Balance abundance profiles (g element / g Total  $\text{PM}_{2.5}$  mass) as entered into the EPA CMB model (v8.2). Values were obtained from the SPECIATE database.

**Table 11.** Constraints and initial “seed” values (IV) for  $\text{SO}_2$  (g/s) used in Park’s model and the iPDRM for the six major  $\text{SO}_2$  sources.

**Table 12.** Scaling factors applied to species concentrations in order adjust the residual size for preferential fitting of species. Resultant maximum scaled concentrations are also listed.

**Table 13.** Emission rate constraints (g/s) used for Step 2.

**Table 14.** Final emission rate constraints (g/s).

**Table 15.** Fraction of predicted SO<sub>2</sub> to ambient SO<sub>2</sub> concentrations apportioned to Big Bend, Gannon, and Gulf Coast (%) from 13:00-15:30.

**Table 16.** Performance statistics for predicted concentrations of SO<sub>2</sub>, NH<sub>3</sub>, and elements. Performance statistics published by Park are compared where available.

**Table 17.** Equations for the calculation of performance statistics shown in Table 16.

**Table 18.** Predicted emission rates (g/s) for SO<sub>2</sub>, NH<sub>3</sub>, and elements.

**Table 19.** Source abundance profiles (relative to Fe) as derived from EPA SPECIATE for a diammonium phosphate fertilizer plant and for Cargill, as predicted by Park and the iPDRM.

**Table 20.** Source abundance profiles (relative to Pb) as derived from EPA SPECIATE for incinerators and for McKay and PCRR, as predicted by this work.

**Table 21.** Ratios of iPDRM emission rate predictions to emission rates reported by NEI-TRI.

**Table 22.** Ratios of predicted and published emission rates (iPDRM/NEI-TRI) grouped within factors of 2.5, 5.5, or > 5.5.

## List of Figures

**Figure 1.** Map of the Tampa Bay area showing the sampling site (Sydney) and major sources of PM. Sources originally modeled by Park et al., 2005 are represented by red-trimmed stars. Additional industrial sources are represented by targets.

©2007, Google

**Figure 2.** Thirty-minute averages of surface 30-minute wind speeds and wind directions measured at Sydney on May 13, 2002.

**Figure 3.** Predicted concentration profiles as determined by Park (adapted from Park et al., 2005a) show over- and under-predictions of the observed concentration profiles for Al, Cu, Fe, Ni, Pb, and Zn.

**Figures 4a. & b.** Surface back trajectories computed every 30 minutes using wind data collected by NOAA at a height of 10 m: trajectories from 12:00-15:30(a) and 16:00-20:30(b) are shown. The surface wind shifted from a Southerly to a Southwesterly flow at 12:30.

**Figure 5.** Concentration-vs.-time-of-day profiles for SO<sub>2</sub> and NH<sub>3</sub> measured at Sydney (courtesy of BRACE database).

**Figure 6.** Forward Trajectories of the plumes originating from Gannon at three different times: 11:30 (turquoise), 12:00 (purple), and 12:30 (gold). The points of closest approach to Sydney occurred: at 14:00 (A), 14:30 (B), and 15:00 (C). The off-axis distances ( $Y$ ) and transport distances ( $x$ ) were calculated from these trajectories.

**Figure 7.** A plume centerline from the source of origin toward Sydney modeled using the head-to-toe alignment of wind direction vectors. Equations shown are used to calculate the off-axis distance,  $Y$ , between the point of closest approach and Sydney.

**Figure 8.** Illustration of plume trajectories originating at Big Bend at 12:00 and 13:00 at heights of 100- and 500-m. Plumes at different heights originating at the same time are observed to travel along different angles indicating a wind rotation aloft.

**Figure 9.** PM<sub>2.5</sub> mass concentration estimates-vs.-time-of-day profiles. PM<sub>2.5</sub> mass concentration was (crudely) estimated as the sum of major ionic species (ammonium, sulfate, nitrate, and chloride) measured at Sydney.

**Figure 10.** Observed concentration-vs.-time-of-day profiles (hybrid dataset; blue) and those predicted (red) using the EPA Chemical Mass Balance v8.2 model.

**Figure 11.** Source contribution estimate (SCE) (ng total PM<sub>2.5</sub> mass / m<sup>3</sup>)-vs-time-of-day profiles predicted by the CMB model for generic source types. The SCE for the soil source includes the smoothed profile (A) input into the PDRM.

**Figure 12.** Flow chart showing our hierarchical steps with input constraints and output solutions.

**Figure 13.** Concentration-vs.-time-of-day profiles for elements in ambient air samples by Graphite Furnace Atomic Absorption Spectroscopy (GFAAZ) (blue) and Inductively Coupled Plasma Mass Spectrometry (ICPMS). Concentration profiles for 11 additional elements determined with ICPMS are shown.

**Figure 14.** Comparison of  $\chi/Q^{\text{iPDRM}}$  profiles (red) and the input  $\chi/Q^{\text{traj}}$  profiles (blue). The  $\chi/Q^{\text{iPDRM}}$  profiles differ from the  $\chi/Q^{\text{traj}}$  profiles due to “conditioning” of the former with the “shapes” of tracer species concentration profiles.

**Figure 15.**  $\chi/Q$ -vs.-time-of-day profiles as calculated by the Gaussian plume module by Park ( $\chi/Q^{\text{MET}}$ , black) and trajectory analysis ( $\chi/Q^{\text{traj}}$ , blue).

**Figure 16a, b, c, & d.** Concentration profiles of selected tracer species vs.  $\chi/Q^{\text{traj}}$  profiles. All datasets shown are normalized to their maximum values.

**Figure 17.** Observed concentration-vs.-time-of-day profiles for species (hybrid dataset; blue) used in iPDRM compared with iPDRM predicted concentration versus time profiles (red).

**Figure 18.** Reported CMB Abundance profiles (g element / g Total PM<sub>2.5</sub> mass; SPECIATE) categorized by source type and compared with predicted emission rate profiles from iPDRM and Park’s model (note: Mg was not reported in literature for the Oil-fired source).

**Figure 19.** Ambient Pb (grey) and predicted (red) Pb concentration profiles (ng/m<sup>3</sup>). Total predicted Pb concentration profiles from major contributing sources are shown. Park’s results are shown in the graph above, iPDRM results in the graph below.

**Figure 20.** Ambient Zn (grey) and predicted (red) Zn concentration profiles (ng/m<sup>3</sup>). Total predicted Zn concentration profiles from major contributing sources are shown. Park’s results are shown in the graph above, iPDRM results in the graph below.

**Figure A1.** The PDRM makes use of source angle and distance relationships. Plume transport distance ( $x'$ ) and displacement ( $y$ ) of the plume centerline from the sampling site are shown.

# 1. Introduction

Source Apportionment is the quantitative determination of the contributions of pollutants from their sources to ambient atmospheric concentrations (Gordon, 1988). It is important to identify contributing sources in order to effectively implement emissions control strategies which reduce ground-level exposures and associated health risks and degradation of air quality (Gordon, 1988). Source apportionment is generally accomplished with either source- or receptor-based models. *Apriori* knowledge of emission rates is necessary for source based models and their accuracy is limited by large uncertainties in modeling plume dispersion. For these reasons receptor models are often preferred. The basis for receptor models is that measurements of ambient pollutant ( $i$ ) concentrations made at a “receptor site”,  $C_{R_i}$ , can be expressed as the linear sum of contributions from sources,  $j$ , which for  $n$  sources is (equation 1):

$$C_{R_i} = \sum_{j=1}^n C_{S_{i,j}} \quad (1)$$

where  $C_{S_{i,j}}$  is the source contribution, i.e., the concentration of that species in air at the receptor site induced by an individual source or a generic source type,  $j$ , both typically in units of  $\mu\text{g}/\text{m}^3$ .

To permit solutions to equation (1), the terms on the right side are factored into products of variables, at least one of which must be known either from measurements or at least estimated by calculation. This is:

$$C_{R_{i,t}} = \sum_{j=1}^n A_{i,j} \cdot B_{j,t} + \text{residual} \quad (2)$$

where the ambient pollutant,  $i$ , concentrations made at the receptor site,  $C_{R_i,t}$ , for each observation,  $t$ , for  $n$  observations. The definitions of  $A_{i,j}$  and  $B_{j,t}$  depend on the receptor model type, but in every case, the products of these factors are the predicted source contribution represented by  $C_{s_{i,j}}$  in equation (1). The residual represents the difference between the  $\sum_{j=1}^n C_{s_{i,j}}$  and  $C_{R_i}$ .

As observed by Park et al., (2005a), receptor models are typically of three types, those that make no use of information other than meteorological and concentration measurements (e.g. Factor Analysis, (FA), Principle Component Analysis, (PCA), notably Positive Matrix Factorization (PMF) and UNMIX, those that require a single unique tracer for each source (i.e. multiple linear regression (MLR)) and those that require detailed information on the relative abundances of each source (Chemical Mass Balance (CMB)).

In the CMB, the terms in equation (2),  $A_{i,j}$ s are the relative abundances of species,  $i$ , in particles emitted from source,  $j$ , and  $B_{j,t}$ s are the mass concentrations of particles at the receptor site induced from each source,  $j$ , in each sampling interval,  $t$ . An advantage of the CMB approach is that only one or more samples are needed, and the use of source compositional information effectively constrains solutions. A disadvantage to the CMB approach is that source profiles must be measured. Published profiles often do not accurately represent emissions from sources in the study area of interest owing in part to differences in analytical methods and the fact that the composition of emissions from a generic source type can be highly variable from plant to plant (Gordon, 1988). Moreover, temporal variability may be great owing to their dependence on such factors as fuel composition and changes in emission controls. Lastly, emission profiles for individual

sources, particularly of the same type, can be too similar to permit resolution. Thus, solutions are often obtained only for generic source types.

Collection of ambient concentration data at resolution times comparable to changes in wind direction has enabled apportionment of species to individual sources. Rheingrover and Gordon (1988) used 2-hour aerosol composition data to estimate the contributions of individual sources to ambient air concentrations using Instrumental Neutron Activation Analysis (INAA) data. More recently Kidwell and Ondov (2001, 2004) developed a system capable of measuring elemental concentrations at 30-minute intervals using Graphite Furnace Atomic Absorption Spectroscopy. The System, now known as the Semi-continuous Elements in Aerosol Sampler (SEAS), enabled both greater temporal resolution and much faster analytical turn-around. The SEAS was deployed in College Park (Kidwell and Ondov, 2004) and later in several studies (Park et al., 2005b, Ondov et al., 2003) including the Tampa Bay area during the Bay Regional Atmospheric Chemistry Experiment (BRACE), where plumes from individual sources were readily identified by correlating excursions in time-series concentration profiles of marker elements with wind directions. This included two sources for which emissions had not been previously detected (Park et al., 2005a).

In many cases, narrow, Gaussian peak shapes were observed (e.g., Pancras et al. 2006). This occurred when the mean wind direction rotated slowly enough such that plumes from stationary sources would be swept across the sampling site. In such cases, it was clear that the widths of the peaks are related to the plume width. Also, as sources were often >10 km from the measurement site, observation of the plumes at the surface sampling sites occurred only after they were well mixed in the boundary layer to the

extent of the mixing height. Thus, sources could be identified by composition wind versus source angle, and because the “peak” widths contain dispersion information, it was postulated that the peak shape could be used to develop parameters required by Gaussian Plume Models (GPM).

To exploit the information contained in these data, Park et al.(2005a, b), applied a new version of a hybrid receptor model previously described by both Yamartino (1982) and Cooper (1982). In these models, the ambient concentrations in the mass balance equation are defined in terms of the products of source emission rates and plume dispersion factors ( $\chi/Q$ ). As implemented by Yamartino (1982) and Cooper (1982), plume dispersion factors were derived deterministically using GPM equations for individual sources, and solutions were sought for single pollutants (i.e., SO<sub>2</sub>, and total suspended particle concentrations (TSP), respectively. Neither attempt met with much success due to the fundamental inaccuracies in the Gaussian Plume Model (GPM). Park et al.,(2005a, b) implemented the same mass balance equation, but recognizing that the plume width parameter,  $\sigma_y$  (defined later), could be inferred from “peak” shape, and that plume width would also constrain transport distances, they used the GPM-derived dispersion factors as initial guesses and to set constraints to solutions rather than applying them deterministically. Inclusion of Gaussian dispersion factors effectively eliminates the contributions from sources which cannot physically influence the sampling site at a given time. Thus, PDRM was designed to exploit directionality based on source angles relative to the sampling site and observed wind direction data, changes in plume width ( $\sigma_y$ ) accompanying dispersion over longer distances, and plume transport speeds inferred from source receptor distances and wind speeds.

PDRM was applied in two different studies, one in Tampa and another in Pittsburgh (Park et al., 2005a; 2005b; the former is henceforth referred to herein as “Park”). In the Tampa study, solutions were obtained for 6 sources, i.e. four power plants, a lead recycling plant, and a phosphate fertilizer plant. Remarkably, the predicted emission rates for SO<sub>2</sub> for the four major power plants in Tampa were within ~8% of those inferred from CEM data and fits to ambient marker element concentrations were generally good. However, significant residuals were observed at various time intervals for several key marker species.

Park designed the PDRM to treat high frequency measurements in situations where the mean wind was constant or slowly rotating so that plumes from point sources that had relatively constant emission rates over the study period would sweep across the measurement site. The dataset from Tampa was modeled because of the availability of reliable ambient SO<sub>2</sub> and elemental data, high quality meteorological and modeled micrometeorological data (Scire, 2000), as well as Continuous Emissions Monitor (CEM) data for SO<sub>2</sub> for the four power plants. These data were available throughout the study period. However, a rapid shift in the mean wind direction during the study period created curvilinear plume trajectories. Park chose to compensate for the wind shift by creating a “transport adjusted” wind direction set for use in computing estimates of the period of plume influences (as revealed by GPM-calculated  $\chi/Q$  profiles). Also, Park used only ambient SO<sub>2</sub> concentrations in the PDRM to determine the modeled dispersion factors and subsequently used those to apportion the elemental constituents of PM<sub>2.5</sub>. Residuals in Park's modeled elemental constituents suggest that the six modeled sources were not the only contributors of PM<sub>2.5</sub>.

In this work, the original data and results for Tampa were thoroughly reanalyzed and an improved PDRM (herein, iPDRM) was implemented to allow its application to a wider range of more complicated scenarios. Specific improvements are as follows: 1) the application of curvilinear forward trajectories to better predict the periods of plume influence, especially during periods of shifting winds, 2) calculation of trajectories for up to three levels to account for wind rotation aloft for sources with high stacks, and the corresponding transport at different wind velocities, 3) inclusion of compositional information (i.e., CMB profiles) to better constrain solutions for sources where marker species exist, 4) use of concentration-versus-time profiles to condition  $\chi/Q$  profiles for sources for which key tracer species were clearly resolved as a means of providing better fits and allowing for intermittent emission rates, 5) inclusion of additional sources, including generic background soil dust, two incinerators, and a shipyard source to improve the apportionment of elemental constituents of  $PM_{2.5}$ , and lastly, 6) the original samples collected for the Tampa study were reanalyzed for up to 14 additional elements in an effort to find useful marker species for additional sources. We describe the model of Park as applied to Tampa and its shortcomings, in the next section. Subsequent sections present the ICPMS analytical method, the expanded species data set developed for the new modeling work, and the iPDRM approach and its results.

## 1.1 Park's PDRM

The PDRM (pPDRM) applied by Park was configured as follows in equation (3):

$$[E_i]_t = \sum_{j=1}^n \overline{ER}_{i,j} \cdot (\chi/Q)_{j,t}^{pPDRM} + residual \quad (3)$$

where  $[E_i]_t$  are the ambient concentration ( $\text{g m}^{-3}$ ); of each species  $i$  measured at the receptor site in the sampling interval,  $t$ .  $\overline{ER}_{i,j}$  is the emission rate of species  $i$  from source  $j$  ( $\text{g s}^{-1}$ ), averaged over the modeling period, and  $(\chi/Q)_{j,t}^{PDRM}$  is the PDRM-determined meteorological dispersion factor ( $\text{s m}^{-3}$ ) for each source  $j$  at each sampling interval,  $t$ .

Initial guesses for  $(\chi/Q)_{j,t}^{PDRM}$  values were derived using the simple GPM and denoted as  $(\chi/Q)_{j,t}^{Met}$  (equation (4)):

$$(\chi/Q)_{j,t}^{Met} = \frac{1}{\pi\sigma_y\sigma_z u} \exp\left(-\frac{Y^2}{2\sigma_y^2}\right) \exp\left(-\frac{H^2}{2\sigma_z^2}\right) \quad (4)$$

where  $\chi$  is the predicted concentration ( $\text{g m}^{-3}$ ) of gas or aerosol species at ground level ( $z = 0$ ),  $Q$  is the average mass emission rate ( $\text{g s}^{-1}$ , i.e.  $\overline{ER}_{i,j}$ ), and  $u$  is the transport speed (m/s) of the plume over its trajectory. Plume dispersion parameters,  $\sigma_y$  and  $\sigma_z$  (m), are the standard deviations of the concentration distributions in the lateral ( $y$ ) and vertical ( $z$ ) directions (in units of m), and increase as the plume disperses downwind with distance traveled,  $x'$ , from the source.  $H$  is the effective stack height (m), i.e. the height to which the stack gas rises above the stack owing to velocity and buoyant forces.

In equation (4), the pre-exponential term ( $\text{s m}^{-3}$ ) is the inverse of the plume dilution rate. This term is a function of transport speed (and hence, distance) because  $\sigma_y$  and  $\sigma_z$  increase with distance (and vary with conditions of atmospheric stability and turbulence). The exponential factors account for the off-axis decay of concentrations from their maxima along the plume centerline in the lateral and vertical directions, as a function of the off-axis distance ( $Y$  and  $H$  in units of m). The first exponential term and  $\sigma_y$  (m) is a powerful constraint when applied to highly time-resolved data as it prevents solutions from being obtained for sources whose source angles do not sufficiently align with their

plume trajectories. The second exponential term employs a ratio of  $H$  to  $\sigma_z$ . Inherent in equation (4), is the assumption that all emitted species are conserved, i.e., are neither removed by gravitational settling, dry or wet deposition, nor by chemical reactions. Horizontal and vertical turbulence are assumed to be homogenous. These simplifications lead to substantial errors in model predictions.

In order to calculate  $\sigma_y$  and  $\sigma_z$ , Park used equations from Draxler (1976), Irwin (1979), and Binkowski (1979). Transport velocity,  $u$ , was calculated from the power law (Panofsky et al., 1960). Briggs' equations (1969, 1971, 1974) were used to calculate buoyancy flux and momentum flux parameters to estimate  $H$ . Details of these calculations are given in Park and are reproduced in **Appendix A**.

Equation (2) was solved using a nonlinear least squares solver ('lsqcurvefit') in MATLAB (MathWorks, Inc, version 7.4). By minimization of the object function, FUN:

$$\text{FUN} = \sum_{i=1}^l \sum_{t=1}^m \sum_{j=1}^n (\overline{ER}_{i,j} (\chi/Q)_{j,t}^{pDRM} - [E_{i,t}])^2 \quad (5)$$

such that the following constraints in equation (5A) were satisfied:

$$(\chi/Q)_{j,t}^{pDRM} = \alpha_j (\chi/Q)_{j,t}^{Met} \quad (5A)$$

where  $\alpha_j$  is a scaling multiplier that is set within lower and upper bounds for which the solver is directed to find solutions. Upper and lower bounds of the meteorological dispersion factors reflect the uncertainty in the solutions of the GPM,  $(\chi/Q)_{j,t}^{Met}$ , as calculated with meteorological data.

Modeled solutions, referred to as  $(\chi/Q)_{j,t}^{pDRM}$ , were constrained to lie within a factor of 0.1 to 2 of the GPM predictions. This was based on information reported in an intentional tracer study (Ondov et al., 1992) conducted at a coal-fired power plant 20km

from an arc of samplers in Maryland, a location which had terrain and land use similar to that in Tampa (Park et al., 2005a).

### 1.1.1. Inputs

Atmospheric measurements used in this study were collected at Sydney, Florida (27.9653N, 82.2273W). The positions of this site and of the 6 sources used in Park's model are shown in **Figure 1**, along with additional PM<sub>2.5</sub> sources in the Tampa vicinity. The measurements consisted of SO<sub>2</sub> and 10 elements determined in particles collected with SEAS by GFAAZ between 12:00-21:00 local time (LT) on 13 May 2002, during which time winds swept from ~200-270° with 30-minute average surface wind speeds from 1-4 m/s (**Figure 2**). Data used in the GPM were as follows: 1) measured (1min) meteorological data from NOAA taken at a height of 10m and averaged to 30-min including wind direction (degrees), surface wind speed (m/s), solar insolation (W/m<sup>2</sup>), and ambient temperature (°C), 2) CALMET derived parameters (Scire et al., 2000) to describe the atmospheric boundary layer (ABL) including: Pasquill Stability class, friction velocity,  $u_*$  (m/s), mixing height,  $z_i$  (m) Monin-Obukhov length,  $L$  (m), and convective velocity scale,  $w_*$ (m/s) (described in detail in Park et al., 2005a), 3) source angles and distances of sources relative to Sydney and 4) stack data (physical stack height, stack inside diameter, exit gas velocity, and exit gas temperature).

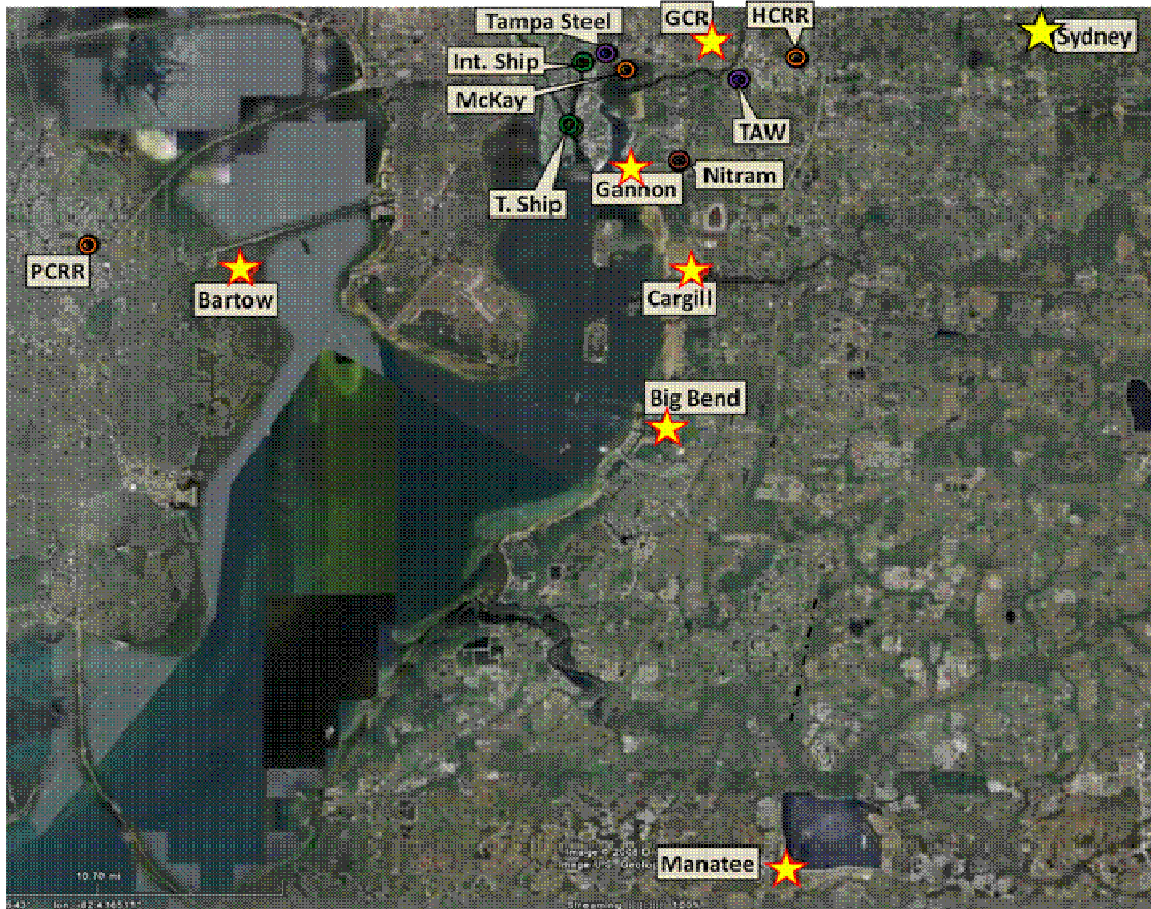


**Figure 1.** Map of the Tampa Bay area showing the sampling site (Sydney) and major sources of PM. Sources originally modeled by Park et al., 2005 are represented by red-trimmed stars. Additional industrial sources are represented by targets.  
©2007, Google

The 108 output dispersion factors,  $\chi/Q^{\text{Met}}$ , were input into equation 2 and the model was solved to obtain a set of 66 emission rates (i.e., 11 species for each of the six sources) and for a set of 108 dispersion factors ( $\chi/Q^{\text{PDRM}}$ , 18 for each of the six sources).

### 1.1.2. Results

Results of Park's PDRM are shown in **Figure 3**, where predicted and measured concentrations are shown for the entire study period for SO<sub>2</sub>, Al, As, Cu, Fe, Ni, Pb, Se, and Zn. Park achieved excellent fits between predicted concentrations of SO<sub>2</sub> and As, and emission rates predicted for SO<sub>2</sub> for the 4 power plants were within 8% of those derived from their CEM data. Many of the predictions for the other elements were also good: the normalized mean square error (i.e. relative mean square error) (%NMSE) in the ratios of predicted-to-observed concentrations for all time periods for Al, Cr, Fe, Mn, and Se were < 10%. However, %NMSE for Cu, Ni, Pb, and Zn were substantially greater, i.e. 13-36%. Moreover, large residuals observed in specific sampling periods, suggest the presence of other sources, or as concluded in this work, errors in the  $\chi/Q$  profiles calculated from the GPM. The following incidences are viewed as important:

1. over-predictions of SO<sub>2</sub>, Al, Cu, Fe, Ni, Pb, and Zn at 12:00, under-predictions for the same species at 12:30,
2. under-predictions in Al, Cu, Fe, and Pb from 13:30-14:00,
3. over-predictions in Al and Fe from 18:00-19:00, over-predictions in Cu and Pb at 18:00,
4. under-predictions at 14:00 for Cu, 15:00 for Fe (peak excluded by Park) and 14:30 in Al.

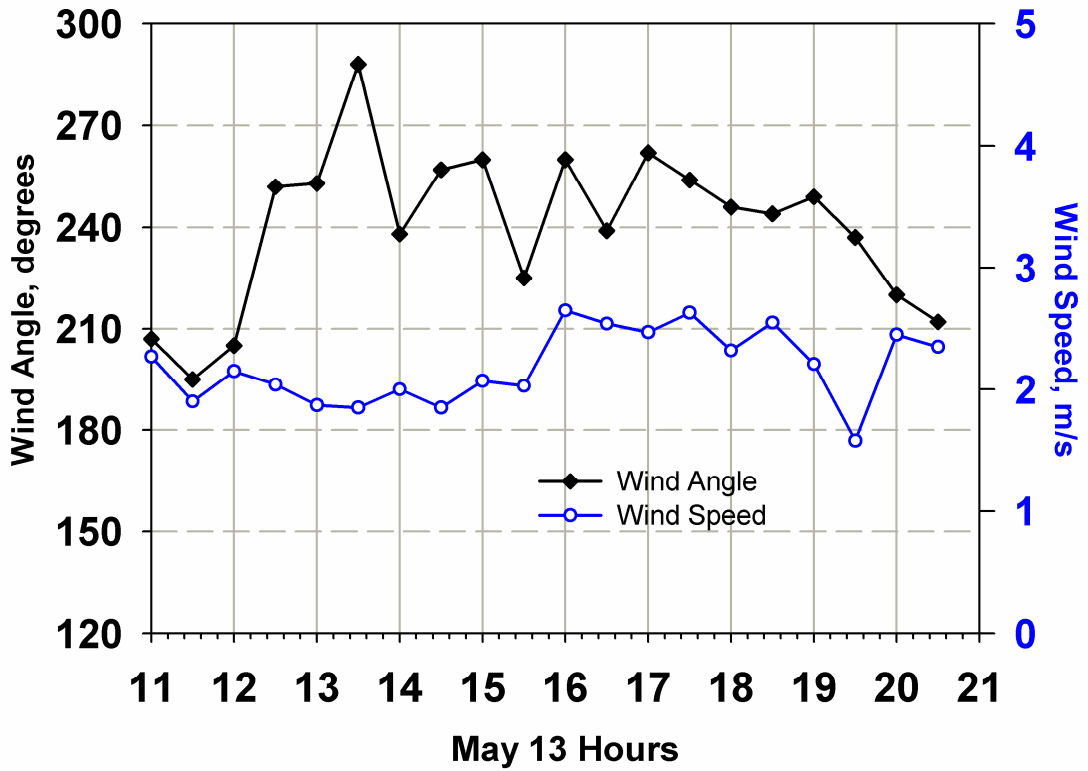


**Figure 2.** Thirty-minute averages of surface 30-minute wind speeds and wind directions measured at Sydney on May 13, 2002.

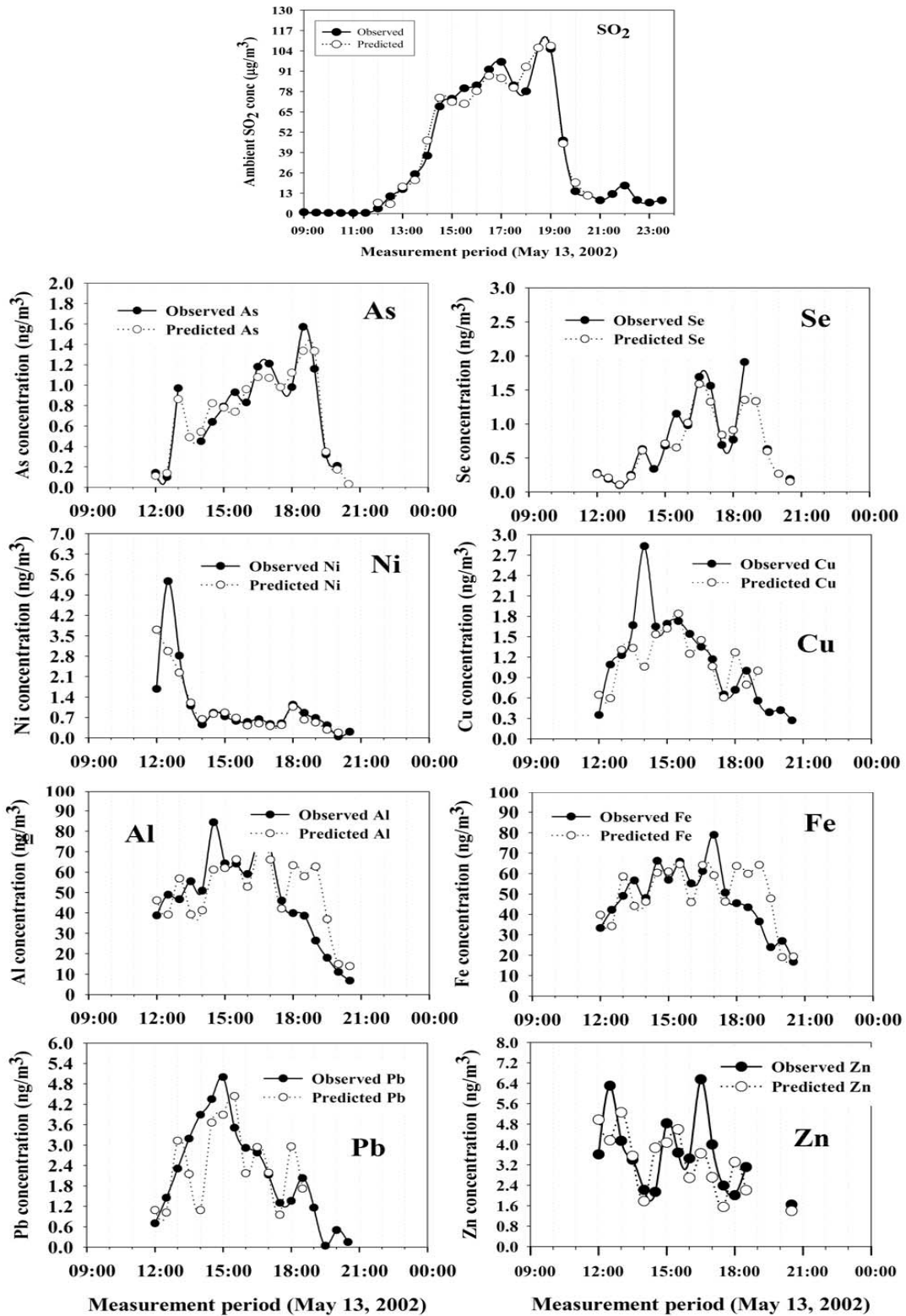
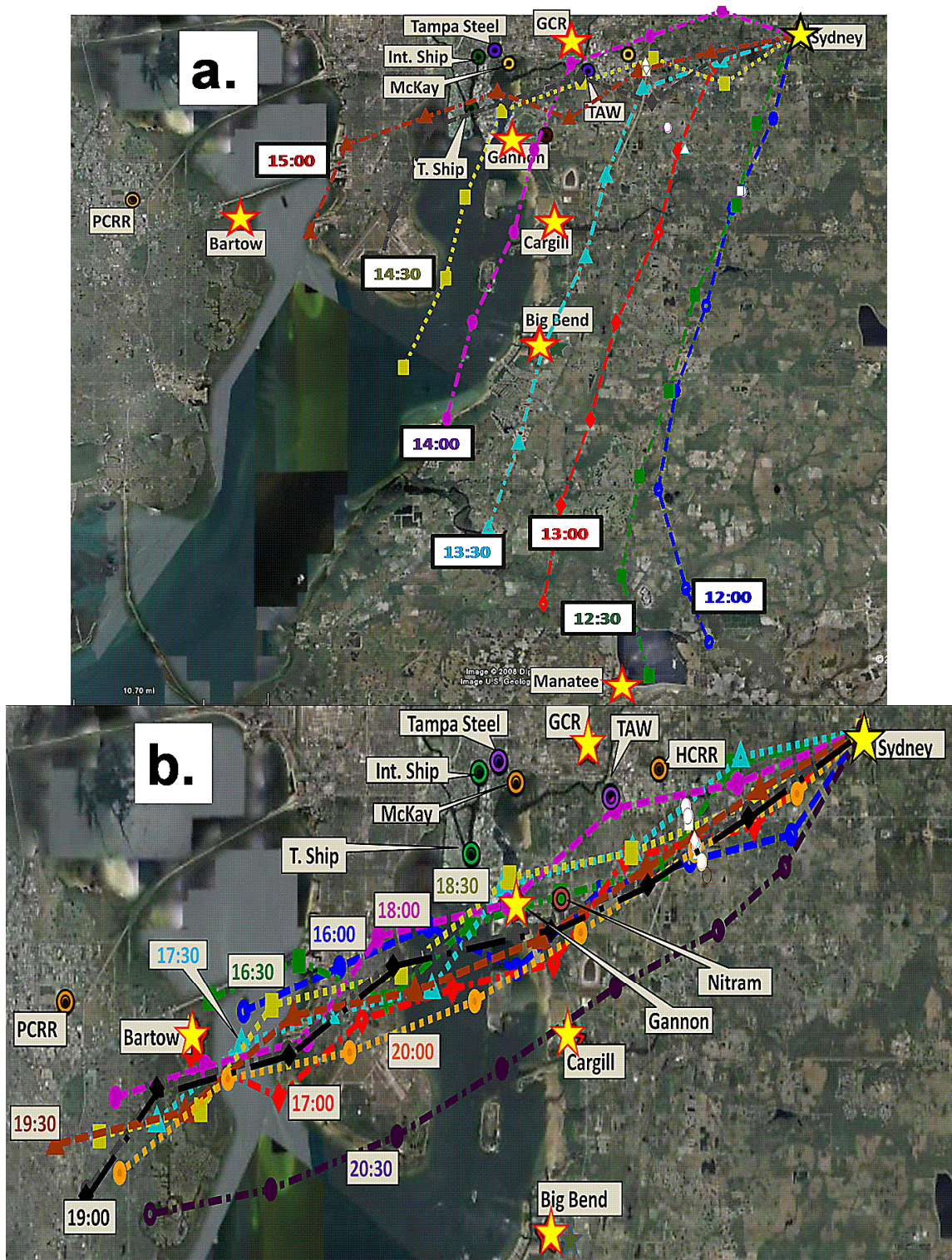


**Figure 3.** Predicted concentration profiles as determined by Park (adapted from Park et al., 2005a) show over- and under-predictions of the observed concentration profiles for Al, Cu, Fe, Ni, Pb, and Zn.

5. the correlation between predicted and observed concentrations for Zn was generally poor, i.e., features are predicted to occur earlier or later than they actually do.

Park reasoned that short-term fluctuations in source emissions were beyond the capability of their model and that over-predictions in Al and Fe were due to poor recoveries in analytical methods for soil particles. However, a cause of some of these residuals is likely to have been the result of the substantial wind shift that occurred at ~12:30 PM, causing errors in the periods of predicted plume influence for plume arriving between 12:30-16:00. (Curvilinear wind paths are shown as back-trajectories calculated from 30-minute average surface wind speeds Sydney in **Figures 4a.** and **4b**). In addition to the residuals, some of the ratios of predicted elemental emission rates do not agree with those reported for similar sources in literature source profiles found in EPA's SPECIATE database (U.S. EPA, 2006; herein referred to as SPECIATE). As discussed in section 3.2.3, this is most evident in the X/Pb ratios for the lead recycling plant (**Table 1**), where Park predicted a Zn/Pb ratio of 1.0 as compared to the reported ratio of 0.005 and in X/Ni ratios for both oil-fired power plants (**Table 2**), where predicted X/Ni are an order of magnitude higher than literature ratios for Cu, Mn, Pb, and Zn, and greater than two orders of magnitude for Al, As, Cr, Fe, and Se. As described below, we were able to explain many of these discrepancies with the improved model.

Park published two cases, the first (Case 1) in which all six source meteorological dispersion parameter solutions were constrained to within 0.1-2 of their values predicted by the GPM, and the second (Case 2) in which separate constraints were applied for the



**Figures 4a. & b.** Surface back trajectories computed every 30 minutes using wind data collected by NOAA at a height of 10 m: trajectories from 12:00-15:30(a) and 16:00-20:30(b) are shown. The surface wind shifted from a Southerly to a Southwesterly flow at 12:30. ©2007, Google

**Table 1.** Source abundance profiles (relative to Pb) as derived from EPA SPECIATE for lead recycling plants and for Gulf Coast, as predicted by Park and this work.

Ratio to Pb	Literature: Secondary Pb			Gulf Coast Recycling	
	Mean*	±	σ	This Work	Park
Ag	0.001	±	0.001	0.017	-
Al	0.09	±	0.05	8	15
As	0.02	±	0.01	0.05	0.10
Ba	0.02	±	0.03	0.01	-
Ca	0.02	±	0.02	0.03	-
Cd	0.01	±	0.02	0.03	-
Cr	0.001	±	0.003	0.001	0.3
Cu	0.006	±	0.007	0.008	0.4
Fe	0.09	±	0.15	0.81	14
Mg	0.02	±	0.01	0.03	-
Mn	0.001	±	0.001	0.130	0.286
Na	0.04	±	0.03	0	-
Ni	0.002	±	0.001	0.007	0.182
Pb	1.0	±	0.2	1.0	1.0
Sb	0.07	±	0.05	0.05	-
Se	0.001	±	0.001	0.01	0.08
Sr	0.001	±	0.001	0.09	-
V	0.0002	±	0.0002	0.0003	-
W	-	±	-	0.2	-
Zn	0.005	±	0.003	0.001	1.0

\* Composite of 5 profiles

**Table 2.** Source abundance profiles (relative to Ni) as derived from EPA SPECIATE for oil-fired power plants and for Manatee and Bartow, as predicted by Park and this work.

Ratio to Ni	Literature: Oil Fired Emissions			Manatee		Bartow	
	Mean*	±	σ	This Work	Park	This Work	Park
<b>Ag</b>	0.003	±	0.004	-	-	4.E-06	-
<b>Al</b>	0.6	±	0.4	0.6	11.5	0.8	75.5
<b>As</b>	0.005	±	0.004	0.004	0.01	0.097	16
<b>Ba</b>	0.1	±	0.1	0.3	-	0.2	-
<b>Ca</b>	1.0	±	0.6	3.6	-	0.7	-
<b>Cd</b>	0.001	±	0.002	0.008	-	0.014	-
<b>Cr</b>	0.03	±	0.01	0.01	0.3	0.18	14
<b>Cu</b>	0.04	±	0.01	0.15	0.14	0.17	2
<b>Fe</b>	0.5	±	0.4	0.4	10	0.3	201
<b>Mg</b>	-	±	-	3.7	-	3.8	-
<b>Mn</b>	0.03	±	0.01	0.14	0.3	0.05	1.0
<b>Na</b>	0.7	±	0.3	1.3	-	0.3	-
<b>Ni</b>	1.0	±	0.5	1.0	1.0	1.0	1.0
<b>Pb</b>	0.3	±	0.1	0.3	0.2	0.4	3
<b>Sb</b>	0.01	±	0.01	-	-	0.02	-
<b>Se</b>	0.002	±	0.002	0.04	0.07	0.15	16
<b>Sr</b>	0.02	±	0.002	0.04	-	0.003	-
<b>V</b>	1.0	±	0.1	1.2	-	1.8	-
<b>W</b>	-	±	-	-	-	0.001	-
<b>Zn</b>	0.5	±	0.4	0.8	1.3	0.2	9

\* Composite of 11 profiles

Cargill and Gulf Coast plants. This was done because Case 1 solutions for SO<sub>2</sub> ERs exceeded reported annual emissions (FDEP) by factors of >3 and >12 for Cargill and Gulf Coast, respectively. Case 2 was run on the hypothesis that effective plume heights (<100 m) for these plants are low compared to the utilities which ranged from 500- 1200 m, and dispersion is expected to be more affected by surface roughness elements. Case 2 assumes that these surface plumes were more coherent. Separate lower and upper bound constraints were 0.4-8.0 (Cargill) and 1.2-24 (Gulf Coast).

## **2. Dataset and Methods**

### **2.1. Reanalysis of Tampa Sources**

The major sources likely to have affected air quality at Sydney are described below. This includes Park's original six sources (four power plants, the Cargill phosphate fertilizer plant, and the Gulf Coast lead recycling plant) and three new sources not modeled by Park. Pertinent source information, including distances and station angles (measured at Sydney from due North), fuel type, emissions control devices, and emissions data are listed in **Table 3**. Stack and stack gas emission parameters listed in **Table 4** were obtained from NEI.



**Table 4.** Stack information compiled from the NEI database.

<b>Source</b>	<b># Stacks</b>	<b>Ave Stack Height (m)</b>	<b>Ave Stack Diameter (m)</b>	<b>Ave Exit Gas Temp. (K)</b>	<b>Ave Exit Gas Velocity (m/s)</b>
<b>Manatee</b>	2	152.1	8.2	441	24.5
<b>Big Bend</b>	4	152.1	7.3	410	14.3
<b>Gannon</b>	6	96.0	3.7	423	28.1
<b>Bartow</b>	3	91.4	2.9	421	33.9
<b>Cargill</b>	4; surface	39.1	2.0	330	15.7
<b>Gulf Coast</b>	2; surface	45.7	0.9	344	16.7
<b>HCRR</b>	1	67.1	1.6	416	22.1
<b>McKay</b>	1	48.8	1.7	505	12.5
<b>PCRR</b>	1	50.3	2.6	405	21.8
<b>Tampa Steel</b>	surface	3.0	0.0	295	0.0
<b>Int. Ship</b>	surface	3.0	0.0	295	0.0
<b>Tampa Ship</b>	surface	3.0	0.0	295	0.0
<b>T. Arm. Works</b>	1	7.2	0.6	978	3.1

**Oil-fired Utility Plants.** Two oil-fired power plants, Manatee and Bartow, are located ~40 km from Sydney (41 and 38 km), at station angles of 196° and 253°, respectively. SO<sub>2</sub> emission rates from Manatee and Bartow (1100 and 1150 g/s) were comparable during the study period. However Manatee is equipped with only a cyclone system to control PM emissions while Bartow's stacks have more efficient Electrostatic Precipitators (ESP). Thus, annual PM emission rates reported for Manatee (9470 metric tons/year) are nearly 4-fold larger than those for Bartow (2600 metric tons/year).

**Coal-fired Utility Plants.** The remaining two utility plants, Gannon (1200 MW) and Big Bend (~1800 MW) are coal-fired units located 20 and 25 km from Sydney at station angles of 222° and 251°, respectively. Gannon is equipped with an Electrostatic precipitator (ESP), while Big Bend is equipped with both an ESP and a wet (forced oxidation lime) scrubber. Both plants burn bituminous coal. SO<sub>2</sub> emissions from the Gannon plant (2667 g/s) were the largest of the 4 utility power plants, while those from Big Bend were the smallest (316 g/s) during the study period.

**Industrial Sources.** Cargill (235°; 20 km) is an ammonium phosphate fertilizer plant that burns sulfur via a double contact process to produce sulfuric acid with SO<sub>2</sub> as a by-product. NH<sub>3</sub> is also used as a reactant to generate ammonium phosphates used as fertilizer. Much of the PM emissions are from phosphate rock dust and calciners and have elemental source profiles similar to soil: Si, Ca, Al, and Fe with enriched P concentrations (SPECIATE). Reported emission rates for Cargill vary, depending on the data source: SO<sub>2</sub> and PM emission rates obtained from the Florida Department of Environment were ~3,400 (108 g/s) and 288 (9 g/s) metric tons/year, respectively, but

only 0.006 g/s and 1.7 g/s as reported by NEI. Reported emission rates of NH<sub>3</sub> are 2.8g/s (NEI) and 6.1 g/s (TRI).

The Gulf Coast (GCR) plant (269°; 15km) recycles lead batteries to produce Pb ingots mixed with Sb, Al, Sn, or other metals. This facility operates two coke-fired blast furnace equipped with bag-houses for collection of PM emissions before discharge through 46 m stacks. The blast furnace feeds molten lead into open topped molds. Material captured by the baghouses is sent to a flash agglomeration furnace to be liquefied and the molten material poured into open crucibles and then crushed before being transferred to the blast furnace feed hoppers for lead recovery. The cooled lead “buttons” are re-melted and mixed with additives, which include Sb, and Al depending on desired product composition. Its SO<sub>2</sub> and PM emission rates are reported to be 487 (16 g/s) and 26 metric tons/year, respectively. However, this plant is located only 15 km from Sydney and it is expected to be a substantial source of Pb, Al, and Sb.

Stack heights for both Cargill and Gulf Coast are 46 m, i.e., much lower than the Utility Plants, and at Gulf Coast, emission of fumes from molten metal pouring operations occurs nearly at ground level.

Ship refurbishing is a major industry in Tampa and two of the largest facilities are Tampa (260°; 22km) and International Ship (266°; 21km). These provide maintenance and repair of vessels of all sizes and encompass large scale fabrication of parts and assemblies involving steel cutting and welding, slag abrasive blasting (for removal of scale, rust, and paint from ship hulls and other steel surfaces), and surface coating. Tampa Ship is cited as one of the busiest shipyards in the Southeast. International Ship repairs and modifies large and small ships, motors, and boilers and in addition to 5 dry docks,

they maintain a 25,000ft<sup>2</sup> steel fabrication area which is only partially covered. Blast cleaning is accomplished with a high-pressure (35,000 psi) water slurry laden with ‘Black Beauty’ slag abrasive (Reed Minerals). This material contains 48.8% SiO<sub>2</sub>, 21% Al<sub>2</sub>O<sub>3</sub>, 19.0% Fe<sub>2</sub>O<sub>3</sub>, 6.0% CaO, 1.7% KO<sub>2</sub>, 0.92% TiO<sub>2</sub>, 0.9% MgO, and 0.62%Na<sub>2</sub>O. For shipyards and other industrial sources, emissions are likely to be episodic in nature as opposed to continuous. Within a km of International Ship is a steel refurbishing yard, Tampa Steel (267°; 20km) which machines and sandblasts steel.

Two incinerators, namely McKay Bay (265°; 21km) and Pinellas County Refuse Recovery (PCRR) (257°; 45km) were included in the iPDRM. Of the two incinerators considered, PCRR is reported to have the largest emissions (NEI). Source profiles (SPECIATE) show significant abundances of Zn (13-21%) and Pb (8-15%) in incinerator emissions. A third incinerator, Hillsborough County Refuse Recovery (HCRR) (264°; 11km) was not included in the iPDRM because we saw no evidence of its influence on Sydney.

## 2.2. Meteorological Data

Meteorological data measured at Sydney was described by Park:

“Two-minute averaged surface meteorological observations were available from a National Oceanic and Atmospheric Administration (NOAA) vertical profiling site at Sydney (NOAA Environmental Technology Laboratory). Thirty-minute averages of the NOAA wind speed and direction measurements made during the study period on 13 May are shown in **Figure 2**. In the predawn hours, light winds blew from the southeast under stable atmospheric conditions. As the sun rose, the winds shifted

clockwise and developed into a southwesterly flow off of the Tampa Bay. The midday high temperature and low relative humidity averaged 33°C and 37%, respectively, with strong convective mixing. The mixing height reached an estimated 2400 m by mid-afternoon under slightly unstable atmospheric conditions and with more westerly winds at 3–4 m/s off of Tampa Bay. Westerly winds continued through the evening, with lower wind speeds and stable atmospheric conditions developing within an hour after sunset. Sunrise was at 0541 Eastern Standard Time (EST), and sunset was at 0711 EST. No precipitation was recorded across the Tampa Bay area.”

In addition to surface wind observations, hourly winds and temperatures for a three-dimensional modeling domain and hourly two-dimensional outputs of mixing heights and surface characteristics were also available from the CALMET model output at the geo-coordinates of the Sydney site [Scire et al., 2000]. These parameters included the: Pasquill stability class, mixing height, coriolis parameter, friction velocity, Monin-Obukhov length and convective velocity scale and were used in constructing upper air trajectories and in the micrometeorological parameterizations used in the GPM in both the original PDRM and in the iPDRM.

### **2.3. Ambient Pollutant Measurements**

Ambient concentrations of SO<sub>2</sub> and NH<sub>3</sub> were those obtained by Park from the BRACE database. The 30-min averages of the native one-minute SO<sub>2</sub> and 20-min NH<sub>3</sub> mixing ratios (ppb, shown in **Figure 5**) were used in the iPDRM.

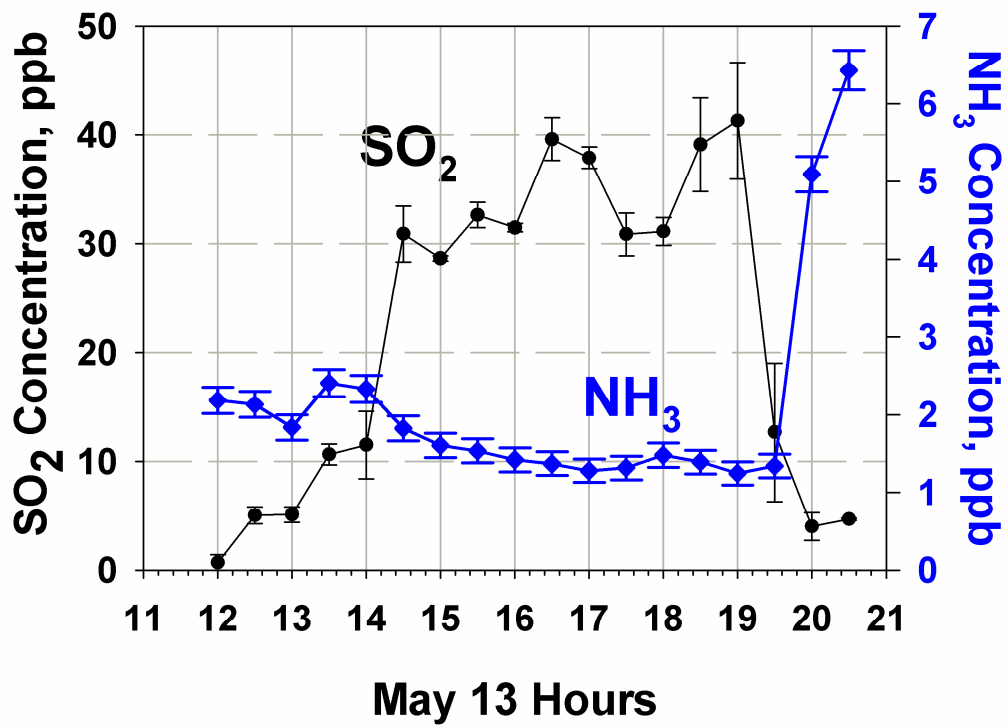


**Figure 5.** Concentration-vs.-time-of-day profiles for SO<sub>2</sub> and NH<sub>3</sub> measured at Sydney (courtesy of BRACE database).

In addition to gases, ambient  $PM_{\text{fine}}$  aerosol was collected in successive 30-min slurry samples for an 8.5-hour period at Sydney using the University of Maryland Semi-Continuous Elemental Aerosol Analyzer (SEAS; Park et al., 2005, Pancras et al., 2005, Kidwell and Ondov, 2001, 2004). Herein, the original eighteen samples were reanalyzed for the 11 elements (Al, As, Cd, Cr, Cu, Cu, Fe, Mn, Ni, Pb, Se, and Zn) originally determined by Park using multielement Graphite Furnace Atomic Absorption Spectroscopy with Zeeman background correction (GFAAZ, Pancras et al., 2004); and 14 additional elements that were potentially useful as point source or background marine and dust aerosol tracers using a Thermo-Systems, Inc., X-series II Inductively Coupled Plasma Mass Spectrometry (ICPMS).

Our Thermo-Electron X-series II ICPMS is equipped with an off-axis quadrupole analyzer with resolution between 0.25 and 0.35 amu, a simultaneously gated analog Faraday cup and dynode-electron-multiplier-pulse-counting detectors, a reaction cell, a tunable hexapole stage for ion Kinetic Energy Discrimination (KED), and a concentric nebulizer with a Peltier cooled spray chamber. All measurements were done in "Collision Cell Technology" (CCT) mode, wherein a mixture of 8%  $H_2/He$  gas is continuously injected to reduce the kinetic energy of all sampled ions with indiscriminate collisions. It is more probable that collisions will be between interference ions (such as  $Ar^+$  ions from the plasma, or polyatomic ions with a greater surface area) than between analyte ions, thus reducing interferences to a greater extent than analytes; in effect, increasing the signal to background ratio and maximizing instrument sensitivity. The KED stage was routinely set to -17 volts to block products of the gas collisions from

entering the quadrupole. The X-series II instrument was controlled with the manufacturer's "PlasmaLab" software version 2.4 (Thermo, Waltham, MA). Specific experimental operating conditions are given in **Table 5**.

Optimization of ion lenses, nebulizer flow, and response tuning were performed at the outset of every experiment using a tuning solution containing elements at low-, mid-, and high-mass ranges. The sampling rate was set via peristaltic pump at 1.0 mL/min, which corresponding to 2.2 minutes per sample, allowing 5 replicate determinations to be made using a sample volume of 2.2 mL. About 1% of the droplets are injected into the instrument. An internal standard mixture containing of Sc (60ppb), Rh (10ppb), and Lu(10ppb), was added along with the sample via a "Y" fitting fitted with a mixing coil and expansion tube (Thermo-Electron Corp., Waltham, MA). Detector cross calibration was performed after approximately every three weeks of use using a solution (Thermo-Electron Corp., Waltham, MA) containing isotopes of 59 elements with mass numbers ranging from 7 to 238, at concentrations ranging from 5-1250 ppb.

Instrumental detection limits for ICPMS and detection limits found in SEAS samples using the GFAAZ (Pancras et al., 2005) and ICPMS are listed in **Table 6**. Detection Limits for SEAS samples achieved with the ICPMS method were much smaller than those for GFAAZ for all elements except Se, which was the same. Pb was 280 times smaller, Al, Cr, Cu, Fe, Mn, and Zn were all smaller by factors ranging from 10-71, and As, Cd, and Ni by factors from 4.5-10.

ICPMS analysis of National Institute of Standards and Technology (NIST) Standard Reference Material (SRM) 1640 "Trace Elements in Natural Water" showed agreement within 5% of certified and reference values for all ppb-level elements (Al, As, Ba, Ca,

**Table 5.** ICPMS operating conditions.

<b>Forward RF Power</b>	1.4	kW	
<b>Argon Gas Flows:</b>			
Support Gas	13	L*min <sup>-1</sup>	
Cool Gas	0.93	L*min <sup>-1</sup>	
Nebulizer Gas	~ 0.86	L*min <sup>-1</sup>	
<b>Interface Cones</b>	Nickel		
<b>Sample Uptake</b>	1.3	mL min <sup>-1</sup>	
<b>Dwell Times:</b>			
Quantified elements	10	ms	<sup>51</sup> V, <sup>52</sup> Cr, <sup>55</sup> Mn, <sup>56</sup> Fe, <sup>59</sup> Co, <sup>60</sup> Ni, <sup>65</sup> Cu, <sup>66</sup> Zn, <sup>88</sup> Sr, <sup>95</sup> Mo, <sup>114</sup> Cd, <sup>121</sup> Sb, <sup>137</sup> Ba, <sup>139</sup> La, <sup>140</sup> Ce, <sup>147</sup> Sm, <sup>208</sup> Pb, <sup>209</sup> Bi, <sup>238</sup> U
	20	ms	<sup>23</sup> Na, <sup>24</sup> Mg
	40	ms	<sup>47</sup> Ti
	100	ms	<sup>39</sup> K, <sup>44</sup> Ca, <sup>75</sup> As, <sup>78</sup> Se
Internal Standards	10	ms	<sup>45</sup> Sc, <sup>103</sup> Rh, <sup>175</sup> Lu
Interfering species	10	ms	<sup>7</sup> Li, <sup>13</sup> C, <sup>33</sup> S, <sup>53</sup> ClO, <sup>77</sup> ArCl, <sup>82</sup> Se, <sup>83</sup> Kr, <sup>86</sup> Sr, <sup>106</sup> Cd, <sup>108</sup> MoO, <sup>118</sup> Sn, <sup>150</sup> Sm, <sup>206</sup> Pb, <sup>207</sup> Pb
<b>Scan Mode</b>	Peak Hopping		
<b>Scans</b>	15		
<b>Acquisition Time</b>	14	s	
<b>Replicates</b>	4 - 5		
<b>CCT Gas Flow</b>	~ 4	mL*min <sup>-1</sup>	
<b>Lens Optimization</b>	Parameters Tuned with respect to cps		
			m/z
max cps.			59, 115, 238
min cps.			78
min Oxide ratio (< 2%).			156/140
min cps RSD.			2%

**Table 6.** Detection limits elements in SEAS samples using ICPMS and GFAAZ compared with reported detection limits from US EPA Speciation Trends Network Protocols.

	ICP-MS (CCT) <sup>1</sup>		Detection Limits, ng/m <sup>3</sup>		
	m/z	ng/mL	GFAAZ <sup>2</sup>	ICP-MS (CCT)	EPA- STN <sup>3</sup>
<b>Al</b>	27	0.57	3.8	0.28	195
<b>As</b>	75	0.014	0.030	0.007	23
<b>Ba</b>	137	0.023	-	0.011	350
<b>Ca</b>	44	2.3	-	1.1	62
<b>Cd</b>	111	0.015	0.040	0.007	109
<b>Cr</b>	52	0.010	0.050	0.005	20
<b>Cu</b>	63	0.031	1.070	0.015	22
<b>Fe</b>	56	0.06	0.72	0.03	23
<b>K</b>	39	5.4	-	2.6	134
<b>Mg</b>	24	0.29	-	0.14	244
<b>Mn</b>	55	0.008	0.140	0.004	21
<b>Na</b>	23	1.5	-	0.7	290
<b>Ni</b>	60	0.040	0.180	0.019	16
<b>Pb</b>	206	0.002	0.310	0.001	49
<b>Sb</b>	121	0.004	-	0.002	230
<b>Se</b>	78	0.043	0.020	0.020	28
<b>Sr</b>	88	0.005	-	0.002	-
<b>V</b>	51	0.004	-	0.002	27
<b>Zn</b>	66	0.26	7.15	0.13	22

<sup>1</sup> Values are averages from five different analytical periods (N=56) wherein detection limits are calculated as the mean reagent blank signal plus 3 times the standard deviation of 3-6 replicate measurements of the reagent blank (Beachley et al., 2007, unpublished results).

Minimum volume (Vmin) for multi element analysis is 1.3

<sup>2</sup> Values (Pancras et al., 2005) listed are derived from the reagent blank signal plus 3 standard deviations of the reagent blank signal. A minimum volume (Vmin) for multielement analysis of 0.5 mL is required for 3 replicates for each of 3 groups of elements.

<sup>3</sup> Method detection limit values are those reported for the US EPA speciation Trends Network (STN) protocol: X-ray fluorescence for all elements except K and Na, for which DLs are reported for analyses by ion chromatography.

Cd, Co, Cr, Cu, Fe, K, Mg, Mn, Mo, Na, Ni, Pb, Sb, Se, Sr, V, and Zn). A total dissolution experiment was performed with the ICPMS for yet-to-be-released NIST atmospheric fine particle Standard Reference Material, for which high-quality elemental constituent analyses are available from NIST. Percent recoveries were within  $\pm 7\%$  (**Table 7**) for all elements (Al, As, Ca, Cd, Cr, Cu, Fe, K, Mg, Mn, Na, Ni, Pb, Sb, Se, Sr, V, and Zn). To investigate the capability of the ICPMS in analysis of a direct slurry, in which complications such as losses of particles to the walls of the sample vials and peristaltic pump tubing, and statistical sampling issues for discrete particles can occur, percent recoveries of direct slurry analysis were compared with total dissolutions of two mock slurries. Procedures for these experiments are outlined in **Appendix B**. The mock slurries consisted of (1) the same NIST atmospheric fine particle SRM diluted to a concentration anticipated to exist in a real SEAS sample, and (2) a pooled slurry of real SEAS samples containing highly refractory aerosol particles collected near Birmingham, AL. Results of these experiments are shown as percent recoveries of elemental concentrations obtained from direct slurry analysis from elemental concentrations obtained from a total dissolution of the slurry in **Table 8**. Percent recoveries in the NIST slurry were within  $\pm 11\%$  of total dissolution values for As, Ba, Ca, Cd, Cu, K, Mg, Mn, Na, Pb, Se, Sr, V, and Zn. Elements which exceeded this range included Al (-45%), Cr (-35%), Fe (-30%), Ni (+23%), and Sb (-21%). Substantial fractions of the masses of these elements (Al, Cr, Fe, and Ni) are often associated with larger, difficult to dissolve particles. Percent recoveries in the pooled slurry were within  $\pm 12\%$  of total digestion values for As, Ba, Cd, Cu, K, Mg, Mn, Na, Ni, Pb, Sb, Se, V, and Zn. Elements which

**Table 7.** Experimental results for ICPMS determination of total dissolution of the yet-to-be-released NIST atmospheric fine SRM.

Element	N	Dilution	NIST values			Total Dissolution			
			Mean ppm	$\sigma$ ppm	% RSD	Mean ppm	$\sigma$ ppm	% RSD	% diff
<b>Al</b>	5	1/100	32200	1600	5	30200	400	1	-6.2
<b>As</b>	8	1/100	116	3	3	116	3.8	3	-0.4
<b>Ca</b>	8	1/100	58300	3300	6	56300	500	0.9	-3.4
<b>Cr</b>	11	1/10	397	14	4	373	1	0.3	-6.0
<b>Cu</b>	11	1/10	600	23	4	624	2	0.3	4.0
<b>Fe</b>	10	1/100	39200	2400	6	37400	100	0.3	-4.6
<b>K</b>	11	1/10	10300	500	5	9930	30	0.3	-3.6
<b>Mg</b>	5	1/10	7930	630	8	7993	118	1	0.8
<b>Mn</b>	11	1/10	822	45	5	765	5	0.7	-6.9
<b>Na</b>	9	1/10	4230	230	5	4297	60	1	1.6
<b>Ni</b>	11	1/100	82	12	15	79.3	5.4	7	-3.3
<b>Pb</b>	10	1/100	6520	250	4	6320	40	0.6	-3.1
<b>Sb</b>	11	1/10	44	2	5	41	0.5	1	-6.8
<b>Se</b>	11	1/10	24	2	8	24.3	1.4	6	1.3
<b>Sr</b>	9	1/10	207	15	7	212	1.72	0.8	2.4
<b>V</b>	9	1/100	121	8	7	124	4.93	4	2.5
<b>Zn</b>	10	1/100	4740	70	1	4384	42	1	-7.5

**Table 8.** Yields for determinations of elements in slurry samples by ICPMS.

<b>Element</b>	<b>iSRM Mock Slurry</b>		<b>Pooled SEAS slurry</b>	
	<b>Ratio</b>	<b><math>\sigma</math></b>	<b>Ratio</b>	<b><math>\sigma</math></b>
<b>Al</b>	0.55	$\pm$ 0.15	0.58	$\pm$ 0.27
<b>As</b>	1.00	$\pm$ 0.06	0.89	$\pm$ 0.18
<b>Ba</b>	0.97	$\pm$ 0.08	0.94	$\pm$ 0.15
<b>Ca</b>	0.96	$\pm$ 0.07	0.57	$\pm$ 0.12
<b>Cr</b>	0.65	$\pm$ 0.18	0.70	$\pm$ 0.05
<b>Cd</b>	1.06	$\pm$ 0.06	0.95	$\pm$ 0.18
<b>Cu</b>	1.05	$\pm$ 0.07	0.91	$\pm$ 0.09
<b>Fe</b>	0.70	$\pm$ 0.05	0.74	$\pm$ 0.04
<b>K</b>	0.96	$\pm$ 0.06	0.96	$\pm$ 0.10
<b>Mg</b>	0.98	$\pm$ 0.07	0.93	$\pm$ 0.18
<b>Mn</b>	0.98	$\pm$ 0.05	0.92	$\pm$ 0.06
<b>Na</b>	1.00	$\pm$ 0.07	0.93	$\pm$ 0.10
<b>Ni</b>	1.23	$\pm$ 0.37	1.00	$\pm$ 0.27
<b>Pb</b>	1.02	$\pm$ 0.07	0.88	$\pm$ 0.06
<b>Sb</b>	0.79	$\pm$ 0.33	1.08	$\pm$ 0.30
<b>Se</b>	1.01	$\pm$ 0.28	1.00	$\pm$ 0.57
<b>Sr</b>	0.99	$\pm$ 0.07	0.46	$\pm$ 0.31
<b>V</b>	1.00	$\pm$ 0.11	0.88	$\pm$ 0.32
<b>Zn</b>	1.11	$\pm$ 0.05	0.90	$\pm$ 0.05

exceeded this range included Al (-45%), Ca (-43%), Cr (-30%), Fe (-26%), and Sr (-54%). These results suggest that direct analysis of SEAS samples will generate confident data ( $\pm 10\%$ ) for most elements while percent recoveries for Al, Cr, and Fe are likely to be ~55-75%.

## 2.4 Modeling Methods

As mentioned above, the improvements to Park's PDRM included: the calculation of trajectories to model plume centerlines, the addition of sources, the application of compositional information from CMB profiles to both condition  $\gamma/Q$  profiles and constrain solutions for emission rates, and the determination of background sources by including CMB terms into the model. The calculation of trajectories and off-axis distances ( $Y$ ) are described below followed by the method of determining the background sources with the CMB model. The configuration of the iPDRM is described in section 2.4.3, along with the hierarchical approach in which it was run.

### 2.4.1. Trajectory Construction and Trajectory-Related Parameters

For each source, trajectories were calculated every half-hour, for up to three heights; and  $Y$ ,  $x'$ , and  $u$  were determined from the trajectories as described in this section.

Distance vectors were created for every half hour and plotted such that the  $xy$  coordinate of the end point of the previous vector is the coordinate of the beginning point of the next vector. For each interval, the components of distances in the  $x$  and  $y$  directions are as follows:

$$\begin{aligned} x_{dist} &= 1800 u_t \cos(\theta_{wind}) \\ y_{dist} &= 1800 u_t \sin(\theta_{wind}) \end{aligned} \tag{11}$$

where  $\theta_{\text{wind}}$  is the wind direction and  $u_i$  is the wind speed in sampling interval  $t$ . The factor of 1800 is applied to convert from m/30 minutes to m/s. A separate trajectory was constructed for each source, every half hour beginning at the source (origin (0,0)). Coordinates for Sydney were likewise referenced to the origin of each source using the station angle and the straight-line distance between the sampling site and each source. Examples of the trajectories calculated from Gannon as they approach Sydney are shown in **Figure 6**.

On each trajectory, the point of closest approach,  $(x_{CA}, y_{CA})$ , was identified and the off-axis distance between that point and Sydney  $(x_{Syd}, y_{Syd})$  was calculated geometrically. As shown in **Figure 7**, the off axis distance,  $Y$ , is calculated from the component distances  $x_{comp}$  and  $y_{comp}$  using equation (12).

$$Y = \sqrt{(x_{comp})^2 + (y_{comp})^2} \quad (12)$$

Because for each trajectory, both the closest approach and Sydney coordinates are referenced to the trajectory's source, the component distances are simply:

$$x_{comp} = x_{CA} - x_{Syd} \quad (13)$$

$$y_{comp} = y_{CA} - y_{Syd}$$

The plume transport distance,  $x'$ , was calculated as the sum of the direction vector magnitudes up until the point of closest approach. Plume transport time,  $t$ , was calculated as the sum of the number of direction vectors up to the point of closest approach. Average transport velocity,  $u$ , along the trajectory is simply the transport distance by the transport time. For trajectories where the point of closest approach fell in between direction vectors, approximations were made to the nearest 10 minutes (1/3 of the

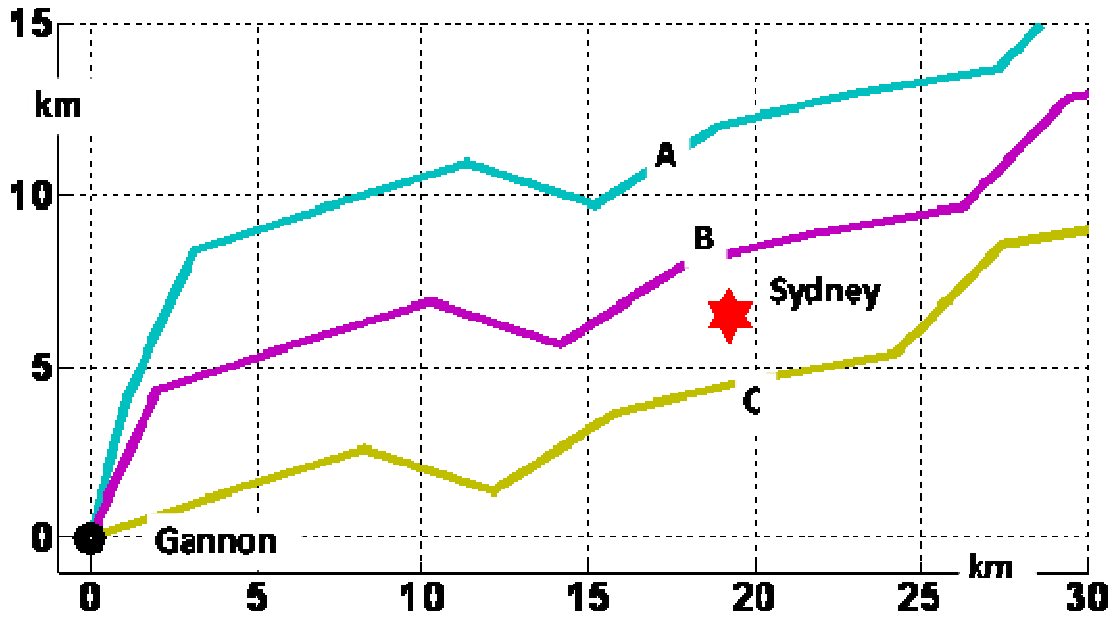


**Figure 6.** Forward Trajectories of the plumes originating from Gannon at three different times: 11:30 (turquoise), 12:00 (purple), and 12:30 (gold). The points of closest approach to Sydney occurred: at 14:00 (A), 14:30 (B), and 15:00 (C). The off-axis distances ( $Y$ ) and transport distances ( $x$ ) were calculated from these trajectories.

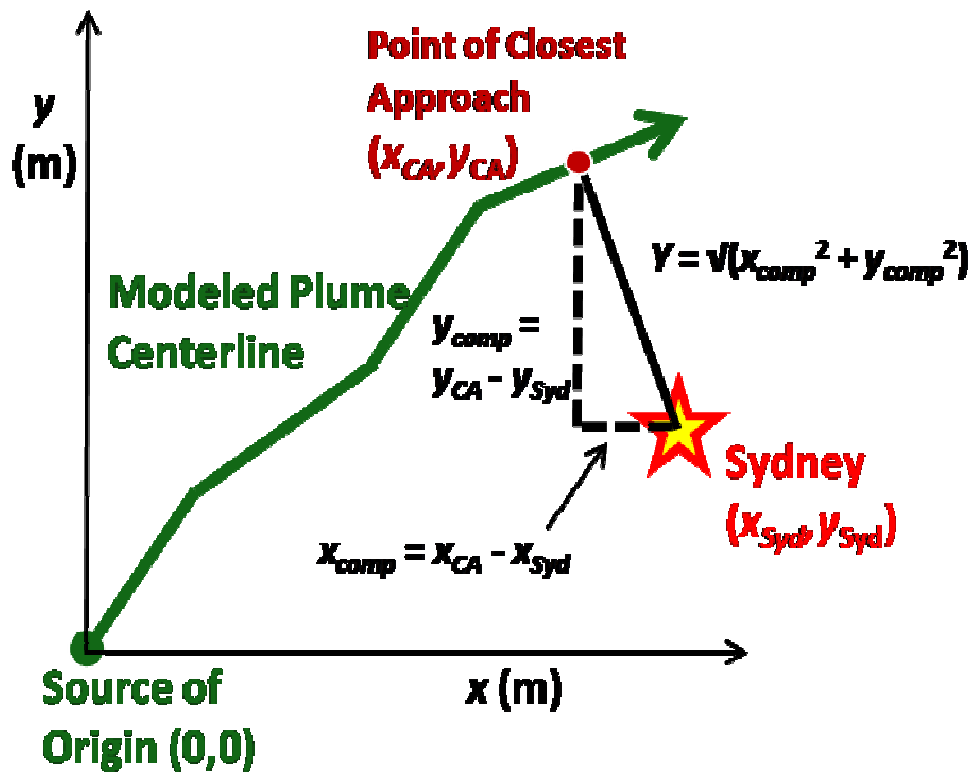


**Figure 7.** A plume centerline from the source of origin toward Sydney modeled using the head-to-toe alignment of wind direction vectors. Equations shown are used to calculate the off-axis distance,  $Y$ , between the point of closest approach and Sydney.

vector). In cases where the point of closest approach for successive trajectories occurred at the same time, the smallest off-axis distance was used.

#### **2.4.1.1. Trajectories at different heights**

As predicted by the power law, wind speed increases with height. Thus for distant sources, we can expect to observe different plume arrival times for portions of the plume transported at different levels. However, differences in wind directions aloft are also likely and because of this, the aloft portion of a plume does not always exhibit a faster time of arrival. This was the case in Tampa, as evidenced by **Figure 8**, wherein we plot plume trajectories for Big Bend beginning at 12:00 and 13:00 at both 100 and 500 m. For this reason, trajectories were calculated at up to three heights. Forward trajectories were calculated at the height of the surface wind measurements (10 m) and at two additional heights 100 m, and 500 m. The trajectories at 100 m were calculated using directions at 10 m, but correcting for the increase in speed with height using the power law (see **Appendix A**). The trajectories at 500 m were constructed using hourly CALMET wind data (Scire, 2000). Thus 60 min intervals were used instead of 30 min. Ten and 100 m trajectories were calculated for all sources, however, 500 m trajectories were also constructed for the power plants, owing to their large effective stack heights (~500-1200 m).

An Ekman angle correction,  $\theta_{\text{Ekman}}$ , included by Park was a uniform  $3.5^\circ$  rotation toward a westerly flow to adjust surface wind directions to reflect wind angles at stack heights. We abandoned this correction, because consistent differences between 10 and 500 m trajectories could not be distinguished, and because the PDRM adjusts the  $\chi/Q$  to

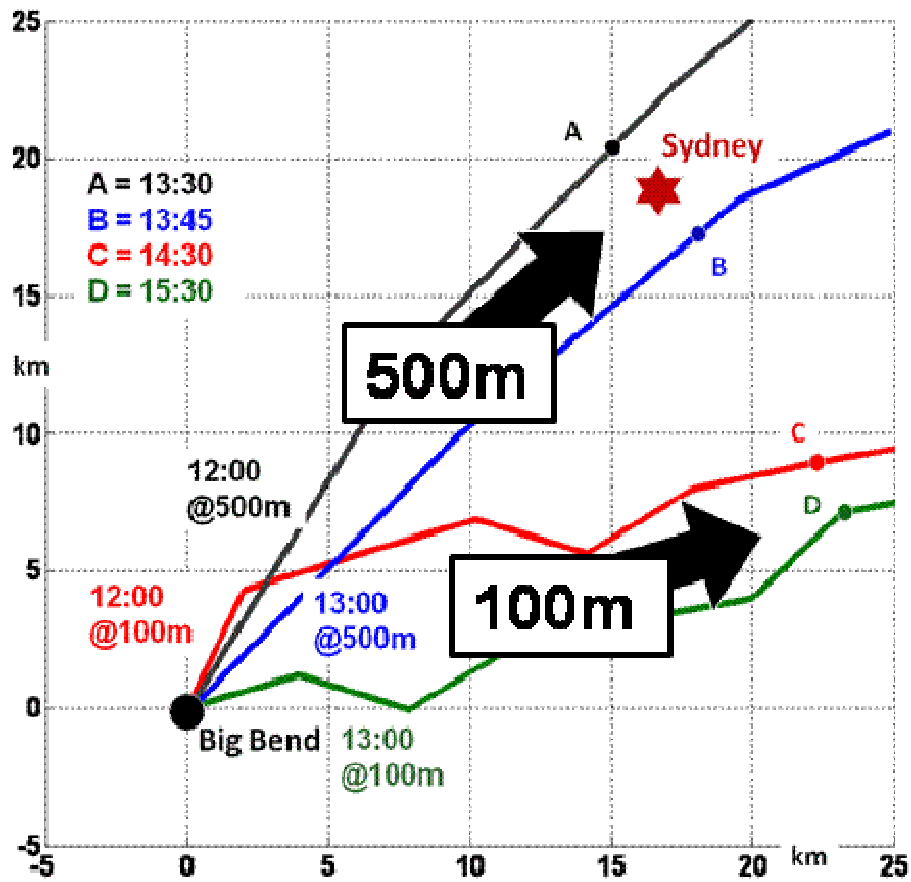


**Figure 8.** Illustration of plume trajectories originating at Big Bend at 12:00 and 13:00 at heights of 100- and 500-m. Plumes at different heights originating at the same time are observed to travel along different angles indicating a wind rotation aloft.

fit the ambient concentrations, it is not highly sensitive to small trajectory errors in  $Y$ . Values for  $Y$ ,  $x'$ , and  $u$  were input into the GPM as described above. In each case, a single trajectory profile was input into the PDRM. For power plants, this consisted of the sum of  $\chi/Q^{\text{traj}}$  values calculated for the 100- and 500-m levels for each time interval. For the shipyard, emissions were so close to the ground that only the 10 m trajectory was used. For all other (industrial) sources, the 100 m trajectories were used.

#### **2.4.2. Estimation of the Background Sources**

Park identified low concentrations at the beginning and end of the study period as background concentrations and linearly interpolated these for the intervening periods. The results were subtracted from the measured concentrations and the PDRM was run with the background-corrected concentrations. The background concentrations for both Park and this work are shown in **Table 9**.

Herein, the EPA CMB model (v 8.2) was run to estimate background contributions throughout the study period as described below.  $PM_{2.5}$  mass concentration measurements were not available for our study period. Instead, ambient mass was (crudely) estimated (**Figure 9**) as the sum of major ionic species (ammonium, sulfate, nitrate, and chloride) available from the BRACE database and used in the CMB model. Seven generic sources included in the model were: a coal fired power plant, an oil fired power plant, an incinerator, a secondary Pb smelter, a steel sandblasting profile, agricultural soil, and sea salt, all obtained from the SPECIATE database. Profiles for these sources are reproduced in **Table 10**. The phosphate fertilizer plant could not be included due to collinearity of its profile with the coal source and to a lesser extent the background soil source. Elements

**Table 9.** Background concentrations (ng/m<sup>3</sup>) as predicted by Park and the iPDRM. Concentration profiles for iPDRM predicted soil and sea salt varied over the course of the study period and are listed as average values.

<b>Species</b>	<b>Park et al., 2005a</b>	<b>Soil*</b>	<b>Sea Salt*</b>
<b>SO<sub>2</sub></b>	520	ND	ND
<b>NH<sub>3</sub></b>	-	2890 <sup>†</sup>	ND
<b>Ag</b>	-	ND	ND
<b>Al</b>	25.0	37.1	1.0
<b>As</b>	0.10	ND	ND
<b>Ba</b>	-	0.82	0.39
<b>Ca</b>	-	87.3	19.2
<b>Cd</b>	-	ND	ND
<b>Cr</b>	0.13	0.62	ND
<b>Cu</b>	0.45	0.04	0.14
<b>Fe</b>	6.8	23.5	ND
<b>Mg</b>	-	8.01	32.8
<b>Mn</b>	0.48	0.05	ND
<b>Na</b>	-	4.6	299
<b>Ni</b>	0.53	0.028	ND
<b>Pb</b>	0.37	0.004	ND
<b>Sb</b>	-	0.016	ND
<b>Se</b>	0.10	ND	ND
<b>Sr</b>	-	0.66	ND
<b>V</b>	-	0.10	0.63
<b>W</b>	-	0.04	ND
<b>Zn</b>	1.72	0.08	ND

\* - average values over study period

ND - values < 0.001

† - not associated with soil aerosol, but included with this source in the iPDRM

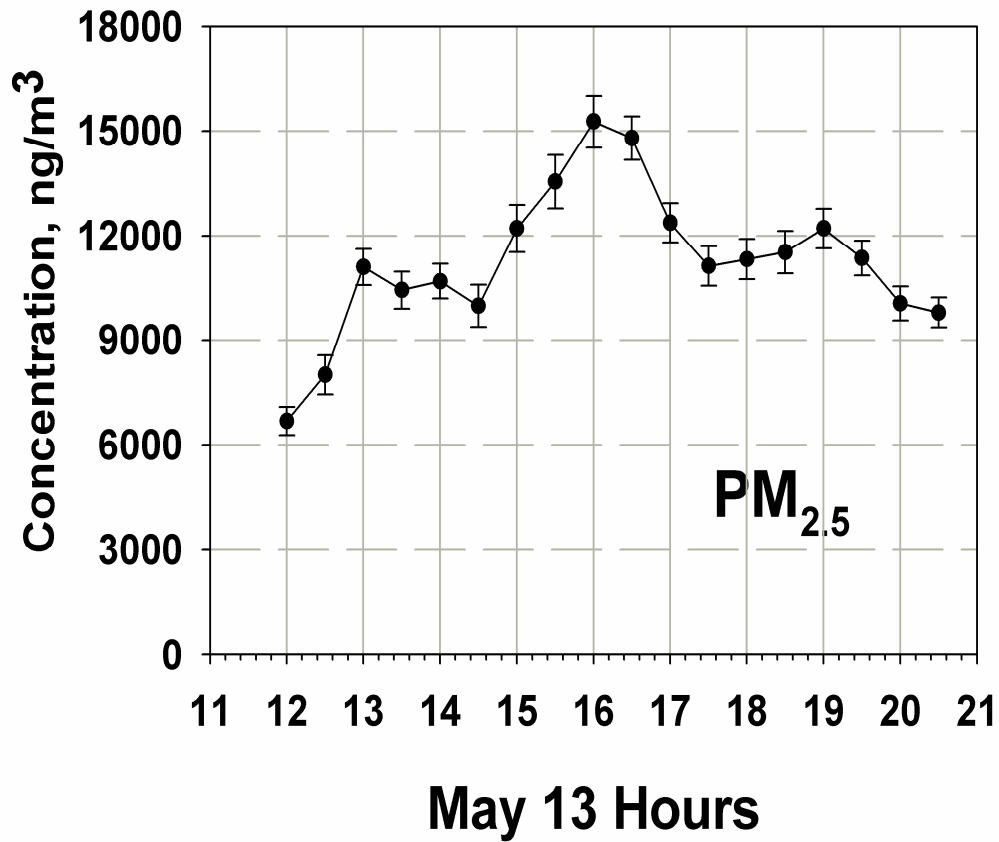


**Figure 9.** PM<sub>2.5</sub> mass concentration estimates-vs.-time-of-day profiles. PM<sub>2.5</sub> mass concentration was (crudely) estimated as the sum of major ionic species (ammonium, sulfate, nitrate, and chloride) measured at Sydney.

**Table 10.** Chemical Mass Balance abundance profiles (g element / g Total PM<sub>2.5</sub> mass) as entered into the EPA CMB model (v8.2). Values were obtained from the SPECIATE database.

	Oil	Coal	Incinerator	Pb Recycling	Sandblasting	Soil	Sea Salt
<b>Al</b>	0.007 ± 0.009	0.071 ± 0.013	0.011 ± 0.007	0.025 ± 0.005	0.013 ± 0.001	0.184 ± 0.018	ND ± ND
<b>As</b>	0.0003 ± 0.0005	0.0011 ± 0.0004	0.0002 ± 0.0001	0.008 ± 0.003	0.0002 ± 0.0001	ND ± ND	ND ± ND
<b>Ba</b>	0.002 ± 0.003	0.016 ± 0.013	0.0005 ± 0.0004	0.016 ± 0.001	ND ± ND	0.0016 ± 0.0002	ND ± ND
<b>Cd</b>	0.0001 ± 0.0007	0.0001 ± 0.0079	0.003 ± 0.035	0.008 ± 0.004	ND ± ND	ND ± ND	ND ± ND
<b>Cr</b>	0.0007 ± 0.0007	0.0002 ± 0.0007	0.0003 ± 0.0017	0.001 ± 0.008	0.010 ± 0.0001	0.0005 ± 0.0001	ND ± ND
<b>Cu</b>	0.0013 ± 0.0007	0.0002 ± 0.0007	0.0024 ± 0.0002	0.005 ± 0.001	0.012 ± 0.001	0.0002 ± 0.0001	ND ± ND
<b>Fe</b>	0.026 ± 0.000	0.050 ± 0.013	0.006 ± 0.001	0.053 ± 0.004	0.111 ± 0.001	0.12 ± 0.0001	ND ± ND
<b>Mn</b>	0.0004 ± 0.0077	0.0016 ± 0.0100	0.0005 ± 0.0024	0.65 ± 0.001	0.002 ± 0.011	0.003 ± 0.012	ND ± ND
<b>Na</b>	0.036 ± 0.009	0.025 ± 0.005	0.09 ± 0.06	0.023 ± 0.001	0.014 ± 0.001	0.0009 ± 0.0001	0.31 ± 0.03
<b>Ni</b>	0.025 ± 0.001	0.0001 ± 0.013	0.0003 ± 0.0004	0.001 ± 0.083	0.0056 ± 0.0002	0.0002 ± 0.0003	ND ± ND
<b>Pb</b>	0.012 ± 0.001	0.001 ± 0.007	0.11 ± 0.0002	0.001 ± 0.0001	0.010 ± 0.001	0.0002 ± 0.0001	ND ± ND
<b>Se</b>	0.0001 ± 0.0005	0.006 ± 0.011	0.0001 ± 0.0286	0.001 ± 0.0002	ND ± ND	ND ± ND	ND ± ND
<b>V</b>	0.018 ± 0.001	0.0002 ± 0.0059	ND ± ND	0.0001 ± 0.0001	0.0001 ± 0.0001	0.0006 ± 0.0001	ND ± ND
<b>Zn</b>	0.006 ± 0.001	0.001 ± 0.013	0.17 ± 0.001	0.003 ± 0.001	0.0083 ± 0.0001	0.0004 ± 0.0001	ND ± ND

ND - values < 0.0001

included in the model were Al, Cd, Cr, Cu, Fe, Pb, Mn, Ni, Se, Na, V, and Zn. CMB predicted and observed fits are shown in **Figure 10**. Of these, Al, Fe, and Na were particularly well-fit. This was fortunate because the main objective of the CMB run was to obtain source contribution estimates (SCE) for soil (high abundances of Al and Fe) and sea salt (large abundance Na) background during the modeling period. Arsenic, Cu, Cr, Mn, Ni, Pb, and V profiles are fit with only minor deviations. Cadmium, Se, and Zn are not fit well, likely because literature source profiles were used instead of profiles representing the actual individual sources in the Tampa area. To minimize the effect of uncertainties in the background concentration estimates on the PDRM, the temporal profiles of the SCEs were smoothed by averaging the  $n-1^{\text{th}}$  through  $n+1^{\text{th}}$  value for each sampling interval. Both the abundances and the smoothed SCE profiles were used directly in the iPDRM as described in section 2.4.3.4. This is possible because their products have units of species concentration ( $C_{i,R}$ ) as do the PDRM terms. Temporal SCE ( $\text{ng PM}_{2.5} / \text{m}^3$ ) profiles are shown prior to smoothing (**Figure 11**) and after smoothing (**Figure 11(A)**).

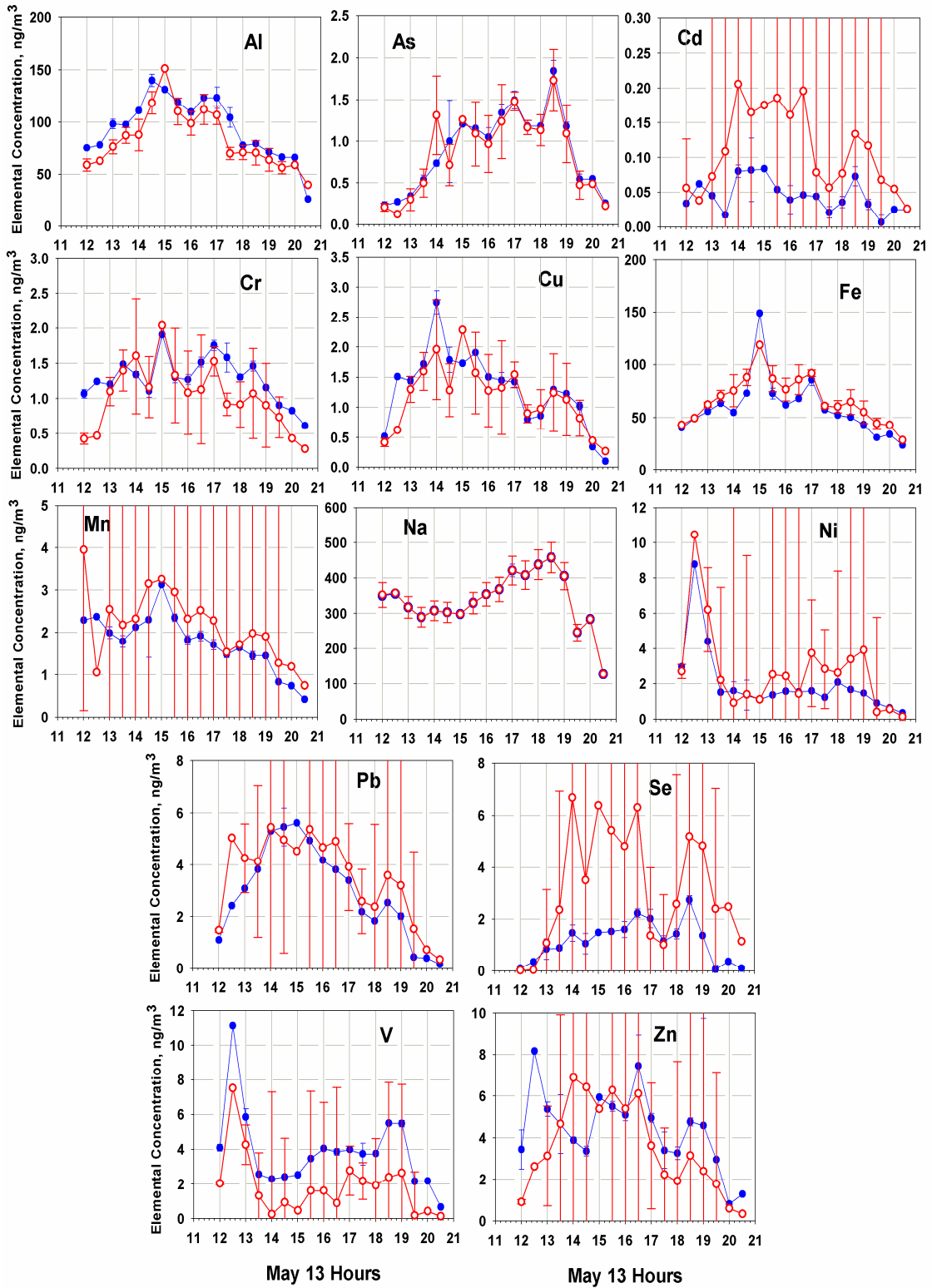


**Figure 10.** Observed concentration-vs.-time-of-day profiles (hybrid dataset; blue) and those predicted (red) using the EPA Chemical Mass Balance v8.2 model.

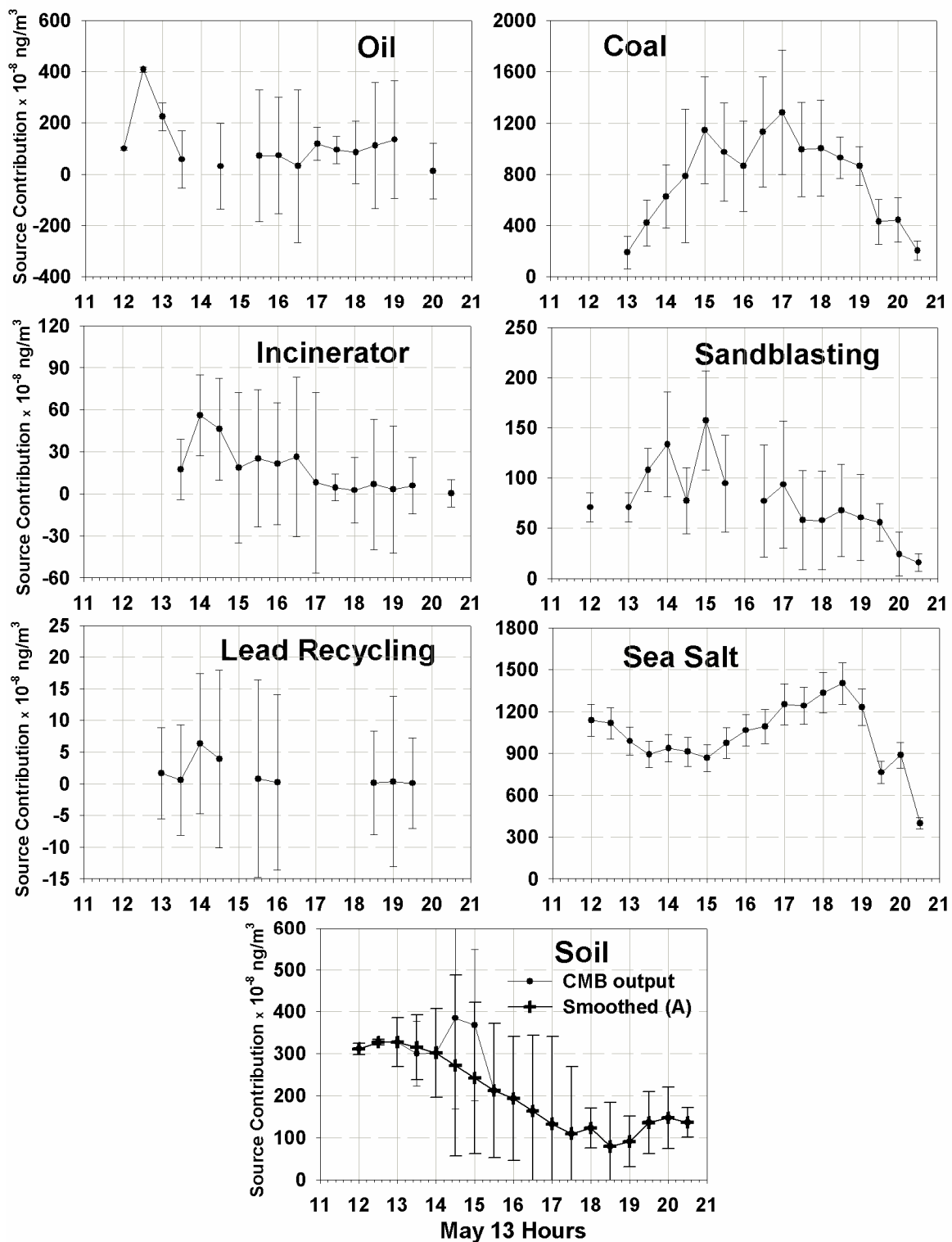


**Figure 11.** Source Contribution Estimate (SCE) (ng total PM<sub>2.5</sub> mass / m<sup>3</sup>)-vs.-time-of-day profiles predicted by the CMB model for generic source types. The SCE for the soil source includes the smoothed profile (A) input into the PDRM.

### 2.4.3. The iPDRM Configuration

The new model was configured as follows:

$$[E_i]_t = \sum_{j=1}^9 \overline{ER}_{i,j} \cdot (\chi/Q)_{j,t}^{iPDRM} + \sum_{j=10}^{11} A_{i,j} [PM_{2.5}]_{j,t} + residual_{i,t} \quad (6)$$

where  $A_{i,j}$  is the abundance of area source  $i$  (g species  $i$  / g total  $PM_{2.5}$  from source  $j$ ) and  $[PM_{2.5}]_{j,t}$  is the source contribution of area source  $i$  (g total  $PM_{2.5}$  from source  $j$  /  $m^3$ ) in the sampling interval,  $t$ . The indices  $j = 1-9$  represent the point sources (6 sources originally modeled by Park, plus the two incinerators and the steel sandblasting source described above), and indices  $j = 10-11$  represent the soil and marine backgrounds, respectively. We denote the  $\chi/Q$  values output by the iPDRM as  $\chi/Q^{iPDRM}$  to differentiate them from  $\chi/Q^{traf}$ .

As done by Park, we sought a single average emission rate for each source and each species  $\overline{ER}_{i,j}$ , corresponding to the periods of influence indicated by the  $\chi/Q_t$  profiles. Herein, solutions were likewise, sought for both  $A_{i,j}$  and  $[PM_{2.5}]_{j,t}$ s for the background sources. The premise for this approach is that both  $A_{i,j}$ s and  $[PM_{2.5}]_{j,t}$ s more aptly describe area sources while the PDRM terms explain the point sources.

In both PDRMs, solutions for  $\chi/Q_{j,t}$ s are also sought. However, in Park's model, the relative values of the  $\chi/Q$  solutions ( $(\chi/Q)_{j,t}^{pPDRM}$ ) were fixed to those obtained by the GPM, i.e., only the magnitude of the profile was allowed to vary but not its shape, as constrained by in Equation 4a. As shown in **Figure 3** and described in section 1.1.2, this led to poor matches between peak shapes for marker species and the predicted times of plume influence.

In the ideal case, peaks revealed by marker species in the ambient time-series data are well resolved, and  $\chi/Q$ s are constrained by their shapes. Such was the case for Ni and V for Manatee, NH<sub>3</sub> for Cargill, and to a lesser extent, Pb for Gulf coast. For this reason, we configured the iPDRM to allow solutions for the  $\chi/Q_{j,t}$ , to vary with sampling interval  $t$  for V, Ni, Pb, and SO<sub>2</sub>, in an iterative process described below. The SO<sub>2</sub> measurements, along with CEM-derived emission rates, provide accurate magnitudes for the  $\chi/Q$ s from the 4 utility sources, while V and Ni provide accurate  $\chi/Q$  profile shapes for the two oil-fired plants.

The above procedure was also applied to Pb and Zn and later to NH<sub>3</sub> to improve profile shapes for Gulf Coast, the two incinerators, and Cargill. As discussed earlier in this section, the practice allows information inherent in the shape to condition the  $\chi/Q$  profiles.

To run the iPDRM, both constraints and seed values are required for all values for which solutions are sought. Initial seed values and constraints used herein and by Park and herein are listed in **Table 11**. As indicated in this table, Park seeded the model with initial SO<sub>2</sub> emission rates that were rough approximations of those determined from CEMs (used as initial values for the iPDRM) and stack volumetric flow rate data, and applied loose constraints to their solutions (**Table 11**). Their constraints on solutions for the elements were, likewise loose, i.e., ranging from 0.0001 to 50 g/s for all sources.

**Table 11.** Constraints and initial “seed” values (IV) for SO<sub>2</sub> (g/s) used in Park’s model and the iPDRM for the six major SO<sub>2</sub> sources.

	Park			iPDRM		
	LB	IV	UB	LB	IV	UB
<b>Manatee</b>	100	2500	3000	1030	1040	1100
<b>Big Bend</b>	100	300	1000	318	335	335
<b>Gannon</b>	100	3000	3500	2490	2550	2750
<b>Bartow</b>	100	1500	2000	1030	1150	1200
<b>Cargill</b>	10	40	500	0.005	28	150
<b>Gulf Coast</b>	10	20	500	0.005	35	500

#### 2.4.3.1. Emission Rate constraints

In iPDRM, the CEM-derived SO<sub>2</sub> emission rate averages were input and their solutions constrained to vary only  $\pm 5\%$ , i.e., our rough estimate of 1 standard deviation of their uncertainties, as SO<sub>2</sub> was viewed to be the most accurate and useful tracer for these sources. Note that for a well resolved source (Manatee),  $\chi/Q$ s may be predicted to within the error of the ratio of the SO<sub>2</sub> measurements made at the sampling site and source; i.e.,  $\sqrt{\sigma_{rel}^2 + \sigma_{rel}^2}$ . In other cases there will be a deconvolution error, as was the case for other sources in Tampa. Emission rate solutions for elements were constrained by an iterative and hierarchical process, as follows.

In the first iteration, the iPDRM was run with SO<sub>2</sub> and the three best marker elements ( $m_{i,j}$ ), i.e., Ni, V, and Pb. The latter were the most well-resolved and definitive marker species: Pb representing the battery recycling plant, and Ni and V representing the oil-fired utility plants (Manatee and Bartow). These marker species help to deconvolute these sources from others that concurrently influence the sampling site. For the first run and all subsequent iterations, lower bounds for Ni, V, and Pb were based on plant-specific rates obtained from the National Emission (NEI) and Toxic Release (TRI) Inventories. For all other elements, emission rate lower bounds (LB) were set to 0. Upper bounds (UB) for all elements were set to 5 g/s, i.e., values greater than could be expected for these elements. In subsequent model runs, lower- and upper-bounds were further constrained using the results derived from the previous run. Specifically, UBs were estimated by dividing the measured concentrations in each sampling interval by  $\chi/Q_{i,j}$  determined in the previous model run, as the former represents the logical upper limit for the predicted concentrations. Emission rate LBs were generally left unchanged

or set to reflect the abundance ratios ( $A_{i,j}$ )s as obtained from the SPECIATE CMB profiles. Abundance profiles for all sources contained V, Ni, and Pb, and therefore ER LBs were obtained by multiplying the emission rates for these marker elements ( $\overline{ER}_{m_{i,j}}$ ) predicted in the previous model run by the appropriate ratio ( $\frac{A_{i,j}}{A_{m_{i,j}}}$ ) in the abundance profile. This is:

$$(ER_{LB})_{i,t} = \frac{A_{i,j}}{A_{m_{i,j}}} ER_{m_{i,j}} \quad (7)$$

The resulting values were reduced by a factor of ~3 to prevent solutions from being too restrictive owing to the known inaccuracy of the CMB Abundance profiles. It was important when developing these constraints to guide the model towards a reasonable solution, but care was taken not to restrict any apportionment without a reasonable basis.

#### 2.4.3.2. $\chi/Q$ constraints

For each of the nine point sources, initial  $\chi/Q_{i,j}$  estimates were calculated using the GPM module as described by Park, except that  $Y$ ,  $x$ , and  $u$  were determined from the 30- or 60-minute trajectories as described above. In the first iteration these were constrained by factors of 0.1 to 2 as done by Park. For the two background source terms, initial  $A_{i,j}$  and source contributions estimates ( $[PM_{2.5}]_{j,t}$ ) were those used in and predicted by, respectively, the CMB analysis (section 2.4.2.). Lower bounds and upper bounds for  $A_{i,j}$ s were derived from the uncertainties for each species in the source profiles as reported in SPECIATE. Specifically,  $1\sigma$ , was subtracted or added to the reported value. These same bounds were used in all model runs.

#### **2.4.3.3. Scaling of Input Concentrations**

Ambient concentrations of all species used in all PDRM runs were scaled to prevent preferential fitting of species with higher concentrations, for which residuals would otherwise dominate the minimization of  $\chi^2$  (Equation 5). This differed from Park's approach in that  $\chi/Q_s$  were derived solely from the SO<sub>2</sub> data and then used as fixed constants in a subsequent run in which emission rates for elements were determined. Essentially, we did not want to ignore the information afforded by the other species, especially Ni, V, Pb and NH<sub>3</sub>, so the scaling factors were selected with resolving power in mind as well. The scale factors used for each element are shown along with its resulting maximum value in **Table 12**. For the first run, an SO<sub>2</sub> scaling factor of 0.001 was used to give a maximum scaled SO<sub>2</sub> concentration of 107. This was adjusted for subsequent iterations to 0.0001 and 10.7, respectively, in order to guide the model to preferentially minimize residuals for tracer species. All other scaling factors remained consistent throughout the iterative runs.

#### **2.4.3.4. Hierarchical Approach.**

The species discussed above were applied in a hierarchical manner, beginning with the most trustworthy data and sources. For each model run, the results from the prior runs were tightly constrained, and additional elements and sources were included in order to guide the modeled solutions based on the best information available. Details from the stepwise "hierarchical" approach used are represented in the flow chart in **Figure 12** and described in detail below:

**Table 12.** Scaling factors applied to species concentrations in order adjust the residual size for preferential fitting of species. Resultant maximum scaled concentrations are also listed.

<b>Species</b>	<b>Scaling Factor</b>	<b>Resultant Maximum</b>
<b>SO<sub>2</sub></b>	0.001*, 0.0001	107*, 10.7
<b>NH<sub>3</sub></b>	0.001	16.7
<b>Ag</b>	103	6.0
<b>Al</b>	0.6	84.0
<b>As</b>	10	18.4
<b>Ba</b>	2	13.6
<b>Ca</b>	0.02	6.0
<b>Cd</b>	75	6.3
<b>Cr</b>	5	9.5
<b>Cu</b>	5	13.7
<b>Fe</b>	0.2	29.8
<b>Mg</b>	0.07	6.0
<b>Mn</b>	5	8.1
<b>Na</b>	0.01	6.0
<b>Ni</b>	10	87.7
<b>Pb</b>	10	56.2
<b>Sb</b>	20	84.0
<b>Se</b>	10	27.3
<b>Sr</b>	3	6.0
<b>V</b>	5	55.7
<b>W</b>	9	6.0
<b>Zn</b>	5	40.9

\*- applied to the first iteration only

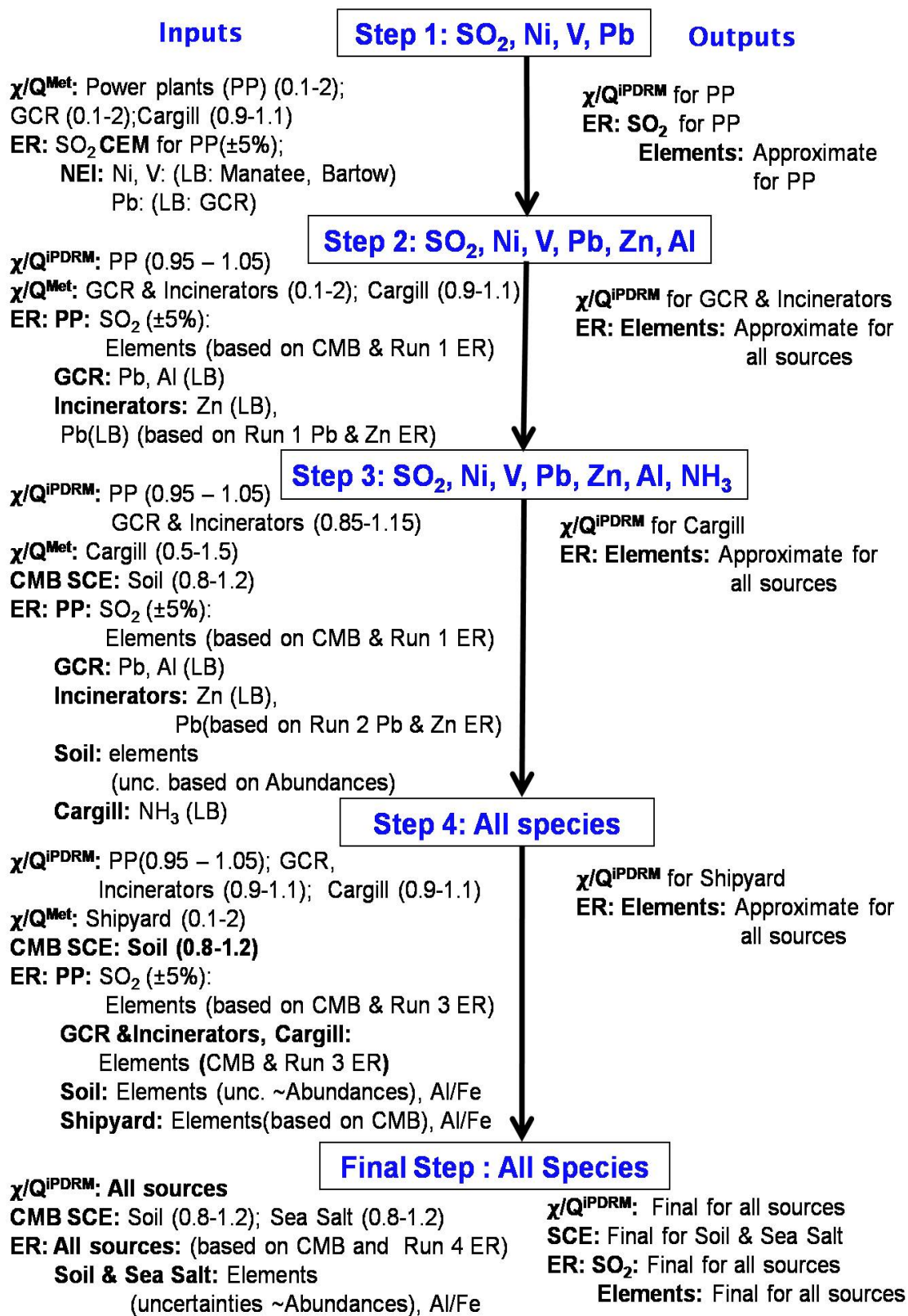


**Figure 12.** Flow chart showing our hierarchical steps with input constraints and output solutions.

**Step 1.** In this step,  $\chi/Q^{\text{traj}}$  for the 4 power plants and Gulf Coast were constrained from 0.1-2 times their input value as described above. Excursions in observed  $\text{NH}_3$  concentrations closely correlate with the  $\chi/Q^{\text{traj}}$  profile calculated for Cargill (see **Figure 16c**). Therefore, solutions for  $\chi/Q^{\text{iPDRM}}$  values for Cargill were constrained to within 10% of the values predicted by  $\chi/Q^{\text{traj}}$ , to preserve its shape. However,  $\text{NH}_3$  was not included in this iteration because of its high background from livestock and other sources in the area. Also, as a water soluble and reactive gas, its chemistry prevents it from being a conservative tracer. Whereas  $\text{SO}_2$  emission rates were tightly constrained for power plants, more relaxed lower and upper bounds (0.005 to 500 g/s) for solutions for Cargill and Gulf Coast were applied in this run owing to the availability of only annual emission rate estimates, instead of contemporaneous values.

In order to prompt the model to apportion Ni and V to Manatee and Bartow, lower bounds for these elements (0.03 (Ni) and 0.1(V); 0.02 (Ni) and 0.003 (V) g/s, respectively) were set at a tenth of their NEI predicted emission rates. We expected significant amounts of Pb emissions from Gulf Coast, so the lower bound for Gulf Coast's Pb emission rate was increased to a third of its NEI predicted emission rate, i.e., at 0.003 g/s.

The output  $\chi/Q^{\text{iPDRM}}$  values for the power plants were considered to be accurate and were input into the remainder of runs. Also useful for use in subsequent iterations were the predicted emission rates. These were not considered highly accurate because all of the sources had yet to be included, but they represented refined guesses.

**Step 2.** In the second step,  $\chi/Q$  solutions for Gulf Coast and the two incinerators were constrained between 0.1-2 times the input  $\chi/Q^{\text{traj}}$  values, while the  $\chi/Q$  solutions for the

power plants were constrained between 0.95-1.05 of the  $\chi/Q^{iPDRM}$  values predicted in the first iteration. The  $\chi/Q$  solution for Cargill was again constrained as described in the first iteration. Ambient concentrations of Pb, Al, and Zn were included along with SO<sub>2</sub>, Ni, V, and Pb to aid in the deconvolution of Gulf Coast and the incinerators. Constraints placed on emission rates (especially the lower bounds) for this run (**Table 13**) were developed to guide the model to apportion Zn to the incinerators and Pb to Gulf Coast and the incinerators. Constraints placed on emission rates of Ni, Pb, V, and Zn from the power plants were estimated from the output emission rates of the first run, literature source profile ratios, and the appearance of the fit (i.e. Manatee emissions were more tightly constrained because it is an isolated source). Al emission rate solutions were constrained widely from 0 to 5 or 10 g/s only to limit the model run time.

**Step 3.** In the third step, for Cargill were constrained from 0.5-1.5 of its  $\chi/Q^{traj}$  values and the SCE values (discussed in the “Estimation of Background Sources” section) for the soil source were constrained between 0.8-1.2 of the input smoothed SCE profile. The  $\chi/Q$  solutions for the power plants were constrained as described in the second iteration. For Gulf Coast, McKay, and PCRR,  $\chi/Q$  solutions for the initial values were those obtained from the second iteration and the constraints applied were from 0.85-1.15. Ammonia (NH<sub>3</sub>) was included along with the elements included in the second iteration. Emission rate constraints for NH<sub>3</sub> were as follows: power plants: 0-100g/s; Cargill: 2-1000g/s; Gulf Coast and the incinerators: 0-1 g/s; and the abundance of the soil source: 1-200.

These constraints were chosen such that the lower bounds were elevated for Cargill and the background source to guide the model to apportion NH<sub>3</sub> to them (Soil would not contain NH<sub>3</sub>, but NH<sub>3</sub> had a large background concentration).

**Table 13.** Emission rate constraints (g/s) used for Step 2.

	Manatee		Big Bend		Gannon		Bartow		Cargill		Gulf Coast		McKay		PCRR	
	LB	UB	LB	UB	LB	UB	LB	UB	LB	UB	LB	UB	LB	UB	LB	UB
<b>SO<sub>2</sub></b>	1037	1100	318	335	2492	2750	1026	1200	0	150	13	500	0	10	0	10
<b>Ni</b>	0.7	0.9	0.02	0.04	0.02	0.04	0.1	1.0	0	5	0	5	0	5	0	5
<b>Pb</b>	0.2	0.3	0.04	0.09	0.03	0.05	0.01	0.25	0	5	0.02	5	0.10	5	0.08	5
<b>V</b>	0.9	1.2	0.03	0.07	0.06	0.11	0.2	0.6	0	5	0	5	0	5	0	5
<b>Zn</b>	0	1	0	0.09	0.04	0.1	0.02	0.25	0	5	0	5	0.003	5	0.003	5
<b>Al</b>	0	10	0	5	0	5	0	5	0	5	0.02	5	0	5	0	5

**Step 4.** In the fourth step,  $\chi/Q$  solutions for the Shipyard source were constrained between 0.1-2 of its  $\chi/Q^{\text{traj}}$  values. Initial guesses for  $\chi/Q$  solutions for the power plants, Cargill, and Gulf Coast and the incinerators were those determined in the 3<sup>rd</sup> iteration and these were constrained to lie between 0.95-1.05 (power plants), 0.9-1.1(Cargill), and 0.85-1.15 (Gulf Coast and the incinerators).

The SCE values for the soil source were constrained as described above. Ambient concentrations modeled were SO<sub>2</sub>, NH<sub>3</sub>, Ag, Al, As, Ba, Cd, Cr, Cu, Fe, Mn, Ni, Pb, Sb, Se, V, W, and Zn. Emission rate constraints for the new elements included were loosely set to 0 – 5 g/s, while the constraints for Fe emission rate of the Shipyard source were set from 0.5-5g/s.

**Final Step.** The SCE for the Sea Salt source was input and constrained (0.8-1.2) in addition to the  $\chi/Q^{\text{iPDRM}}$  values for all other sources as described in the fourth iteration. Ca, Mg, and Na were included to the element set used in fourth iteration. Constraints for these elements were initially loose for all sources (0-10g/s), with constraints for the Sea Salt source reflecting uncertainties in its abundance reported in literature for Ca, Mg, and Na (listed in **Table 13**) . Upper bounds for all other elements were set as 0.001 as they are reported to be < 0.1% of the chemical composition of sea salt.

Once all of the sources had  $\chi/Q^{\text{iPDRM}}$  or SCE values determined, the output emission rates were evaluated and compared with literature source profile abundances and elemental ratio. Constraints were added to emission rates as needed to improve the agreement with literature source types, keeping in mind that variation between individual sources and literature reported generic source types is expected. Final emission rate constraints are listed in **Table 14**.

**Table 14.** Final emission rate constraints (g/s).

	Manatee		Big Bend		Gannon		Bartow		Cargill		Gulf Coast		McKay		PCRR		Shipyard		Soil		Sea Salt	
	LB	UB	LB	UB	LB	UB	LB	UB	LB	UB	LB	UB	LB	UB	LB	UB	LB	UB	LB	UB	LB	UB
SO <sub>2</sub>	1030	1100	318	335	2490	2750	1030	1200	0.005	150	0.005	500	0	10	0	10	0	5.000	0	1E-05	0	0.001
NH <sub>3</sub>	0.0001	35	0.0001	30	0	20	0.0001	20	2	1000	0	1	0	1	0	1	0	2E-06	1	200	0	0.001
Ag	0	1E-06	0	1E-06	0	5E-05	0	5E-05	0	5E-05	0	0.003	0	5E-05	0	5E-05	0	5E-05	0	1E-05	0	5E-05
Al	0.39	0.5	0.1	2.0	0.35	2	0.1	0.2	0.002	1	0.025	5	0.002	0.04	0.002	0.04	0.016	0.27	0.076	0.2	0	0.001
As	0.001	0.03	0.001	0.011	0.011	0.035	0.013	0.033	0	4E-05	0.0001	0.02	0.0002	0.02	0.0002	0.02	0.002	0.004	0	3E-05	0	0.001
Ba	0.0001	0.5	0.025	0.5	0.12	0.5	0.0001	0.5	0.0001	0.5	0.0001	0.003	0.0001	0.003	0.0001	0.015	0.00	1E-05	1E-04	0.5	0	0.001
Ca	0	3.2	0	10	0	10	0	1.1	0	10	0	0.005	0	0.19	0	0.43	0.00	0.36	0.05	0.4	0.011	0.018
Cd	0	0.04	0	0.0001	0.0001	0.0004	0	0.009	0	7E-05	0	0.05	3E-05	0.001	3E-05	0.004	0.0	1E-05	0	1E-06	0	0.001
Cr	0.0001	0.3	0.0001	0.5	0.0001	0.5	0.0001	0.1	0.0001	0.5	0.0001	0.001	0.0001	0.002	0.0001	0.002	0.02	0.21	0.003	0.5	0	0.001
Cu	0.1	0.16	0.03	0.04	0.001	0.025	0.008	0.08	1E-05	0.0003	3E-05	0.001	0.0002	0.005	0.0002	0.005	0.015	0.25	0.0002	0.0005	0	0.001
Fe	0.0001	1.0	0.0001	2.00	0.0001	2	0.01	1	0.0001	0.5	0.0001	0	0.0001	0.12	0.0001	0.12	0.900	2.3	0.0001	0.5	0	0.001
Mg	0	3.3	0	10	0	10	0	10	0	0.009	0	0.005	0	0.06	0	0.13	0	0.25	0.002	0.04	0.024	0.033
Mn	0.0001	0.5	0.0001	0.50	0.0001	0.5	0.0001	0.5	0.0001	0.5	0.0001	0.5	0.0001	0.5	0.0001	0.5	0.003	0.05	0.0001	0.5	0	0.001
Na	0	1.32	0	0.45	0	10	0	0.3	0	0.05	0	0.005	0	0.15	0	0.35	0	0.3	0.0009	0.02	0.27	0.34
Ni	0.7	0.9	0.01	0.035	0.009	0.04	0.2	1	0	0.0003	2E-05	0.001	5E-05	0.001	0	0.001	0.007	0.12	0	0.0002	0	0.001
Pb	0.21	0.30	0.015	0.09	0.005	0.05	0.09	0.25	0	0.0002	0.025	5	0.06	5	0.08	5	0.01	0.2	2E-05	0.0005	0	0.001
Sb	0	1E-06	0	1E-06	0	0.05	0	0.05	0	0.05	0	0.05	0	0.05	0	0.05	0	0.0005	0	0.049	0	0.0002
Se	0.03	0.04	0.018	0.025	0.01	0.055	0.002	0.05	1E-06	6E-05	0	0.02	6E-06	0.02	6E-06	0.02	0	1E-05	0	1E-06	0	0.001
Sr	0	0.04	0	0.5	0	0.5	0	0.01	0	0.5	0	0.5	0	0.5	0	0.5	0	0.008	0	0.5	0	0.001
V	0.9	1.2	0.01	0.07	0.006	0.06	0.2	0.6	0	0.002	2E-06	3E-05	2E-07	0.001	0	0.001	0.001	0.001	0.001	0.0006	0	0.001
W	0	1E-06	0	1E-06	0	0.0004	0	0.0004	0	1E-05	0	0.5	0	1E-05	0	1E-05	0	1E-05	0	0.5	0	0.0002
Zn	0.29	1.0	0.005	0.09	0.02	0.1	0.03	0.25	0.0001	5	0	0.001	0.003	5	0.003	5	0.01	0.03	0.0004	0.003	0	0.001

### 3. Results and Discussion

The results of the Analytical analyses are discussed in the following section, 3.1, followed by the modeled results in section 3.2.

#### 3.1. Analytical Results

The results of the ICPMS analyses along with Park's GFAAZ results are shown in **Figure 13**. For 5 elements analyzed with GFAAZ and reanalyzed with ICPMS, results agreed to within their uncertainties. However, for Al, Fe, As, and Cr, and Cu, ICPMS results were often 1.2 to 2-fold greater than those determined by GFAAZ. These differences are attributed to the more rigorous sample heating procedures before analysis with the ICPMS, the small statistical sampling of suspended particles (which is always a concern for GFAAZ analysis), and the slow leaching of particles stored in the slurry over long periods of time.

For these reasons, a hybrid dataset was constructed for modeling. ICPMS concentrations were preferably used when possible; however, weighted averages of the GFAAZ and ICPMS concentrations were used to replace GFAAZ data after scaling the former to match the latter. Uncertainties in the resulting dataset were the larger of i) the weighted average of the individual uncertainties in each pair of concentrations and ii) the difference between the two values, expressed as  $1\sigma$ . We argue that the difference between pair amounts to  $2\sigma$  and, therefore,  $1\sigma$  values were estimated at one of half of the difference. The resulting finalized observed concentration dataset used in the model runs are shown later in **Figure 14**.

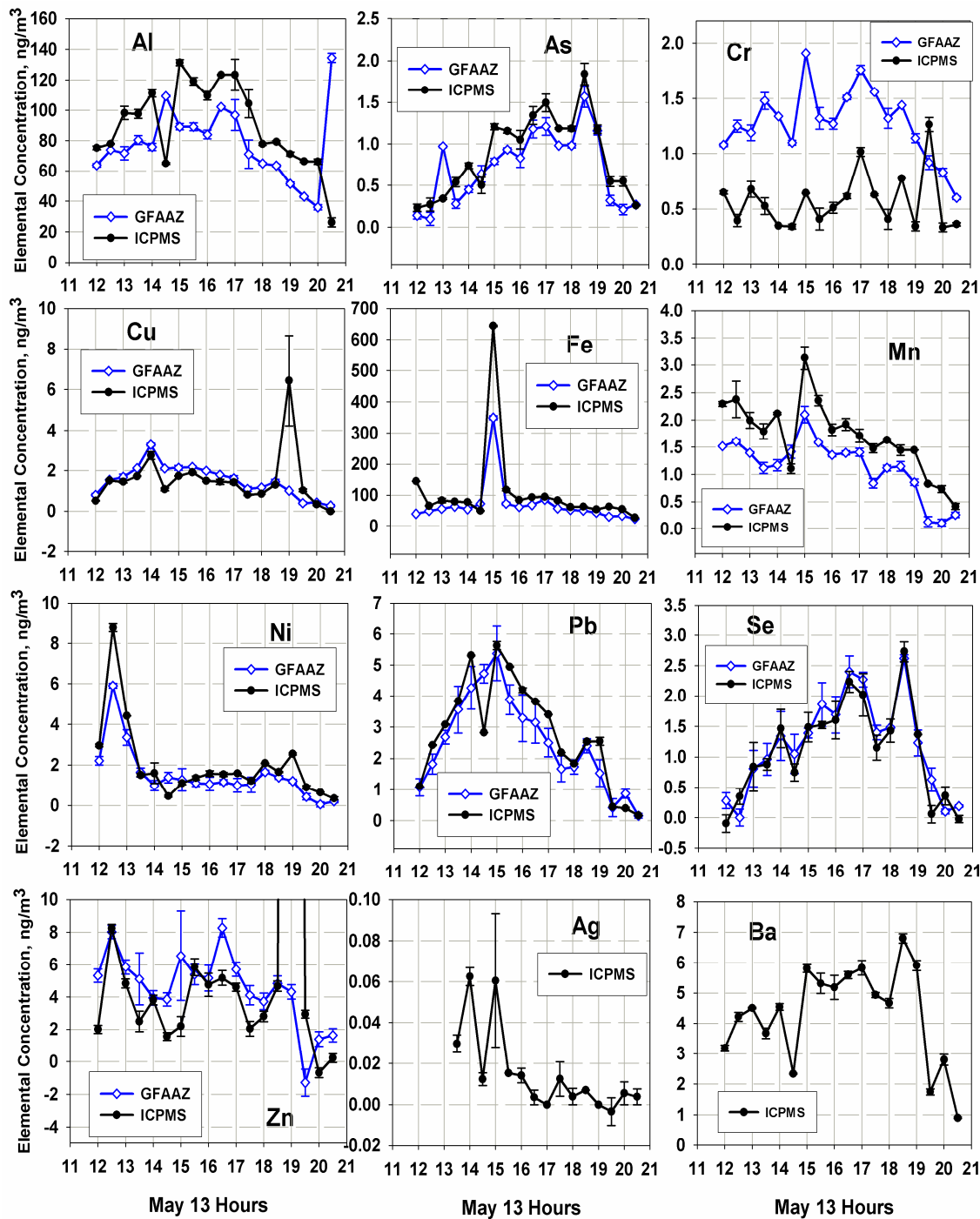


**Figure 13.** Concentration-vs.-time-of-day profiles for elements in ambient air samples by Graphite Furnace Atomic Absorption Spectroscopy (GFAAZ) (blue) and Inductively Coupled Plasma Mass Spectrometry (ICPMS). Concentration profiles for 11 additional elements determined with ICPMS are shown.

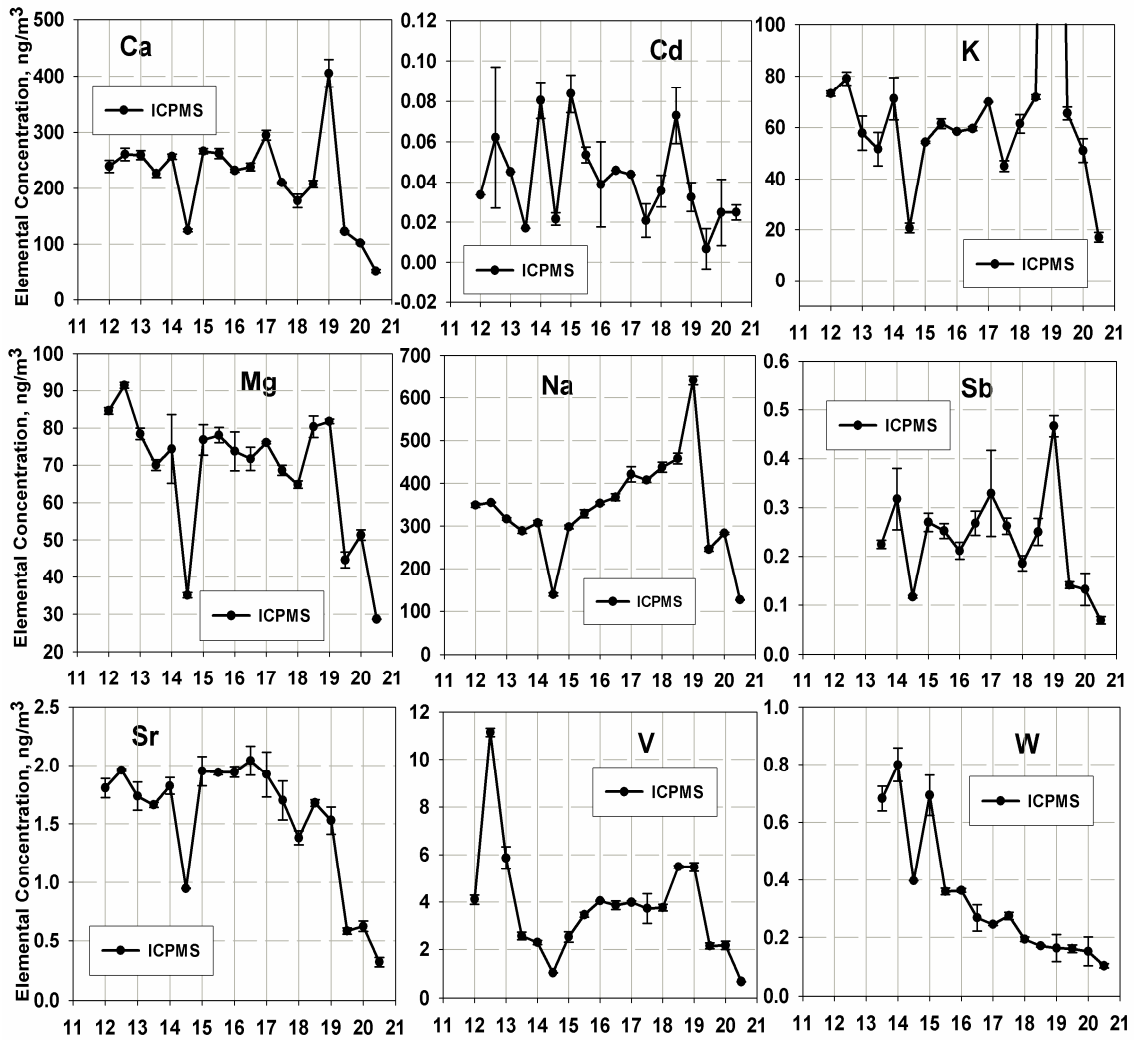


**Figure 13.** continued from previous page.

In addition, six discrepancies were identified and resolved as follows:

1. Cd was not well detected by GFAAZ, and was deemed unreliable by Park. The ICPMS was substantially more sensitive for Cd and produced results with much smaller uncertainties. Cd is not volatile or otherwise subject to losses upon storage. The ICPMS dataset was used.
2. A large excursion in Al appeared at 20:30 in the GFAAZ data set, but not in the ICPMS data set. Al is typically associated with large, difficult to dissolve alumina-silicate dust particles and generally better-measured by ICPMS coupled with our more aggressive sample preparation method. This excursion was ignored by Park, a decision which is now supported by the ICPMS data.
3. A sharp peak in As was detected at 13:00 in the GFAAZ data set, but not in the ICPMS data set. This peak was predicted to coincide with the period of influence of the plume from the Big Bend by Park, but not by the trajectory analysis method used herein. It is possible that As was lost during storage and in acidic solutions and that the peak was due to pressure treated lumber burning as described by Pancras et al., 2005. There is no known source to the Southwest of the site and such a source would be difficult to model. Therefore, the ICPMS data were used.
4. ICPMS results were low for all of the 14:30 samples. We attribute this to differences in efficiency of sample aspiration between GFAAZ and ICPMS analyses. In this case GFAAZ probably sampled one or more insoluble particles not aspirated by ICPMS.

As noted above, we have observed evidence of settling of larger particles in the ICPMS sample vials. This appears to have created dips most noticeably in Ag, Al, Ba,

Ca, Cd, K (not included in model run), Mg, Mn, Na, Pb, Sb, Sr, and W, and to a lesser extent in As, Cu, Ni, Se, V, and Zn. Inspection of **Figure 13** suggests that these “dips” appear artificial. Therefore, the ICPMS value at 14:30 was corrected to the GFAAZ value by interpolation of the surrounding data points at 14:00 and 15:00 in the latter and scaling them to the former.

5. A very large peak in Fe appears at 15:00 along with smaller but distinct peaks in Mn and Cr. Park attributed the Fe, but not Mn and Cr, to contamination and removed excess Fe from this peak. However, reanalysis with the ICPMS confirmed the same excursion at 15:00, in Fe, Cr, and Mn. Because elevated levels of all three elements occur at 14:30 and 15:30 directly before and after the excursion, it was deemed not likely to be isolated sample contamination. After correction of Fe, Cr, and Mn for background (based on the previous sampling interval), the composition was seen to correspond to low alloy steel. The fingerprint of the resulting composition ( $\text{Cr/Fe} = 0.009$ , and  $\text{Mn/Fe} = 0.007$ ) is consistent with the average composition ( $\text{Cr/Fe} = 0.008$ ;  $\text{Mn/Fe} = 0.008$ ) reported for an average of more than 1000 samples of low alloy steel (MatWeb, 2009). As described above, plumes from two large shipyards and a steel machining facility were predicted to influence the site during the 15:00 sampling period. All three sources perform sandblasting, welding, and machining of steel and are likely to be non-continuous regarding their emissions.

6. In the 19:00 sample, large excursions appear in the ICPMS data for Zn with Cu, and Cr, but are not present in the GFAAZ data for these elements. These were accompanied by substantial excursions in K, Ca, and Na, and to a lesser extent V, Sr, Ba, and possibly Sb, all elements not determined by GFAAZ. All values have large

uncertainties associated with them. The corresponding sample had little remaining volume when it was reanalyzed, and we attribute this behavior to the aspiration of one (or possibly a few), large, particle(s).

When ICPMS concentrations (ppb (mass/slurry volume)) are converted to  $\text{ng}/\text{m}^3$ , they are multiplied by the total volume of slurry collected. Thus, erroneously high concentrations will result if particles settle during storage or are trapped in the meniscus owing to surface tension (may be likely for contaminants), resulting in large apparent mass/volume concentrations when subsequent analyses are performed after the total volume is reduced by prior analyses. Also, of the elements measured, the major constituent is Zn ( $134 \text{ ng}/\text{m}^3$ ). The presence of such a large amount of Zn might normally be attributed to trash incinerators as these typically emit particles containing up to 20-50%  $\text{ZnCl}_2$  by mass (Ondov and Wexler, 1998). However, Zn in this form is quite soluble, and wouldn't have been missed by GFAAZ. For this reason, the GFAAZ data, after scaling to the adjacent ICPMS values as described above, was used.

### 3.2. Discussion of Modeling Results

The  $\chi/\text{Q}$  profiles are described in the section immediately below.  $\chi/\text{Q}^{\text{traj}}$  profiles are compared to the modeled  $\chi/\text{Q}^{\text{iPDRM}}$  profiles in **Figure 14**, to Park's  $\chi/\text{Q}^{\text{Met}}$  profiles in **Figure 15**, and to selected ambient species concentration profiles in **Figures 16a, b, c, and d**. The predicted species concentration profiles resolved by source are shown with the ambient observed concentration set determined as described in the Analytical Results section (3.1) in **Figure 17**. The fits between these data and the goodness-of-fit statistics (**Table 15**) are discussed in **section 3.2.2**, and the iPDRM predicted emission rates

(Table 17) are discussed in section 3.2.3. In section 3.2.4., the iPDRM predicted emission rates are compared with published NEI and TRI emission rates.

### 3.2.1. Source $\chi/Q$ profiles and Discussion

**Manatee.** As shown in Figure 14, the  $\chi/Q^{\text{traj}}$  profile for Manatee contains a single excursion that has already begun at 12:00, peaks at 12:30 ( $1.2 \cdot 10^{-8} \text{ s/m}^3$ ), and departs at 13:00. The  $\chi/Q^{\text{traj}}$  profile is only calculated from 500-m trajectories in which emissions from Manatee from 9:00-10:00 have an average transport velocity of 4.1 m/s for the trajectory predicted to reach the sampling site at 12:30. The 100-m  $\chi/Q$  profile was not used for the following reasons. The 100-m plume beginning at Manatee between 6:30-7:00 is predicted to influence Sydney at 13:00. The trajectories used for these  $\chi/Q$  values encompassed early morning wind velocities  $< 1.0 \text{ m/s}$ , i.e. for which the power law adjustment does not apply (Park, 2005). The early morning atmosphere was stable (Pasquill Stability class: E), thus downward mixing was limited at this time such that the trajectory did not carry a significant portion of the Manatee plume. By the time the atmosphere destabilizes at 7:30 (Pasquill stability class: C), the trajectories carry the plume too far to the South of Sydney to have any influence.

Figure 15 shows that Manatee  $\chi/Q^{\text{traj}}$  profile peaks (12:30) a half hour later than Park's  $\chi/Q^{\text{Met}}$  profile (12:00) which is in better agreement with ambient concentration profiles for Ni and V (Figure 16a) and explains the over-predictions at 12:00 and under-predictions at 12:30 made by Park for  $\text{SO}_2$ , Al, Cu, Fe, Ni, Pb, and Zn. The  $\chi/Q^{\text{iPDRM}}$  profile is relatively unchanged from the  $\chi/Q^{\text{traj}}$  profile (Figure 14), suggesting the GPM

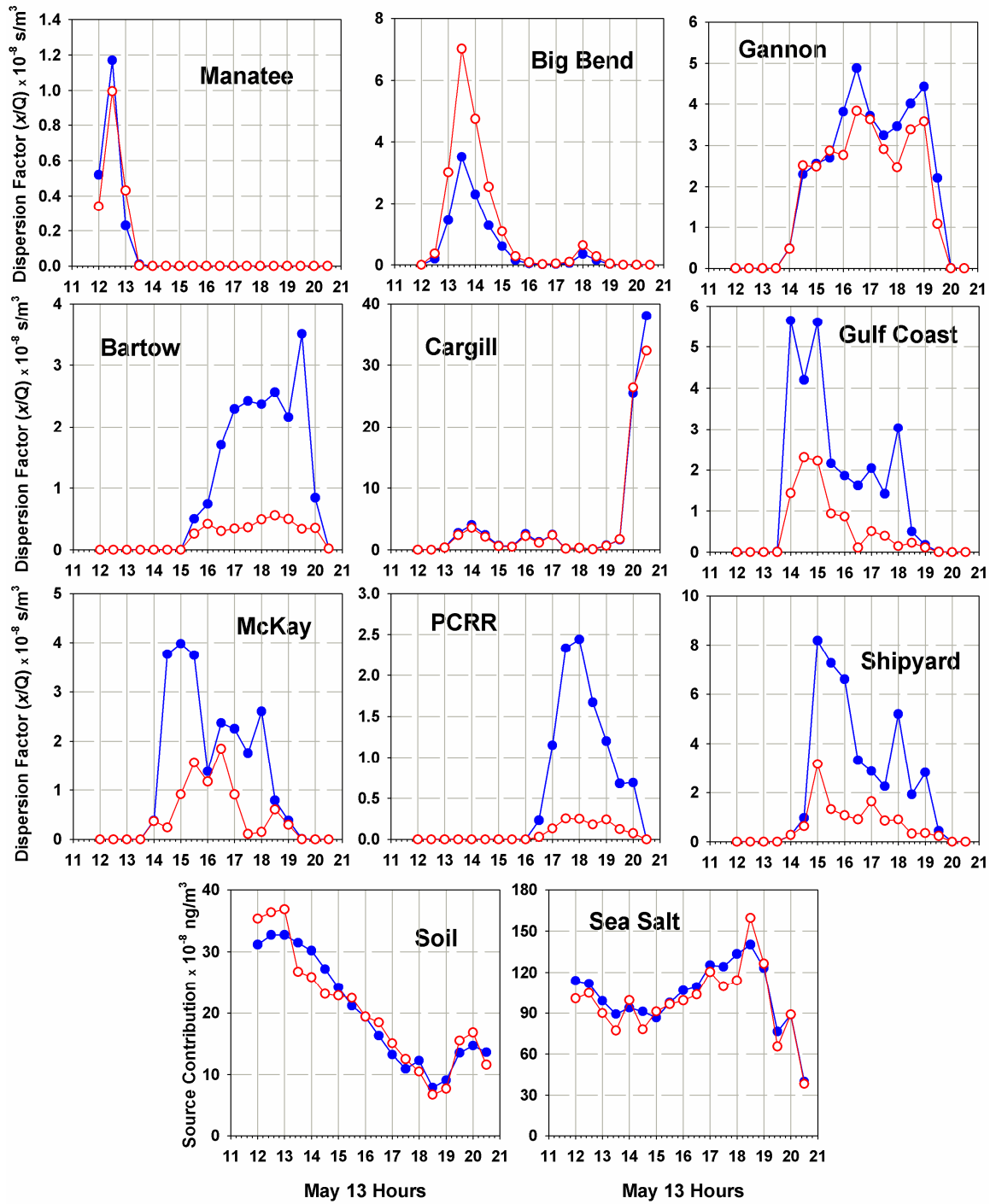


**Figure 14.** Comparison of  $\chi/Q^{iPDRM}$  profiles (red) and the input  $\chi/Q^{traj}$  profiles (blue). The  $\chi/Q^{iPDRM}$  profiles differ from the  $\chi/Q^{traj}$  profiles due to “conditioning” of the former with the “shapes” of tracer species concentration profiles.

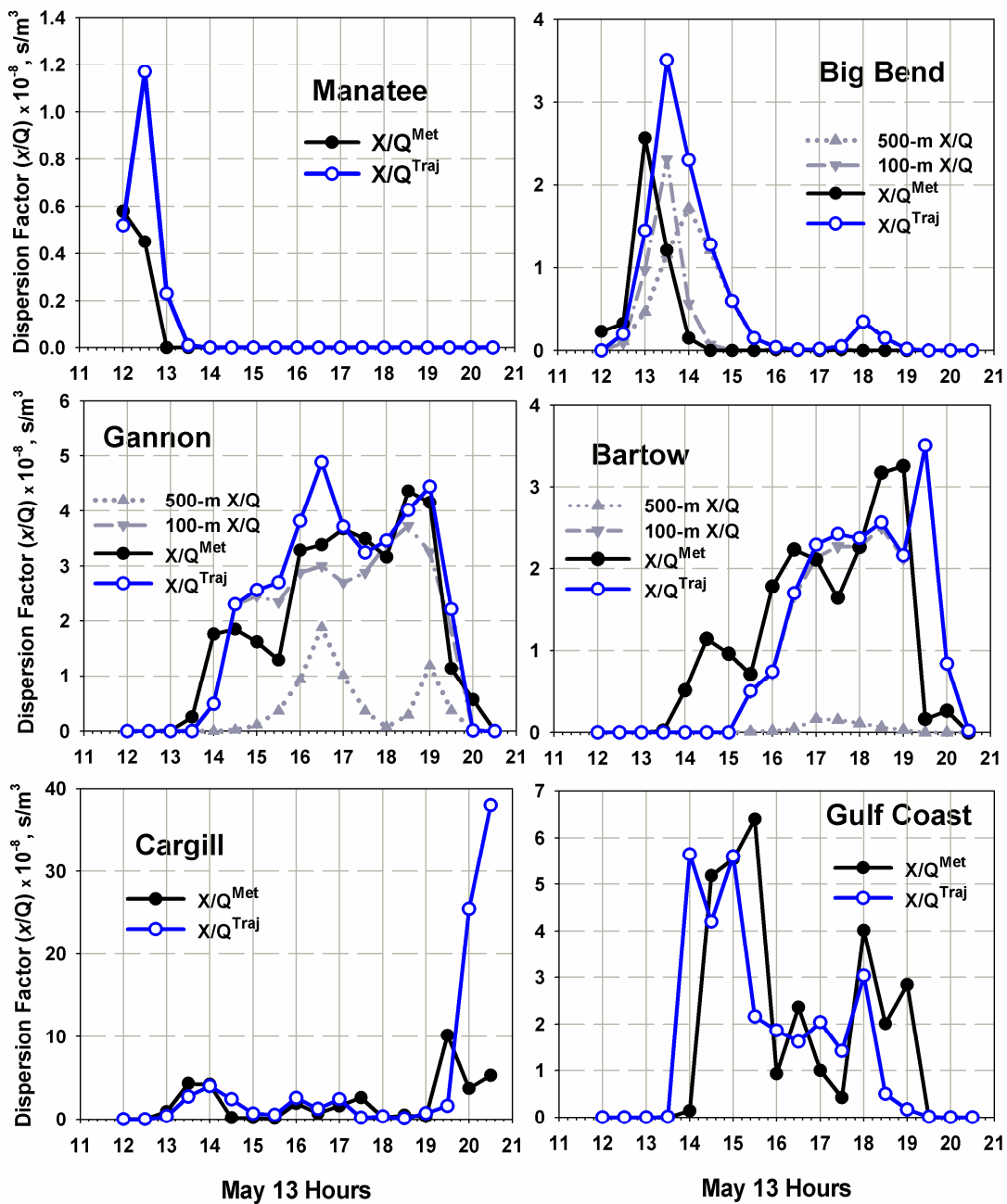


**Figure 15.**  $\chi/Q$ -vs.-time-of-day profiles as calculated by the Gaussian plume module by Park ( $\chi/Q^{\text{MET}}$ , black) and trajectory analysis ( $\chi/Q^{\text{traj}}$ , blue).  $\chi/Q$  profiles from 100- and 500-m used to calculate the  $\chi/Q^{\text{traj}}$  profiles for the power plants are shown in grey (The 500-m  $\chi/Q$  profile is the same as the  $\chi/Q^{\text{traj}}$  profile for Manatee).

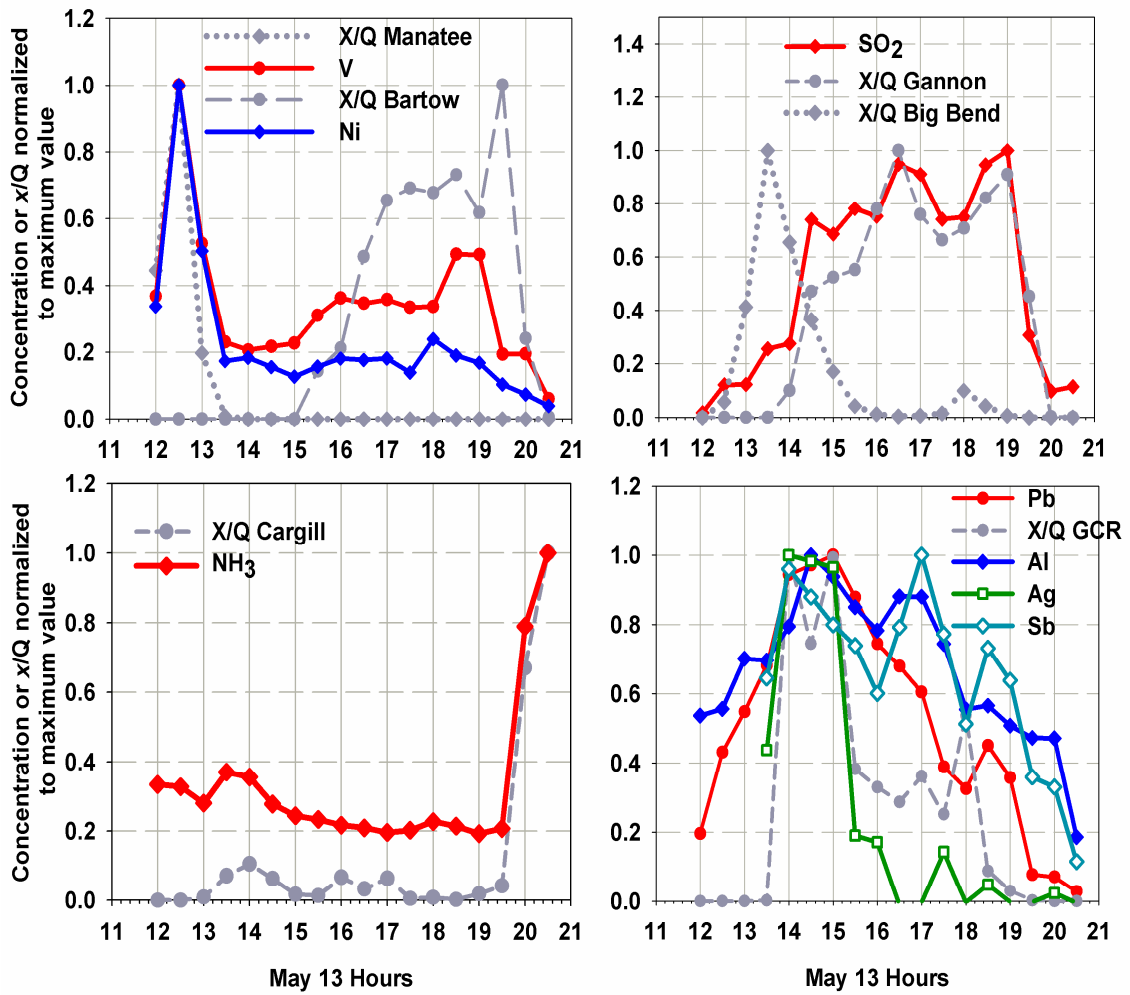


**Figure 16a, b, c, & d.** Concentration profiles of selected tracer species vs.  $\chi/Q^{\text{traj}}$  profiles. All datasets shown are normalized to their maximum values.

using trajectories was an accurate assessment. The magnitude of the  $\chi/Q^{iPDRM}$  at 12:30 is  $1 \cdot 10^{-8} \text{ s/m}^3$  is relatively unchanged from the  $\chi/Q^{traj}$  peak ( $1.2 \cdot 10^{-8} \text{ s/m}^3$ ). As expected, the magnitude of this value is smaller than those predicted for nearby sources (15-25km) and is consistent with the maximum  $\chi/Q^{iPDRM}$  values of Bartow and PCRR ( $0.6 \cdot 10^{-8}$  and  $0.2 \cdot 10^{-8} \text{ s/m}^3$ ), both of comparable distance (~40km) to Sydney.

**Big Bend.** Big Bend's  $\chi/Q^{traj}$  profile shows its plume arriving at 13:00, peaking at 13:30 ( $3.5 \cdot 10^{-8} \text{ s/m}^3$ ), and departing at 15:00. The  $\chi/Q^{traj}$  profile input into the iPDRM is the sum of 100-m and 500-m  $\chi/Q$  profiles. The 100-m  $\chi/Q$  profile predicted for Big Bend's plume shows its plume arriving at Sydney at 13:00 with a maximum influence there at 13:30. The estimated time of origin is from 10:00-11:00, and the average transport velocity was 2.5m/s. During this period, the atmosphere was unstable (Pasquill class: B) and the plume was expected to mix down into the 100-m layer. The 500-m profile for the Big Bend plume was predicted to arrive at 13:30 with a maximum influence at 14:00. The estimated time of origin and average transport velocity were 12:00 (~11:30-12:30) and 4.1m/s, respectively. The two profiles overlap considerably, such that the sum of both the 100m and 500m profiles peaks at 13:30. The contribution of the 500-m profile was 33% at 13:30 and 75% at 14:00.

The  $\chi/Q^{traj}$  profile for Big Bend also peaks (13:30) a half hour later than predicted by Park's  $\chi/Q^{Met}$  profile (13:00) (**Figure 15**). This difference in time correlates better with the ambient  $\text{SO}_2$  concentration profile (**Figure 16b.**), and addresses the under-predictions in Al, Cu, Fe, and Pb from 13:30-14:00 obtained with Park's model. The magnitude of the  $\chi/Q^{iPDRM}$  (**Figure 14**) at 13:30 is  $7 \cdot 10^{-8} \text{ s/m}^3$  which is increased by a factor of 2 from the  $\chi/Q^{traj}$  profile at this time.

**Gannon.** The  $\chi/Q^{\text{traj}}$  profile for Gannon predicts the plume arrival at 14:00, significant excursions at 14:30 ( $2.5 \cdot 10^{-8} \text{ s/m}^3$ ), 16:30 ( $5 \cdot 10^{-8} \text{ s/m}^3$ ), and 18:30-19:00 ( $4.5 \cdot 10^{-8} \text{ s/m}^3$ ), and departure at 20:00. This profile is the sum of 100-m and 500-m  $\chi/Q$  profiles. The 100-m  $\chi/Q$  profile predicts plume arrival at 14:00, a relative maximum at 14:30 which increases to another maxima at 16:30, and a main excursion between 18:30-19:00 before departure at 20:00. The average transport velocity is 2.7m/s and the estimated time of origin was from 11:00-17:30. The 500-m  $\chi/Q$  profile arrives at 15:30, has maximum influences at 16:30 and 19:00 with a relative minimum at 18:00, and departs at 20:00. The estimated period of origin for the 500-m plume is from 14:00-18:00 with an average transport velocity of 4.0m/s. At Sydney, the contribution of the 500-m trajectory  $\chi/Q$  value was 34% at 16:00; 48% at 16:30; 36% at 17:00; and 27% at 19:00.

The  $\chi/Q^{\text{traj}}$  profile for Gannon arrives (14:30) a half hour later than predicted by Park's  $\chi/Q^{\text{Met}}$  profile (14:00) along with significantly greater values (14-77%) from 14:30-16:30 (**Figure 15**). These differences correlate better with the ambient  $\text{SO}_2$  concentration profile as observed in **Figure 16b**. The  $\chi/Q^{\text{iPDRM}}$  profile (**Figure 14**) is similar in shape to the  $\chi/Q^{\text{traj}}$  profile, values from 16:00-16:30 and between 18:00-19:00 the iPDRM adjusted its values by factors from 0.8-0.95 in order to fit the  $\text{SO}_2$  profile better. The magnitude of the  $\chi/Q^{\text{iPDRM}}$  at its peak at 16:30 is  $4 \cdot 10^{-8} \text{ s/m}^3$ .

**Bartow.** The predicted  $\chi/Q^{\text{traj}}$  profile for Bartow arrives at 15:30, has a relative maximum from 17:00-19:00 ( $\sim 2.5 \cdot 10^{-8} \text{ s/m}^3$ ) which increases to a peak at 19:30 ( $3.5 \cdot 10^{-8} \text{ s/m}^3$ ) and departs at 20:30. This profile is the sum of 100-m and 500-m  $\chi/Q$  profiles; however, the magnitude of the 100-m  $\chi/Q$  is much greater than the 500-m  $\chi/Q$  profile and therefore has virtually the same shape as the summed  $\chi/Q^{\text{traj}}$  profile. The 100-m Bartow

plume influencing Sydney is estimated to have originated from 10:30-17:00 with an average transport velocity of 2.8m/s. The 500-m  $\chi/Q$  profile arrives at 15:30, has a maximum influence from 17:00-17:30 ( $0.003 \cdot 10^{-8} \text{ s/m}^3$ ), and departs at 20:00. The contribution of the 500-m  $\chi/Q$  value to the overall  $\chi/Q^{\text{traj}}$  was only 12% at 17:00 and 10% at 17:30, and for all other periods <7%.

The  $\chi/Q^{\text{traj}}$  profile begins an hour and a half later than Park's  $\chi/Q^{\text{Met}}$  profile predicted (**Figure 15**). Bartow (station angle:  $253^\circ$ ) is more significantly affected by the wind shift than Gannon (station angle:  $251^\circ$ ) because of its large source distance (38km). When the wind shift occurs at 12:30, westerly winds are sustained long enough to bring the plume from Gannon (20km distant) to Sydney by 14:30, however, the Bartow plume had a larger distance to cover and therefore a longer transport time and is not predicted to reach Sydney until 15:30. The  $\chi/Q^{\text{traj}}$  profile aligns much better with broad excursions in Ni and V from 15:30-20:00 (**Figure 16a.**). The  $\chi/Q^{\text{iPDRM}}$  (**Figure 14**) profile is ~0.1 times the magnitude of the  $\chi/Q^{\text{traj}}$  profile and its peak value of  $0.3 \cdot 10^{-8} \text{ s/m}^3$  occurs at 17:30. It is feasible that more dispersion than the GPM estimated occurred during the long plume transport during unstable conditions.

**Cargill.** Cargill's predicted  $\chi/Q^{\text{traj}}$  profile arrives at 13:00, peaks at 14:00 ( $5 \cdot 10^{-8} \text{ s/m}^3$ ), and departs at 14:30. Cargill's plume arrives again at 20:00 and has a maximum peak at 20:30 ( $39 \cdot 10^{-8} \text{ s/m}^3$ ). The profile is calculated from 100-m trajectories with estimated emission origins from 10:30-12:00 and 18:30-19:00, at average transport velocities of 2.6 and 2.9 m/s, respectively. At the end of the study period: 20:00-20:30, wind directions shift toward Cargill and its influence on conditions at Sydney are large,

possibly due in part to stabilizing atmospheric conditions and low effective plume heights.

Comparison of the  $\chi/Q^{\text{traj}}$  profile with Park's  $\chi/Q^{\text{Met}}$  profile (**Figure 15**) shows that both have a minor excursion from 13:30-14:00, but the  $\chi/Q^{\text{traj}}$  profile has only a large excursion from 20:00-20:30, and does not have the peak at 19:30 as Park's profile does. The agreement between the  $\chi/Q^{\text{traj}}$  profile and the ambient  $\text{NH}_3$  concentration profile supports the  $\chi/Q^{\text{traj}}$  values, as Cargill is reported to be a significant  $\text{NH}_3$  source. The  $\chi/Q^{\text{iPDRM}}$  and the  $\chi/Q^{\text{traj}}$  profiles are very similar (**Figure 14**).

**Gulf Coast.** The  $\chi/Q^{\text{traj}}$  profile for Gulf Coast arrives at 14:00, peaks from 14:00-15:00 ( $5 \cdot 10^{-8} \text{ s/m}^3$ ), peaks at 18:00 ( $3 \cdot 10^{-8} \text{ s/m}^3$ ), and departs at 19:00. The profile is calculated from 100-m trajectories with estimated emission origins from 12:00-18:00, and an average transport velocity of 2.8 m/s.

The  $\chi/Q^{\text{traj}}$  profile predicts that the Gulf Coast plume arrives a half hour earlier than Park's  $\chi/Q^{\text{Met}}$  profile (**Figure 15**). As shown in **Figure 16d**, this earlier arrival time correlates better with the ambient concentration profiles for Ag, Al, Pb, and Sb, all of which Gulf Coast is reported to emit (see Tampa sources section). This shift, in conjunction with the  $\chi/Q^{\text{traj}}$  profile shifts for Big Bend and Gannon, help to address the under-predictions in Al, Cu, Fe, and Pb from 13:30-14:00 obtained with Park's model.

The magnitude of the  $\chi/Q^{\text{iPDRM}}$  profile ( $2.4 \cdot 10^{-8} \text{ s/m}^3$ ) is ~2-3 times less than the  $\chi/Q^{\text{traj}}$  profile for all values (**Figure 14**), and the  $\chi/Q^{\text{traj}}$  profile peak at 18:00 is not present in the  $\chi/Q^{\text{iPDRM}}$  profile. We can conclude from the species concentration data that if Gulf Coast was responsible for Ag, Al, Pb, and Sb concentrations from 14:00-15:00, then it is not

influencing Sydney at 18:00 despite what is predicted in the  $\chi/Q^{\text{traj}}$  profile. This is either due to an error in the wind trajectory or a change in the emission rate from this source.

The “conditioned” changes in the  $\chi/Q^{\text{iPDRM}}$  profile shape take this conclusion into account and are primarily dependent on the shape of the ambient Pb and Zn concentration profiles, as Pb was apportioned to this plant and Zn was not. The ratios of these two elements were used to deconvolute Gulf Coast from the incinerators as described in the Second iteration.

Thus, the “conditioning” of the  $\chi/Q^{\text{iPDRM}}$  profiles prevented the large over-predictions seen in Park’s model (i.e. over-predictions at 18:00 and 19:00 for Al, Cu, Fe, and Pb).

**McKay.** The  $\chi/Q^{\text{traj}}$  profile for McKay arrives at 14:00, peaks from 14:30-15:30 ( $\sim 4 \cdot 10^{-8} \text{ s/m}^3$ ), has peaks at 16:30 ( $2.2 \cdot 10^{-8} \text{ s/m}^3$ ) and 18:00 ( $2.5 \cdot 10^{-6} \text{ s/m}^3$ ), and departs at 19:30. The profile is calculated from 100-m trajectories with estimated emission origins from 12:00 to 18:00, with an average transport velocity is 2.8 m/s.

The  $\chi/Q^{\text{iPDRM}}$  profile for McKay predicts the plume to arrive at 14:00, but does not peak until 15:30, the maximum peak occurs at 16:30 ( $2 \cdot 10^{-8} \text{ s/m}^3$ ), with a secondary peak at 18:30 (**Figure 14**). As was the case with Gulf Coast, changes made by the iPDRM to the input  $\chi/Q^{\text{traj}}$  profile were most dependent on the shape of the ambient Pb and Zn concentration profiles, as both elements are apportioned to this source. The inclusion of the incinerators, McKay and PCRR, improved the significant residuals in Zn observed for Park’s results.

**PCRR.** The  $\chi/Q^{\text{traj}}$  profile for PCRR arrives at 16:30, peaks from 17:30-18:00 ( $2.4 \cdot 10^{-8} \text{ s/m}^3$ ), and departs at 20:30 (**Figure 14**). The profile is calculated from 100-m

trajectories with estimated emission origins from 11:00 to 16:30, with an average transport velocity is 2.8 m/s.

As observed in Bartow (also ~40 km from Sydney), the  $\chi/Q^{\text{iPDRM}}$  profile was ~0.1 times the input  $\chi/Q^{\text{traj}}$  profile which is attributed to the long plume transport distance during unstable atmospheric conditions. The  $\chi/Q^{\text{iPDRM}}$  profile peaks at 17:30-18:00 ( $0.25 \cdot 10^{-8} \text{ s/m}^3$ ).

**Shipyard.** The predicted  $\chi/Q^{\text{traj}}$  profile for the Shipyard arrives at 14:30, peaks at 15:00 ( $8 \cdot 10^{-8} \text{ s/m}^3$ ), has relative peaks at 18:00 and 19:00, and departs at 20:00 (**Figure 14**). The profile is calculated from 100-m trajectories with estimated emission origins from 12:00-18:00, with an average transport velocity of 2.8 m/s.

The shipyard is likely an intermittent source and potential plumes from this location are likely to influence Sydney at 15:00 when peaks in Cr, Fe, and Mn concentrations are observed. The magnitude of the  $\chi/Q^{\text{iPDRM}}$  profile is ~2-4 times less than the input  $\chi/Q^{\text{traj}}$  profile and the resulting peaks at 15:00 ( $3.2 \cdot 10^{-8} \text{ s/m}^3$ ) and 17:00 are conditioned as the result of ambient Fe, and to a lesser extent, Cr and Mn concentration profiles.

**Background Soil.** The input SCE profile for soil peaks from 12:30-13:00 ( $3.3 \cdot 10^{-8} \text{ g/m}^3$ ) then decreases throughout the study period and has a relative peak from 19:30-20:00. The SCE profile was only allowed to vary from 0.8-1.2 times its input value in the iPDRM, thus the shape of the output SCE is similar, with a maximum value at 13:00 ( $3.7 \cdot 10^{-8} \text{ s/m}^3$ ) (**Figure 14**). The changes that occur are dependent on the Al, Ca, and Fe concentration profiles as they are the most abundant species.

**Sea Salt.** The input SCE profile for sea salt closely resembles the ambient Na concentration profile. Na is by far the most abundant species (excluding anions of  $\text{Cl}^-$ ,

and  $\text{SO}_4^{2-}$ ) in sea salt and sea salt is typically responsible for nearly all of the airborne Na in the Tampa Bay area (Poor, private communication) The profile begins the study period (12:00) at  $\sim 120 \cdot 10^{-8} \text{ g/m}^3$ , dips from 13:00- 16:30, peaks at  $140 \cdot 10^{-8} \text{ g/m}^3$  at 19:00, then sharply decreases, with a relative peak at 20:30, before its lowest value of  $30 \cdot 10^{-8} \text{ g/m}^3$  at the end of the study period (**Figure 14**). As was the case with the soil source, the input SCE values were only allowed to vary from 0.8-1.2 times their input values, thus the modeled output SCE profile only differs with a couple of minor peaks at 12:30, 14:00, and 17:00, and a sharpened maximum peak at 19:00 ( $160 \cdot 10^{-8} \text{ g/m}^3$ ).

**Tampa Armature Works.** The observed Cu profile has excursions at 14:00 and 15:30 of which are not consistent with any other species concentration profile. Tampa Armature Works is reported to operate a Cu reclamation incinerator and its  $\chi/Q^{\text{traj}}$  profile has peaks at 14:00-15:00, that could account for the observed excursions. However, outside of expecting that Cu is abundant in emissions from a Cu reclamation incinerator, no other information could be found on this source or generic source type and it was decided to exclude it from the model.

As a result of the changes in the shapes of the  $\chi/Q^{\text{traj}}$  profiles and conditioned  $\chi/Q^{\text{iPDRM}}$  profiles, the iPDRM predicted a major reappportionment of  $\text{SO}_2$ . The times of  $\chi/Q^{\text{traj}}$  profile peaks for Manatee, Big Bend, Gannon, and Cargill correlate to peaks observed in the observed  $\text{SO}_2$  profile. The  $\text{SO}_2$  concentration of 0.7 ppb at 12:00 increases to 5 ppb at 12:30 (Manatee  $\chi/Q$  peak), then to 10.6 ppb at 13:30 (Big Bend  $\chi/Q$  peak), to a substantial increase to 30.9 ppb at 14:30 which fluctuates from 29 - 41ppb until 19:00 before decreasing at 19:30 to 13 ppb (Gannon  $\chi/Q$  peak). From 20:00-20:30, the  $\text{SO}_2$  concentration increases slightly from 4.0 to 4.6 ppb (Cargill  $\chi/Q$  peak).

As shown in **Table 15**, Park predicted significant SO<sub>2</sub> residuals from 13:00-14:00: +32%, -35%, +44%, respectively. Our predicted SO<sub>2</sub> residuals showed substantial improvement for that period: +13%, -11%, and +6%. Because of the half hour delay in Gannon's  $\chi/Q^{\text{traj}}$  profile, the majority of the observed SO<sub>2</sub> is apportioned to Gannon (83-99% from 14:30-19:30) in our model. Park had apportioned 50-59% of observed SO<sub>2</sub> to Gulf Coast and 31-47% to Gannon from 14:30-15:30. Our model apportions 1-2% of SO<sub>2</sub> to Gulf Coast and 83-90% to Gannon at this time. This is a substantial reapportioning of SO<sub>2</sub>. This is a reasonable result as Gannon is the largest SO<sub>2</sub> emitter in the region and has reported SO<sub>2</sub> emission rates over 150 times those reported for Gulf Coast.

Regarding the differences between the  $\chi/Q^{\text{traj}}$  profiles and the  $\chi/Q^{\text{iPDRM}}$  profiles, it appears that those for Manatee, Gannon, and Cargill are the most similar. The profile shape for Big Bend does not change but it is increased by a factor of 2. We expect that aloft sources with high effective heights (~400-1200 m) would be more likely to disperse in a Gaussian manner and would thus, be more accurately modeled with the GPM.

Sources with shorter stacks, excepting Cargill, showed significant differences between their  $\chi/Q^{\text{traj}}$  and the  $\chi/Q^{\text{iPDRM}}$  profiles. We hypothesize that because these emit closer to the ground (effective heights from 50-150 m) are closer to dispersive surface roughness elements.

This is likely to accelerate dispersion and larger  $\sigma_y$  and  $\sigma_z$  values have been reported for plumes in urban environments, i.e., with larger surface roughness elements than in rural settings (McElroy & Pooler, 1968; McElroy, 1969; Shum, Loveland, & Hewson, 1975).

**Table 15.** Fraction of predicted SO<sub>2</sub> to ambient SO<sub>2</sub> concentrations apportioned to Big Bend, Gannon, and Gulf Coast (%) from 13:00-15:30.

	Park				This Work			
	Total Pred.	Big Bend	Gannon	GCR	Total Pred.	Big Bend	Gannon	GCR
<b>13:00</b>	132	122	1	0	113	77	0	0
<b>13:30</b>	65	28	18	0	89	86	0	0
<b>14:00</b>	144	3	119	4	106	54	42	4
<b>14:30</b>	99	0	47	50	100	11	83	2
<b>15:00</b>	104	0	44	58	100	5	89	2
<b>15:30</b>	91	0	31	59	98	1	90	1

The fact that sources with shorter or no stacks are also less likely to have continuous emissions, especially those with processes such as sandblasting or welding, is likely to create differences between  $\chi/Q^{\text{traj}}$  and the  $\chi/Q^{\text{iPDRM}}$  profiles. The GPM calculates the  $\chi/Q^{\text{traj}}$  on the assumption that the source is emitting at a constant rate, and if this is not the case, then the  $\chi/Q^{\text{traj}}$  profile will be incorrect and not correlate with observed concentration profiles. In adapting the iPDRM to constrain chemical compositional information, we can address this scenario and we conclude that our predicted  $\chi/Q^{\text{iPDRM}}$  profiles are a more accurate estimate of actual plume influence.

### 3.2.2. Predicted vs. Observed Fits

iPDRM predicted concentrations are shown with the ambient species concentration profiles in **Figure 17**. The fits obtained with the iPDRM are visibly improved from Park's fits and correct all of the significant under- and over-predictions described in section 1.1.2. Reasons for the improved fits are: 1) the improved determination of  $\chi/Q^{\text{traj}}$  profiles, 2) the conditioning of  $\chi/Q^{\text{traj}}$  profiles with chemical compositional information, 3) and the increased number of sources (6 to 11). The emission rate constraints used in the iPDRM, however, were much more restrictive than those used in Park and contribute to the residuals observed in this work.

Statistical measures of the iPDRM fits and model performance are shown in **Table 16** and are compared to Park's published results. The statistical analysis tools used are the same as used in Park's study and the equations are defined in **Table 17**.

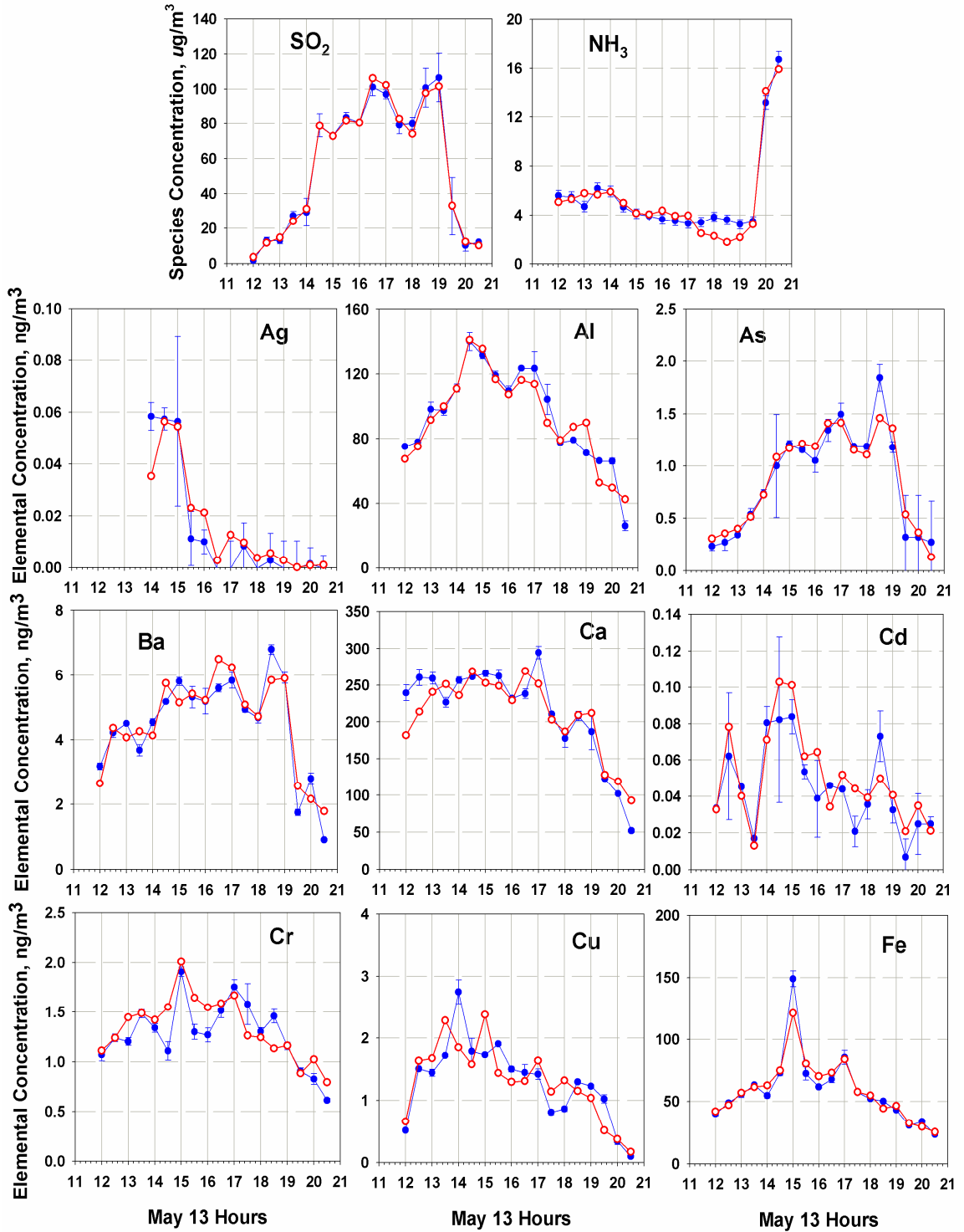


**Figure 17.** Observed concentration-vs.-time-of-day profiles (hybrid dataset; blue) for species used in iPDRM compared with iPDRM predicted concentration versus time profiles (red).

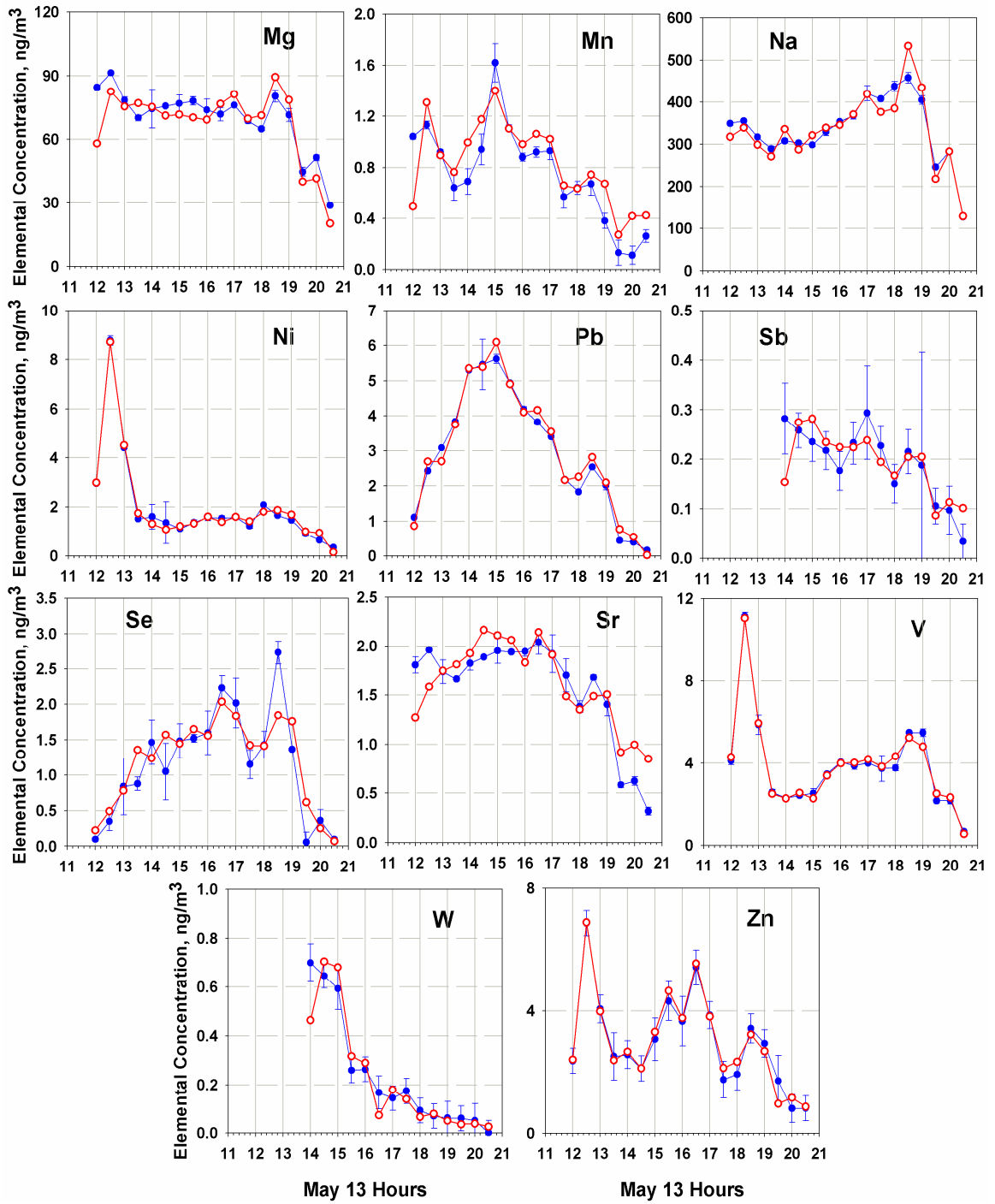


Figure 17. continued from the previous page.

**Table 16.** Performance statistics for predicted concentrations of SO<sub>2</sub>, NH<sub>3</sub>, and elements. Performance statistics published by Park are compared where available.

	Units	SO <sub>2</sub> <sup>b</sup>		NH <sub>3</sub> <sup>b</sup>		Ag		Al		As		Ba		Ca		Cd		Cr		Cu		Fe	
		This Work	Park Work	This Work	Park Work	This Work	Park Work	This Work	Park Work	This Work	Park Work	This Work	Park Work	This Work	Park Work	This Work	Park Work	This Work	Park Work	This Work	Park Work	This Work	Park Work
Observed (avg)	ng/m <sup>3</sup>	56.7	57.2	5.46	0.01	94.3	47.1	0.87	0.78	4.49	214	0.045	1.28	1.15	1.30	1.28	59.1	47.6					
Predicted (avg)	ng/m <sup>3</sup>	56.6	57.3	5.28	0.01	92.5	49.8	0.88	0.77	4.55	211	0.050	1.35	1.12	1.30	1.16	59.2	49.9					
Ratio (avg)	-	1.06	1.00	0.95	-	1.01	1.22	1.06	1.02	1.07	1.03	1.25	1.07	1.01	1.08	1.04	1.02	0.95					
MB	ng/m <sup>3</sup>	0.03	-0.08	0.18	-0.001	1.75	-2.62	-0.01	0.01	-0.06	3.36	-0.005	-0.07	0.03	-0.004	0.120	-0.12	-2.28					
MNB	%	-5.8	-6.5	5.0	888	-0.5	-22.4	-6.1	-2.1	-6.7	-3.3	-25	-7.2	-1.0	-8.3	-4.4	-1.9	-10					
MFB	%	-3.5	-2.7	7.6	-62	1.0	-12.6	-3.3	-0.6	-3.9	-1.5	-14	-5.7	2.0	-3.5	3.5	-1.5	-5.4					
MAGE	ng/m <sup>3</sup>	0.7	4.7	0.004	7.5	0.1	11.7	0.5	0.1	21.4	0.01	0.16	0.31	0.24	4.9	0.33	7.0	10.1					
MNGE	%	12	18	16	924	11	37	17	15	16	13	38	13	21	27	30	7.5	25					
RMSE	ng/m <sup>3</sup>	3.0	6.2	0.8	0.01	9.6	14.8	0.1	0.12	0.56	26.7	0.01	0.2	0.29	0.4	0.53	7.8	12.7					
NMSE	%	0.2	0.9	1.6	11.3	1.0	8.4	1.8	2.0	1.4	1.5	7.2	2.4	6.2	7.5	18	1.5	6.4					
Fa2	%	94	94	100	33	100	83	100	100	100	100	89	100	100	100	93	100	94					
CC (R <sup>2</sup> )	-	1.00	0.98	0.98	0.94	0.94	0.73	0.96	0.96	0.93	0.91	0.86	0.79	0.52	0.80	0.51	0.96	0.65					

	Units	Mg		Mn		Na		Ni		Pb		Sb		Se		V		W		Zn	
		This Work	Park Work																		
Observed (avg)	ng/m <sup>3</sup>	70.0	0.75	0.82	336	2.01	1.23	2.93	2.64	0.15	1.15	0.84	3.87	0.19	3.02	3.56					
Predicted (avg)	ng/m <sup>3</sup>	67.7	0.83	0.82	333	2.02	1.09	3.01	2.39	0.15	1.20	0.76	3.88	0.18	3.05	3.32					
Ratio (avg)	-	0.96	1.35	1.07	0.99	1.01	0.99	1.03	1.00	1.14	1.66	0.96	1.00	0.90	1.03	0.99					
MB	ng/m <sup>3</sup>	2.35	-0.08	0	2.92	-0.01	0.13	-0.08	0.25	0.001	-0.05	0.08	-0.01	0.009	-0.039	0.25					
MNB	%	4.2	-35	-3.3	1.1	-0.6	1.1	-3.1	-0.3	-10.7	-66	3.3	-0.4	7	-2.9	0.5					
MFB	%	5.2	-19	0.0	1.3	1.7	7.5	2.4	9.0	-3.7	-14	5.1	-0.04	10.5	-1.5	7.0					
MAGE	ng/m <sup>3</sup>	0.2	21.8	0.16	0.16	0.2	0.47	0.03	0.82	0.24	0.2	0.1	0.04	0.2	0	1.1					
MNGE	%	10.6	42	21	6.2	14.1	28	17	28	22	81	13	6	18	10	32					
RMSE	ng/m <sup>3</sup>	8.8	0.2	0.2	28.7	0.2	0.9	0.2	1.1	0.04	0.3	0.2	0.3	0.1	0.3	1.3					
NMSE	%	1.56	6.3	5.0	0.7	0.5	35.6	0.5	16	5.6	6.3	5.8	0.3	5.9	0.6	12.7					
Fa2	%	100	89	100	100	100	93	100	93	72	89	100	100	72	100	100					
CC (R <sup>2</sup> )	-	0.87	0.85	0.82	0.94	1.00	0.72	0.99	0.61	0.91	0.90	0.94	0.99	0.95	0.98	0.51					

**Table 17.** Equations for the calculation of performance statistics shown in Table 16.

$$MB = \left(\frac{1}{N}\right) \sum_{i=1}^N (O_i - P_i) \quad MNB = \left(\frac{1}{N}\right) \sum_{i=1}^N \left(\frac{(O_i - P_i)}{O_i}\right)$$

$$MFB = \left(\frac{2}{N}\right) \sum_{i=1}^N \left(\frac{(O_i - P_i)}{(O_i + P_i)}\right)$$

$$MAGE = \left(\frac{1}{N}\right) \sum_{i=1}^N |O_i - P_i| \quad MNGE = \left(\frac{1}{N}\right) \sum_{i=1}^N \left(\frac{|O_i - P_i|}{O_i}\right)$$

$$RMSE = \left[ \left(\frac{1}{N}\right) \sum_{i=1}^N (O_i - P_i)^2 \right]^{\frac{1}{2}} \quad NMSE = \frac{\left[ \left(\frac{1}{N}\right) \sum_{i=1}^N (O_i - P_i)^2 \right]}{\left[ \left(\frac{1}{N}\right) \sum_{i=1}^N (O_i P_i)^2 \right]}$$

Fa2 = fractions of the predictions within a factor of 2 of the observed values

CC = Coefficient of Correlation ( $R^2$ )

These include measures of fit that identify bias: Mean Bias (MB), Mean Normalized Bias (MNB), and Mean Fractional Bias (MFB), and tests that measure the overall fit and consider the absolute residual or the square of the residual including: Mean Absolute Gross Error (MAGE), Mean Normalized Gross Error (MNGE), Root Mean Square Error (RMSE), and Normalized Mean Square Error (NMSE). All “Normalized” terms are divided by their observed value. The fraction of predictions within a factor of 2 of the observed concentration value (Fa2) is reported in addition to the Correlation Coefficient (CC). According to Kumar et al. [1993], model performance is deemed acceptable if  $NMSE \leq 0.5$  (50%),  $-0.5 \leq MFB \leq 0.5$ , and  $Fa2 \geq 0.8$  (80%).

The bias test measures whether the residuals have a preference to be negative (over-prediction in Park’s orientation) or positive (under-prediction). Results for MFB are  $\leq \pm 8\%$  for SO<sub>2</sub>, NH<sub>3</sub>, Al, As, Ba, Ca, Cr, Cu, Fe, Mg, Na, Ni, Pb, Sb, V, W, and Zn. Species that show significant bias include: Ag (90%), Cd (-14%), Mn (-19%), and Se (-14%). Only Ag exceeded Kumar’s criteria for acceptability.

This is a considerable improvement on Park’s results in that our model outperformed Park’s for every element, except As and Se. These elements are subject to high uncertainties and Park removed several outliers from this dataset including As at 13:30 and Se at 18:30. In particular, the predicted Se value at 19:30 contributes to large values for MNB and MNGE, both of which are highly sensitive to differences in small observed concentrations.

Analysis of the NMSE (measures the overall fit) values suggest very good iPDRM fits. These are  $< 2.5\%$  for SO<sub>2</sub>, NH<sub>3</sub>, Al, As, Ba, Ca, Cr, Fe, Mg, Na, Ni, Pb, V, and Zn; and are under 8% for all other species, except for Ag (11%). All iPDRM NMSE values

except those for Mn and Se are improved from Park's results and those are not significantly worse, +1.3% and +0.5%, respectively. Values for Al, Cu, Ni, Pb, and Zn improved by 7-35%. Of Park's results, only NMSEs for SO<sub>2</sub> and As are <2.5%; Al, Cu, Mn, and Se are within 10% and Cu, Fe, and Pb range from 13-36%. By these criteria, our results are considerably improved in comparison to Park's.

Average ratios of predicted to observed elements were within 10% of unity for all elements considered except Cd, Mn, Sb, and Se (1.25, 1.35, 1.14, and 1.66). Cadmium and Se suffer from a single large residual at 19:30, which if removed, improves the ratios of these elements (1.14, 1.12, respectively).

Correlation Coefficients for SO<sub>2</sub>, NH<sub>3</sub>, As, Fe, Ni, Pb, V, W, and Zn are > 0.95; for Ag, Al, Ba, Ca, Na, Sb, and Se > 0.90; for Cd, Mg, and Mn >0.85; only Cu (0.80) and Cr (0.79) are <0.85. Park's CC are substantially smaller: SO<sub>2</sub>, As, and Se are > 0.94; Mn, Ni, and Al are >0.70; Fe and Pb are >0.60; and Cr, Cu, and Zn are >0.50.

### 3.2.3. Emission Rates

iPDRM predicted average emission rates are shown in **Table 18**. As described, emission rates were primarily constrained on the basis of elemental ratios observed in literature source profiles, and preliminary PDRM results. Thus, the emission rate ratios of species are in good agreement with the literature source profiles. **Figure 18** shows the abundance profiles reported in the literature sources, and those derived from emission rates predicted with the iPDRM and with Park's PDRM. In general, iPDRM derived emission rates better agree with NEI-TRI data. The effects on emission rates for individual sources owing to our changes to the iPDRM are analyzed below.

**Table 18.** Predicted emission rates (g/s) for SO<sub>2</sub>, NH<sub>3</sub>, and elements.

	Manatee	Big Bend	Gannon	Bartow	Cargill	GCR	McKay	PCRR	Ship yard	Soil*	Sea Salt
<b>SO<sub>2</sub></b>	1064	333	2668	1151	31	113	2	7	3	NS	NS
<b>NH<sub>3</sub></b>	5	11	19	17	44	0.1	0.1	0.8	NS	14.3	NS
<b>Ag</b>	-	-	NS	NS	NS	0.002	NS	NS	NS	NS	NS
<b>Al</b>	0.50	0.69	1.97	0.20	0.06	1.19	0.04	0.04	0.27	0.18	0.001
<b>As</b>	0.003	0.004	0.02	0.02	NS	0.007	0.008	0.014	0.003	NS	NS
<b>Ba</b>	0.23	0.039	0.13	0.046	0.004	0.0022	0.0002	0.002	NS	0.0041	0.0004
<b>Ca</b>	3.14	1.69	4.25	0.17	0.11	0.005	0.15	0.12	0.35	0.43	0.02
<b>Cd</b>	0.007	0.0001	0.0001	0.003	0.0001	0.004	0.0003	0.001	NS	NS	NS
<b>Cr</b>	0.010	0.009	0.017	0.044	0.001	0.0001	NS	0.001	0.024	0.003	NS
<b>Cu</b>	0.13	0.03	0.01	0.042	0.0003	0.001	0.005	0.001	0.05	0.0002	0.0001
<b>Fe</b>	0.34	0.42	0.82	0.07	0.04	0.12	0.05	0.03	2.09	0.12	NS
<b>Mg</b>	3.16	0.58	0.80	0.92	0.009	0.005	0.012	0.014	0.19	0.04	0.03
<b>Mn</b>	0.119	0.010	0.012	0.012	0.001	0.0191	0.02	0.02	0.010	0.0002	NS
<b>Na</b>	1.08	0.44	1.35	0.069	0.031	NS	0.008	0.12	0.031	0.023	0.31
<b>Ni</b>	0.86	0.024	0.01	0.24	0.0003	0.001	0.001	NS	0.019	0.0001	NS
<b>Pb</b>	0.25	0.053	0.01	0.10	NS	0.15	0.18	0.28	0.016	NS	NS
<b>Sb</b>	-	-	0.004	0.004	0.0003	0.007	0.003	0.015	NS	0.0001	NS
<b>Se</b>	0.03	0.018	0.04	0.04	0.0001	0.001	0.019	0.010	NS	NS	NS
<b>Sr</b>	0.04	0.013	0.03	0.001	0.0015	0.014	0.025	0.079	0.0004	0.003	NS
<b>V</b>	1.02	0.026	0.05	0.43	0.0005	NS	0.001	0.0004	0.001	0.0005	NS
<b>W</b>	-	-	NS	0.0001	NS	0.028	NS	NS	NS	0.0002	NS
<b>Zn</b>	0.67	0.032	0.02	0.05	0.0025	0.0002	0.23	0.36	0.006	0.0004	NS

NS - not significant (< 0.0001 g/s); \* - Contains Background NH<sub>3</sub>

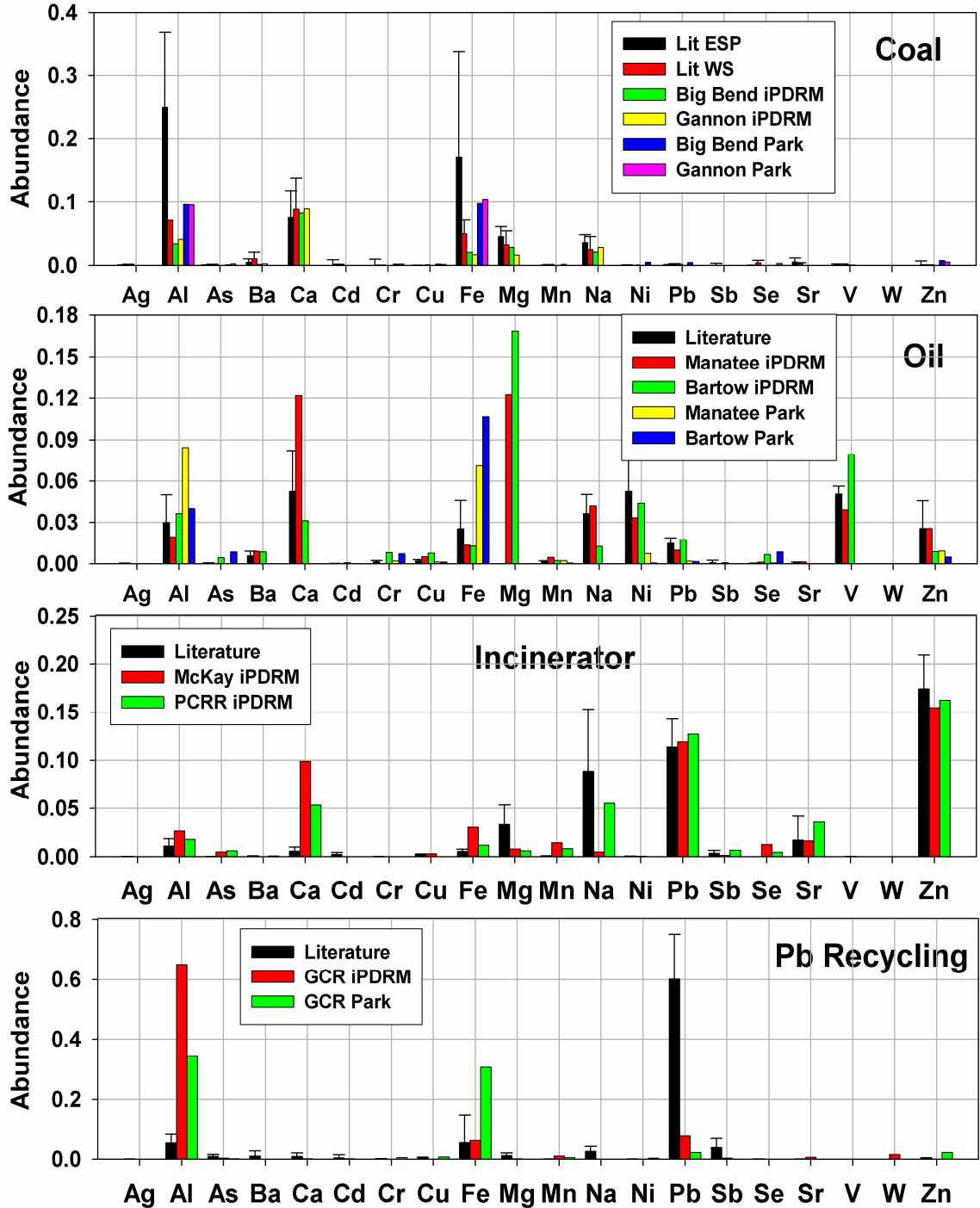


**Figure 18.** Reported CMB Abundance profiles (g element / g Total PM<sub>2.5</sub> mass; SPECIATE) categorized by source type and compared with predicted emission rate profiles from iPDRM and Park's model (note: Mg was not reported in literature for the Oil-fired source).

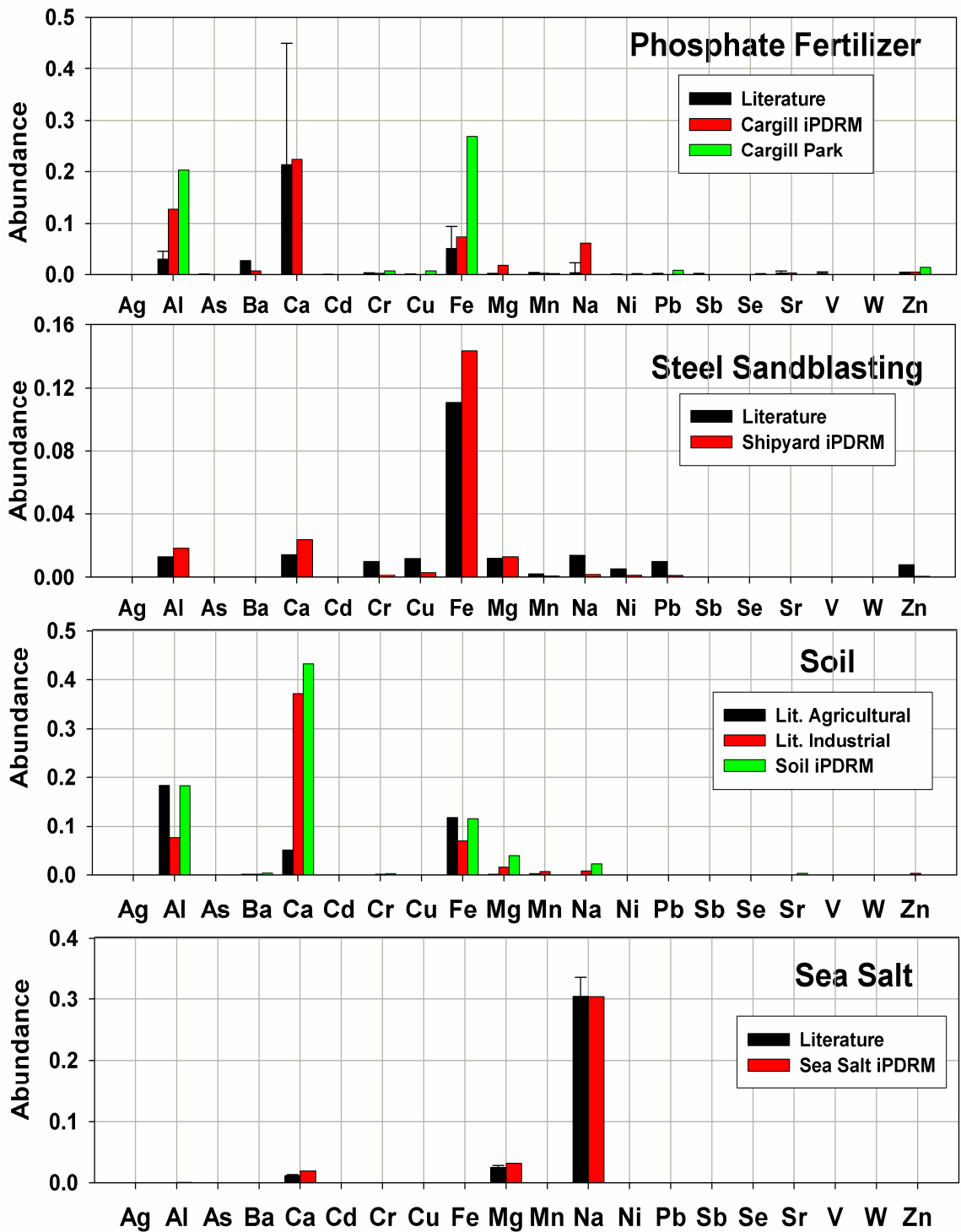


Figure 18. continued from the previous page.

### **Effects of Bartow $\chi/Q$ profile shape**

The effect of the discrepancy in shape between Park's  $\chi/Q^{\text{Met}}$  (and the  $\chi/Q^{\text{pPDRM}}$ , since the shape is not modified in Park's PDRM) and the [Ni] profile was that Ni was apportioned to sources other than Bartow (mostly Gannon and Gulf Coast) in Park's model. For example, Park's predictions for Ni were 0.002 g/s (Case 1) and 0.011 g/s (Case 2) as compared to 0.23 g/s by the iPDRM. This caused Park's X/Ni ratios for Bartow to greatly exceed their values reported in CMB literature source profiles (SPECIATE) by factors ranging from >10 (Cu, Mn, Pb, and Zn) to >100 (Al, As, Cr, Fe, and Se). As shown in **Table 2**, the ratios predicted by iPDRM for 11 elements (Al, Ba, Ca, Fe, Mn, Pb, Sb, and V) were within factors of 2 of their CMB reported values; within factors of 5 for Cu, Na, and Zn; within factors of 10 for Cr and Sr; within factors of 14- and 19 for Cd and As; and 75 for Se (compared with 800 for Park). The improvement in the agreement of the iPDRM predicted abundances for both Bartow and Manatee with CMB abundances is shown in **Figure 18**. For Manatee, agreement between the iPDRM and CMB X/Ni ratios are within a factor of 2 for all elements except Ba, Ca, Cu, Zn (2.6 to 3.7), Mn (4.7), Cd (8), and Se (35). The re-apportionment of Ni to Bartow and Manatee clearly affected the Ni/Al and Ni/Pb ratios computed for Gannon and Gulf Coast.

### **Effects of the addition of a shipyard source**

As discussed above, soil and shipyard  $\chi/Q$  profiles overlapped with those of Bartow and Manatee. Consequently, the inclusion of the soil and shipyard sources likewise improved iPDRM emission profiles for Al and Fe for these two sources as shown in

**Figure 18.** Al and Fe were predicted to be much more abundant in Park's emission profiles for these two sources.

Abundances reported by Park for Al and Fe were 8 and 7% for Manatee and 4 and 11% for Bartow whereas those found with the iPDRM were 2 and 1.3% for Manatee and 4 and 1.3% for Bartow. Literature reported abundances (from 11 profiles) for Al and Fe for oil-fired power plants are  $3\pm 2\%$  and  $2.6\pm 2.1\%$ , respectively.

Another result was that Al and Fe were also reappportioned from both Cargill and Gulf Coast to the background and shipyard sources. This improved agreement between Cargill's iPDRM-derived emission profile and CMB reported (SPECIATE) profiles for a diammonium phosphate plant (**Table 19**). For Gulf Coast, Park reported an Fe/Pb ratio of 14 as compared with the iPDRM value of 0.8 and a SPECIATE value of  $0.1\pm 0.2$ .

For the shipyard source, iPDRM predicted Al-, Cr-, and Mn-to-Fe ratios of 0.11, 0.011, and 0.02, respectively, are in good agreement with literature ratios for sandblasting of steel, i.e. 0.12 (SPECIATE), 0.008 (MatWeb, 2009), and 0.009 (MatWeb, 2009).

For the background-soil source, the final iPDRM abundance profile is similar to the input source abundance (CMB) profile. As described above, abundances and SCE profiles for the background source was constrained by uncertainties derived from multiple literature CMB profiles (SPECIATE), so this agreement is expected. The predicted abundance ratios for Al-, Cr-, and Mn-to-Fe were: 1.7 (SPECIATE: 1.6), 0.002 (SPECIATE: 0.005), and 0.01 (SPECIATE: 0.02).

### **Effect of Adding the Incinerator Sources**

Another key reappportionment, i.e. that of Pb and Zn concentrations with the iPDRM is the result of the addition of the two incinerators. Park predicted a Pb/Zn emission rate

**Table 19.** Source abundance profiles (relative to Fe) as derived from EPA SPECIATE for a diammonium phosphate fertilizer plant and for Cargill, as predicted by Park and the iPDRM.

Ratio to Fe	Literature: Phosphate Fertilizer Plant			Cargill	
	Mean*	±	σ	This Work	Park
<b>Ag</b>	-	±	-	0.0001	-
<b>Al</b>	0.6	±	0.3	1.7	1
<b>As</b>	0.005	±	0.005	0.001	0.00
<b>Ba</b>	0.5	±	-	0.1	-
<b>Ca</b>	4.3	±	4.7	3.0	-
<b>Cd</b>	0.002	±	0.002	0.001	-
<b>Cr</b>	0.03	±	0.04	0.04	0.0
<b>Cu</b>	0.008	±	0.002	0.007	0.0
<b>Fe</b>	1.0	±	0.9	1.0	1
<b>Mg</b>	0.02	±	0.01	0.24	-
<b>Mn</b>	0.036	±	0.036	0.033	0.007
<b>Na</b>	0.1	±	0.4	0.8	-
<b>Ni</b>	0.010	±	0.006	0.007	0.007
<b>Pb</b>	0.029	±	0.006	0.0003	0.0
<b>Sb</b>	0.046	±	-	0.008	-
<b>Se</b>	0.001	±	-	0.002	0.01
<b>Sr</b>	0.06	±	0.07	0.04	-
<b>V</b>	0.05	±	0.05	0.01	-
<b>W</b>	-	±	-	0	-
<b>Zn</b>	0.06	±	0.03	0.07	0.1

\* Composite of 3 profiles

ratio of 1.0 for Gulf Coast which is in significant disagreement with reported Pb/Zn ratios for Pb recycling plants from literature source profiles which range from 67-440 (SPECIATE). With the addition of the incinerators, especially McKay (which concurrently influenced Sydney from 14:00-19:00), the Zn and a portion of the Pb were reapportioned to those sources. The iPDRM predicted Pb/Zn ratio for Gulf Coast was 734, and for McKay and PCRR, 0.77 and 0.78, respectively, in good agreement with averaged literature values (N=5),  $0.66 \pm 0.07$  (Greenberg, 1978; SPECIATE; Han, 1992).

iPDRM predicted X/Pb ratios for Gulf Coast (**Table 2**) show that: Ba, Ca, Cr, Cu, Mg, Sb, and V ratios are within a factor of 2 of literature ratios; As, Cd, Ni, and Zn are within a factor of 5; Fe and Se are within a factor of 8; only Ag (22), Al (89), Mn (127), and Sr (95) are excessively higher than reported. This is much improved over Park's X/Pb ratios, of which only As (6), Cu(62), and Se(71) are within a factor of 100 of literature ratios; the remaining elements, Al, Cr, Fe, Mn, Ni, and Zn all exceed a factor of 100. However, it is expected that predicted Al emissions are much higher for Gulf Coast than literature emissions for a generic Pb recycling plant source, owing to the use of the production of Pb-Al alloy products.

X/Pb ratios for McKay (**Table 20**) show that: Al, Ba, Cr, Cu, Fe, Mg, Ni, Sb, Sr, and Zn are within a factor of 5 of literature ratios; Ag (0), As(20), Ca (16), Cd, (0.06), Mn(26), Na (0.06), Se (192), and V(94) exceed this range. X/Pb ratios for PCRR (**Table 20**) show that: Al, Ba, Cr, Fe, Na, Sb, Sr, and Zn are within a factor of 2; Ca, Cd, Cu, and Mg are within a factor of 10; and Ag(0.01), As (23), Mn (14), Ni (0.03), Se (65), and V(23) exceed this range.

**Table 20.** Source abundance profiles (relative to Pb) as derived from EPA SPECIATE for incinerators and for McKay and PCRR, as predicted by this work.

Ratio to Pb	Literature: Incinerators			This Work	
	Mean*	±	σ	McKay	PCRR
Ag	0.002	±	0.001	NS	NS
Al	0.1	±	0.1	0.2	0.1
As	0.002	±	0.001	0.043	0.049
Ba	0.004	±	0.004	0.001	0.008
Ca	0.05	±	0.04	0.83	0.42
Cd	0.024	±	0.015	0.001	0.004
Cr	0.002	±	0.001	0.001	0.005
Cu	0.021	±	0.005	0.027	0.003
Fe	0.05	±	0.02	0.26	0.09
Mg	0.30	±	0.17	0.07	0.05
Mn	0.005	±	0.004	0.12	0.07
Na	0.8	±	0.6	0.04	0.43
Ni	0.003	±	0.002	0.007	NS
Pb	1.0	±	0.25	1.0	1.0
Sb	0.03	±	0.03	0.01	0.05
Se	0.001	±	0.0002	0.11	0.04
Sr	0.2	±	0.2	0.1	0.3
V	0.0001	±	0.0001	0.006	0.001
W	-	±	-	-	-
Zn	1.5	±	0.3	1.3	1.3

\* Composite of 5 profiles

NS - not significant (< 0.001);

**Figure 19** shows the observed and predicted Pb concentration profiles along with the predicted Pb concentration profiles induced by key sources for Park's model and the iPDRM.

Park apportioned the Pb to 3 main sources, Gulf Coast, Big Bend, and Gannon. As discussed in section 1.1.2., Park's results under-predict the Pb concentration from 13:30-15:00 by 31-80% and over-predict Pb at 18:00 and 19:00 by 230 and 235%. Gulf Coast is predicted to contribute 63-105% of the ambient Pb concentration from 14:30-15:30, Big Bend contributes 128% at 13:30, and Gannon contributes 8-44% from 14:00-17:00. The iPDRM fits between ambient and predicted Pb concentrations are much improved; with residuals from 12:30-19:00 ranging from -13% to 23%. The iPDRM predicts that the major sources of Pb are Gulf Coast, Big Bend, McKay, and PCRR with most of the Pb that Park had attributed to Gannon now being apportioned to McKay and PCRR. Big Bend is predicted to contribute 98% of the observed Pb at 13:30 and 48% at 14:00; Gulf Coast contributes 40-58% of the Pb from 14:00-15:00; McKay contributes 48-86% of the Pb from 15:30-17:00; and PCRR is responsible for 20-34% of ambient Pb from 17:30 – 19:00. The Pb contribution predicted from Gannon is reduced to 2-9% from 14:30-19:00, and reduces its Pb/Al ratio from 0.007 to 0.003 in good agreement with that reported for a CFPP with an ESP ( $0.003 \pm 0.002$ ) (SPECIATE).

**Figure 20** shows the observed and predicted Zn concentration profiles along with the predicted Zn concentration profiles induced by key sources for Park's model and the iPDRM. Park apportioned the Zn to 3 main sources, Gulf Coast, Big Bend, and Gannon. Residuals in Park's predicted vs. observed fits for 11 of 18 sampling intervals exceed  $\pm 30\%$  (12:00, 12:30, 14:30, 15:00, 16:30, 18:00, and 19:00-20:30); and 14 of 18

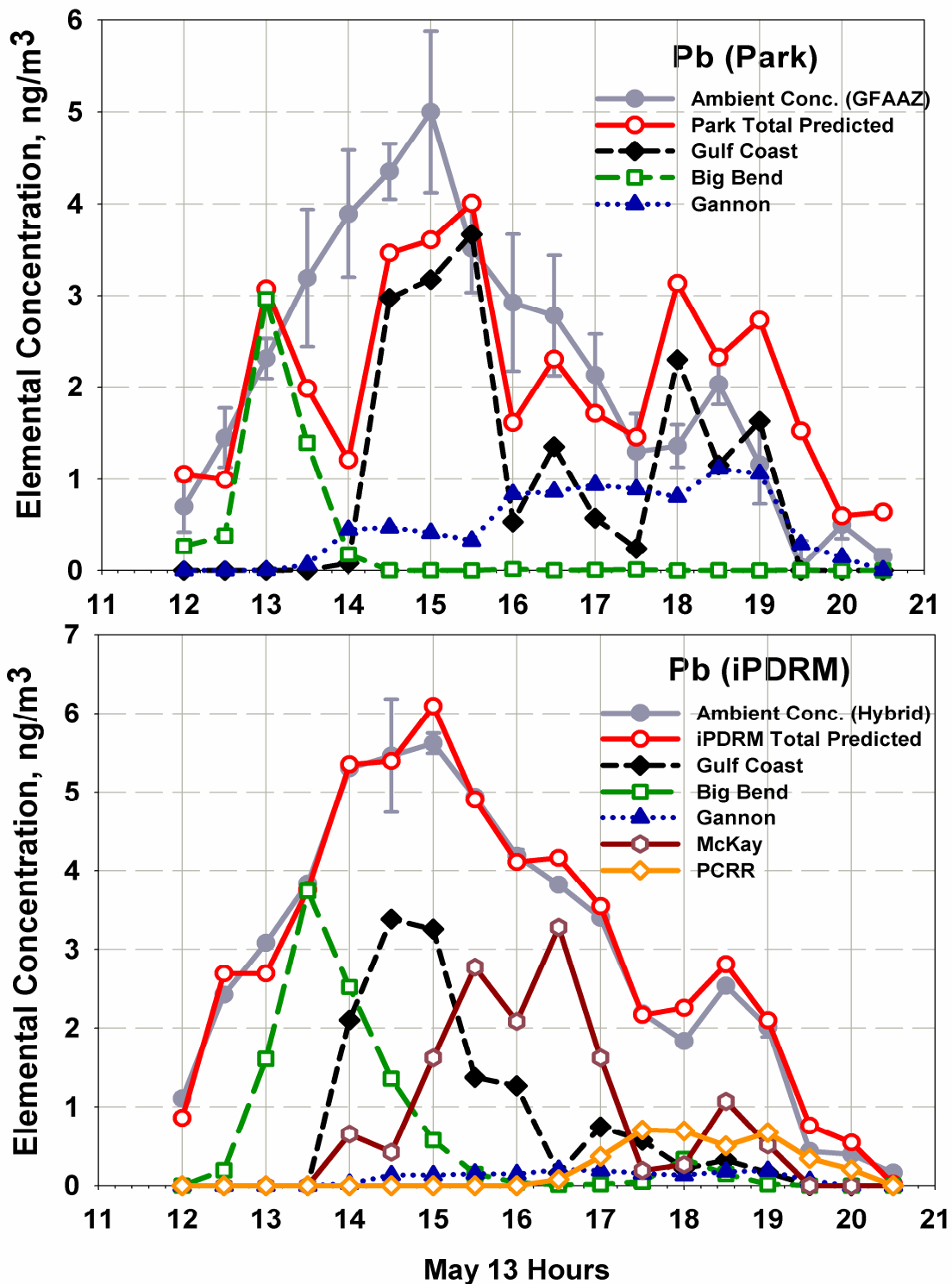


**Figure 19.** Ambient Pb (grey) and predicted (red) Pb concentration profiles ( $\text{ng}/\text{m}^3$ ). Total predicted Pb concentration profiles from major contributing sources are shown. Park's results are shown in the graph above, iPDRM results in the graph below.

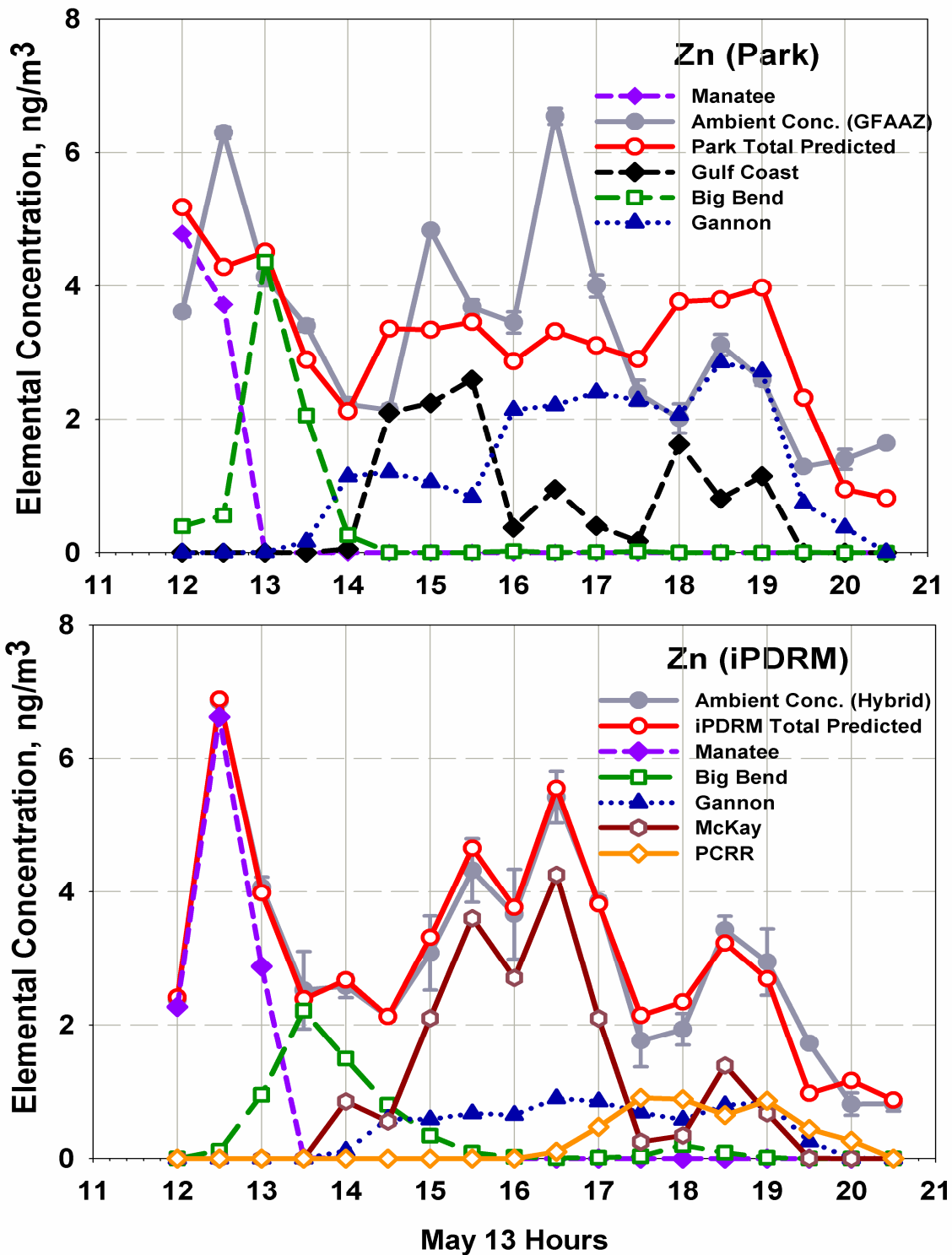


**Figure 20.** Ambient Zn (grey) and predicted (red) Zn concentration profiles (ng/m<sup>3</sup>). Total predicted Zn concentration profiles from major contributing sources are shown. Park's results are shown in the graph above, iPDRM results in the graph below.

sampling intervals exceed  $\pm 20\%$  (17:00, 17:30, and 18:30). The iPDRM reapportions the Zn from Gulf Coast and Gannon to the incinerators, McKay and PCRR. As discussed above, the agreement of the Pb/Zn ratios with literature ratios for lead recycling plants and incinerators suggest that the Zn apportionment predicted with the iPDRM is reasonable. Also, Zn residuals are  $\leq 8\%$  for 14 of 18 sampling intervals and  $\leq 21\%$  for 16 of 18 sampling intervals indicating an excellent fit.

#### **3.2.4. Comparison to NEI and TRI reported emission rates**

iPDRM predicted SO<sub>2</sub> emission rates for the power plants are within  $\pm 5\%$  of CEM reported average emission rates as they were constrained to be. The predicted SO<sub>2</sub> emission rates were 113 g/s and 31 g/s for Gulf Coast and Cargill, respectively. These compare to reported emission rates for Gulf Coast: 16.6 g/s (NEI), 21.3 g/s (NET), and 25 g/s (FDEP). Park predicted emission rates of 340 g/s (Case1) and 31 g/s (Case 2) for Gulf Coast and 130 g/s (Case 1) and 49 g/s (Case 2). These reported rates (as the case with all NEI, TRI, or FDEP emissions; shown in **Table 3**) are converted from annual tons/year numbers and do not translate well to the time resolution of our study period. The annual rates were converted assuming that the sources were continuous throughout the entire year, including overnight and weekends. This conversion means that the g/s estimates are likely lower than calculated, which is why the fractions (i.e., 1/10) of NEI values were only used in the iPDRM as lower bounds. Species that were reported by NEI/TRI include: SO<sub>2</sub>, NH<sub>3</sub>, As, Cd, Cr, Mn, Ni, Pb, Se, V, and Zn.

Park's Case 2 SO<sub>2</sub> emission rate agreed best with reported values, however, the iPDRM value was only ~4-7 times these and is a reasonable estimate given the method of

conversion used, especially when considering that the iPDRM predicted Pb emission rate (0.15 g/s) is 4 times that reported by NEI (0.032 g/s). Reported SO<sub>2</sub> emission rates for Cargill varied greatly depending on the source: 0.006 g/s (NEI), 115g/s (NET), and 40 g/s (FDEP). Our value agrees well with FDEP value as does Park's Case 2.

Ratios of PDRM predicted emission rates predicted both by Park and our work to reported NEI or TRI (herein referred to as NEI-TRI) emission rate ratios are shown in **Table 21**. In **Table 22**, the iPDRM to NEI-TRI ratios are grouped by source and into groups as follows: within a factor of 2.5, within a factor of 5.5, and  $\geq 5.5$ . Agreement between these ratios is much better for power plants, in which SO<sub>2</sub>, and Ni ratios are within a factor of 2.5 for each one. For 10 of 12 species, iPDRM emission rates for Big Bend agree within a factor of 2.5; NH<sub>3</sub> which is not a conservative tracer is within a factor of 5.5, and only Cd (0.01) does not agree well. Predicted emission rates for Gannon are also in similarly good agreement with 9 of 12 species within a factor of 5.5, and Cd (0.06), Se(26), and V(7) exceed that range. For the oil-fired power plants, 7 of 10 iPDRM predicted species emission rates are within a factor of 5.5 of NEI-TRI data (Mn(6), Pb(28), and Se(7) are greater than 5.5 times the NEI-TRI value), and 7 of 11 species for Bartow agree within 5.5 times (NH<sub>3</sub>(7), As (10), Cr (21), and Se (30) are substantially greater). It is likely that iPDRM results are more accurate for certain elements such as As and Se as they are likely to form volatile compounds and have substantial gas-phase concentrations. The iPDRM As emission rates for CFPPs agreed within a factor of 2 for TRI reported emissions, however, NEI reported As emission rates were 450-700 times smaller than those reported for TRI. iPDRM emission rates and NEI-TRI data do not correlate as well for non-continuous sources. This makes sense as

**Table 21.** Ratios of iPDRM emission rate predictions to emission rates reported by NEI-TRI.

	Manatee		Big Bend		Gannon		Bartow		Cargill		Gulf Coast		McKay	PCRR
	This Work	Park	This Work	Park	This Work	Park	This Work	Park	This Work	Park	This Work	Park	This Work	This Work
<b>SO<sub>2</sub></b>	1	1	1	1	2	2	2	2	5598	23500, 8850	7	20, 2	6	3
<b>NH<sub>3</sub></b>	1	-	4	-	4	-	6	-	7	-	-	-	2	5
<b>As</b>	0.4	0.8, 0.1	1	3	2	2	10	14	35	869	12	2, 7	13300	11
<b>Cd</b>	3	-	0.01	-	0.06	-	5	-	7	-	9	-	29	3
<b>Cr</b>	2	33, 44	1	2	2	3	21	13, 10	152	227, 795	0.3	2, 24	32	0.4
<b>Mn</b>	6	9, 11	0.5	1	0.6	0.2, 0.6	1	0.2, 1	274	224, 449	8	0.4, 4	25030	2
<b>Ni</b>	2	1	0.8	1, 2	1	0.2, 1	1	0.01, 0.05	18	131	1	1, 6	194	0.01
<b>Pb</b>	28	15, 18	2	2, 3	0.3	0.5, 2	3	0.2, 0.7	2	792, 1585	4	0.1, 1	5140	33
<b>Sb</b>	-	-	-	-	5	-	0.4	-	-	-	-	-	-	-
<b>Se</b>	7	10, 12	0.4	0.04	26	22	30	22	695	11500, 23200	5	4, 13	-	-
<b>V</b>	0.7	-	1	-	7	-	1	-	-	-	-	-	-	-
<b>Zn</b>	-	-	2	7, 8	3	2, 7	-	-	-	-	-	-	-	-

**Table 22.** Ratios of predicted and published emission rates (iPDRM/NEI-TRI) grouped within factors of 2.5, 5.5, or > 5.5.

	< 2.5	< 5.5	> 5.5
<b>Manatee</b>	SO <sub>2</sub> , NH <sub>3</sub> , Cr, Ni, V	As, Cd	Mn, Pb, Se
<b>Big Bend</b>	SO <sub>2</sub> , As, Cr, Mn, Ni, Pb, Se, V, Zn	NH <sub>3</sub>	Cd
<b>Gannon</b>	SO <sub>2</sub> , As, Cr, Mn, Ni	NH <sub>3</sub> , Pb, Sb, Zn	Cd, Se, V
<b>Bartow</b>	SO <sub>2</sub> , Mn, Ni, Sb, V	Cd, Pb	NH <sub>3</sub> , As, Cr, Se
<b>Cargill</b>	Pb	-	SO <sub>2</sub> , NH <sub>3</sub> , As, Cd, Cr, Mn, Ni, Se
<b>Gulf Coast</b>	Ni	Cr, Pb, Se	SO <sub>2</sub> , As, Cr, Mn
<b>McKay</b>	NH <sub>3</sub>	-	SO <sub>2</sub> , As, Cd, Cr, Mn, Ni, Pb
<b>PCRR</b>	Cr, Mn	SO <sub>2</sub> , NH <sub>3</sub> , Cd	As, Ni, Pb

the NEI-TRI values are estimated from monthly CEM-reports (at best and only for larger sources) along with other variables such as fuel-type, heat generated, and emissions controls. Non-continuous sources are only required to update emissions data once every three years (U.S. EPA, 2006). The iPDRM/NEI-TRI emission rate ratios do show agreements: For Gulf Coast ratios for 4 of 8 of the species were less than a factor of 5.5, and for PCRR, 5 of 8 species. Ratios indicated substantially poorer agreement for Cargill and McKay.

Our predicted emission rates support that the NEI-TRI data are reasonable to within a factor of 5 for power plants and should be trusted less for non-continuous sources. Thus, our results suggest that NEI-TRI values provide a good qualitative estimate of the toxic substances emitted by sources, but are not necessarily useful as seed values in a predictive model to quantify source emissions.

#### **4. Summary and Conclusions**

An improved hybrid PDRM, combining features of a least squares mass balance receptor model, a deterministic Gaussian Plume Model, and a Chemical Mass Balance model was constructed and applied to a dataset for Tampa consisting of highly time-resolved ambient SO<sub>2</sub>, NH<sub>3</sub>, and elemental constituents of PM<sub>2.5</sub> measured during the Bay Regional Atmospheric Chemistry Experiment to apportion their contributions from local stationary sources. The model was designed by Park to exploit known information such as the number and location of known sources in relation to the receptor site, their respective stack and emission parameters, and meteorological conditions during sampling, and improved to exploit additional information such as wind trajectories and the chemical composition of both point and area source emissions.

In this work, ICPMS analysis of 30-minute SEAS samples enabled the expansion of the set of elements determined (whilst reducing the analysis time and achieving superior analytical precision). The resulting dataset included additional marker species (i.e. Ag, Cd, Sb, V, and W) and improved data for Zn. These were used to improve the resolving power of the model and provide more information on the influence of individual sources, including soil and marine background aerosol, i.e. area sources not included by Park. The addition of V corroborated the Ni data reported by Park and allowed us to confirm the arrival and times of influence of the Manatee and Bartow plumes. Both elements were well-fit by new  $\chi/Q^{\text{traj}}$  profiles.

Using the Pb/Zn ratios derived from the CMB source profiles, the  $\chi/Q^{\text{iPDRM}}$  profile for Gulf Coast became similar to the concentration profiles of Ag, Cd, and W allowing these elements to be apportioned to Gulf Coast. The Pb/Zn constraints were thus effective in achieving the resolution of the Gulf Coast, McKay, and PCRR sources. Ratios of Al, Ca, Cr, Fe, and Mn allowed the resolution of the shipyard and soil sources, and Na allowed the resolution of the marine source. With the improved dataset, we were able to conclude that the  $\chi/Q$  profiles predicted by Park were incorrect and that the application of curvilinear forward plume trajectory method provided a more accurate prediction of  $\chi/Q$  profiles for all of the sources (as evidenced by good correlation with tracer species concentration profiles). The inclusion of both 500-m and surface trajectory-derived profiles were especially important for three of the four power plants. Surprisingly, ground plumes for Big Bend and Gannon plants arrived earlier than their plumes aloft, owing to differences in their trajectories, despite lower transport velocities of the former.

The iPDRM performed well despite the wind shift, giving confidence in its application to more complicated situations such as encountered in the Tampa study. The inclusion of bi-level trajectory analysis and additional sources eliminated the need for separate scaling of  $\chi/Q$  bounds for sources with smaller effective heights or near-ground emissions as done by Park.

Predicted  $\chi/Q$  profiles were effectively constrained by hourly CEM-derived  $SO_2$  emission rates for the power plants, as these could be determined with the accuracy of their measurements, degraded only by deconvolution error. For Manatee and Bartow, predicted  $\chi/Q$  profiles were further constrained by the widths of the Ni and V peaks in their concentration profiles.  $\chi/Q$  profiles were likewise constrained by  $NH_3$  (Cargill), and to a lesser extent Pb and Zn (Gulf Coast and the incinerators). All of these improved the resolution of all sources. Improvements were also made by applying constraints based on chemical compositions for generic source types as mentioned above. These were most important in the background soil and marine sources, incinerators, shipyard, and Gulf Coast. In particular, chemical compositional constraints allowed the iPDRM to predict average emission rates and ambient pollutant contributions from sources with intermittent emissions (as was evidenced for Gulf Coast, the two incinerators, and the shipyard). The  $\chi/Q^{traj}$  profile for these intermittent sources can be regarded as a prediction of their expected influence (if they are operating at a constant rate) whereas the  $\chi/Q^{iPDRM}$  profiles were able to account for fluctuations in emission rates of the sources.

In summary, the iPDRM results were greatly affected by the improved Gaussian Plume Model-derived  $\chi/Q$  profiles, the inclusion of extra sources, and the ability of the  $\chi/Q$  profiles for sources to be “conditioned” with chemical compositional constraints and

ambient tracer species concentration profiles. These improvements to the model allowed the apportionment of ambient species to sources based on more available information, resulting in arguably more accurate results as evidenced by improved performance statistics and better agreement with published source profiles and emission inventory estimates (NEI and TRI).

In conclusion, the performance of the iPDRM in a complex scenario, with a wind shift and many sources concurrently influencing the receptor site suggests that iPDRM, when used with highly time-resolved data and CEM reported SO<sub>2</sub> emission rate data can be used as an effective tool that requires minimal amount of computational power to remotely predict and monitor emission rates of toxic and or other non-criteria pollutants.

A significant improvement can be made to future version of the iPDRM by accounting for the uncertainties in the measured ambient concentrations. Residuals for concentration profile data points with large uncertainties should be down-weighted to prevent the iPDRM from compensating for uncertain data by over- or under-predicting data points with smaller uncertainties. This can likely be accomplished with the addition of a normalizing uncertainty term into the least squares function to be minimized.

# Appendices

## Appendix A.

Section reproduced from Park on the calculation of  $\sigma_y$  and  $\sigma_z$ , transport velocity,  $u$ , effective plume height,  $H$ , and the off-axis distance,  $y$ .

### 3.2 Gaussian Dispersion Parameters ( $\sigma_y$ and $\sigma_z$ )

The values of  $\sigma_y$  and  $\sigma_z$  vary with turbulence, height above the surface, surface roughness, and downwind distance above the surface, surface roughness, and downwind distance from the source and, hence, transport wind speed and time. Herein,  $\sigma_y$  and  $\sigma_z$  were determined from correlations as follows:

$$\sigma_y = \sigma_v t F_y \quad (4)$$

$$\sigma_z = \sigma_w t F_z \quad (5)$$

where  $\sigma_v$  and  $\sigma_w$  are the standard deviations of the wind velocity in the  $y$  and  $z$  directions, respectively,  $t$  is the travel time from the source to the location of interest, and  $F_y$  and  $F_z$  are universal functions of parameters that specify the characteristics of the atmospheric boundary layer. Specifically, these are friction velocity,  $u^*$ ; the Monin-Obukhov length,  $L$ ; the mixed layer depth,  $z_i$ ; the convective velocity scale,  $w^*$ ; the surface roughness,  $z_o$ ; and the effective stack height,  $z$ , i.e., the height of pollutant release above the ground. Different formulae are used for different stability classes [Draxler, 1976; Binkowski, 1979; Irwin, 1979].

Likewise,  $\sigma_v$  and  $\sigma_w$  are calculated from friction velocity ( $u^*$ ) and  $L$ , using formulae appropriate for different stability classes. Hourly values of the Pasquill stability class,  $z_i$  (m),  $u^*$  (m/s),  $L$  (m) and  $w^*$  (m/s), were obtained from the CALMET model [Scire et al.,

2000] output at the geocoordinates of Sydney, Florida, as described above. These were interpolated to produce half-hourly estimates for use in the model. A surface roughness length of 0.25 m was used in this analysis.

### 3.3. Transport Wind Velocity $u$

The wind profile power law was used to estimate horizontal transport speed,  $u$ , at the effective plume height,  $z$ , given the horizontal surface wind speed,  $u_1$ , at height  $z_1$  (i.e., the 10 m, meteorological tower height). The power law equation is of the form

$$u = u_1 \left( \frac{z}{z_1} \right)^p \quad (6)$$

where  $p$  is given by equation (6) [Panofsky et al., 1960].

$$p = \frac{\Phi_m \left( \frac{z}{L} \right)}{\frac{U\kappa}{u_*}} \quad (7)$$

where the nondimensional wind shear,  $\Phi_m(z/L)$ , and the nondimensional wind speed,  $U\kappa/u_*$ , are universal functions; and  $\kappa$  is the von Karman constant, which is equal to 0.4. Equation (5) is invalid for wind transport speeds less than 1.0 m/s. Therefore a minimum value of 1.0 m/s was used.

Transport speeds calculated in this manner were relatively constant during the 9-hour modeling period. Thus the transport speed was calculated for each 30-min interval and an average transport speed was used in the receptor model. Likewise, transport time was calculated from the average transport speed at stack height and source-to-receptor site distance. Transport times were assumed to be constant over the 9-hour period, despite shifts in the wind angle, which lead to differences in  $x$  for each source.

### 3.4. Effective Plume Height H

The plume height is used in the calculation of the vertical term described in equation (2) and in calculating the transport velocity, as described above. The effective stack height is taken to be the sum of the actual stack height ( $h_s$ ) and the plume rise ( $\Delta H$ ).

$$H = h_s + \Delta H \quad (8)$$

Herein, plume rise ( $\Delta H$ ) is calculated by the formulas expressed by Briggs [1969, 1971, 1974] and U.S. EPA [1995]. The detailed mathematical formulas can be found in Briggs' papers, and a brief description is given below. The effective stack height ( $H$ ) is determined for conditions at the stack exit. If the plume is dominated by buoyancy, the buoyancy flux parameter,  $F_b$  ( $\text{m}^4/\text{s}^3$ ), is given by

$$F_b = g v_s d_s^2 \left( \frac{\Delta T}{4 T_s} \right) \quad (9)$$

where  $g$  is gravitational acceleration ( $\text{m}/\text{s}^2$ ),  $v_s$  is the stack gas exit velocity ( $\text{m}/\text{s}$ ),  $d_s$  is the inside stack top diameter ( $\text{m}$ ),  $u_s$  is mean wind speed ( $\text{m}/\text{s}$ ) at stack height,  $\Delta T = T_s - T_a$ ,  $T_s$  is the stack gas temperature ( $\text{K}$ ), and  $T_a$  is the ambient air temperature ( $\text{K}$ ).

The plume height ( $H$ ) for unstable or neutral atmospheric conditions is determined by two different flux parameters: (1) For  $F_b < 55$ ,

$$H = h_s + 21.425 \frac{F_b^{3/4}}{u_s} \quad (10)$$

(2) For  $F_b \geq 55$ ,

$$H = h_s + 38.71 \frac{F_b^{3/5}}{u_s} \quad (11)$$

The plume height ( $H$ ) for stable atmospheric conditions is given by equation (12)

$$H = h_s + 2.60 \left( \frac{F_b}{u_s s} \right)^{1/3} \quad (12)$$

If the plume is dominated by momentum, the momentum flux parameter,  $F_m$  ( $\text{m}^4/\text{s}^3$ ), is given by

$$F_m = v_s^2 d_s^2 \left( \frac{T_a}{4T_s} \right) \quad (13)$$

The plume height ( $H$ ) for an unstable or neutral atmospheric condition is given by

$$H = h_s + 3.0 d_s \frac{v_s}{u_s} \quad (14)$$

The plume height ( $H$ ) for a stable atmospheric condition is given by

$$H = h_s + 1.5 \left( \frac{F_m}{u_s \sqrt{s}} \right) \quad (15)$$

where  $s = g(\partial\theta/\partial z)/Ta$  is a stability parameter indicating the potential temperature gradient with height.

Emission parameters required to calculate the effective plume height ( $H$ ) in the Gaussian plume dispersion equation (2) are listed in Table 2.

### 3.5. Distance Between the Plume Centerline and the Sampling Site ( $y$ )

According to equation (2), the plume concentration decays exponentially with increasing distance,  $y$ , from the plume centerline. As illustrated in **Figure A1**, wherein  $x'$  is the plume transport distance,  $y$  is related to the deviation,  $\theta_{DS}$ , between the wind angle,  $\theta_{wind}$ , and station angle,  $\theta_{station}$ , and the source-to-sampling site distance,  $x$ , as follows:

$$y = \sin \theta_{DS} \cdot x \quad (16)$$

$$\theta_{DS} = \theta_{station} - 180^\circ - \theta_{wind} - \theta_{Ekman}$$

where  $\theta_{\text{Ekman}}$  is the wind angle rotation at transport height relative to the surface wind direction (in degrees) due to the Ekman effect. In **Figure A1**, we show a station angle ( $251^\circ$ ) corresponding to the Gannon power plant. Both  $\theta_{\text{wind}}$  and  $\theta_{\text{station}}$  are measured from true north. In the model, we used an average wind angle, computed from the 15-min surface wind data measured at the meteorological tower, i.e., averaged during the period of transport for each source (case 2).

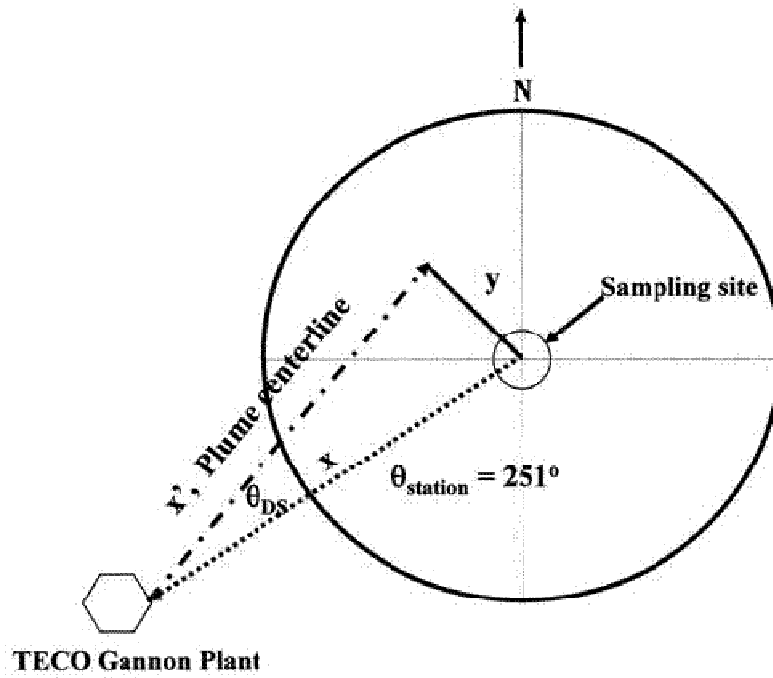


**Figure A1.** The PDRM makes use of source angle and distance relationships. Plume transport distance ( $x'$ ) and displacement ( $y$ ) of the plume centerline from the sampling site are shown.

## **Appendix B.**

Procedures (adapted from Pancras et al., 2005) for experiments to determine the capability of the ICPMS in direct analysis of SEAS samples are included in this Appendix.

### **B1. Cleaning Procedures**

In order to reduce the problem of contamination in determining ppb and sub-ppb concentration ranges, all materials that contact both sample and standards were acid-washed low contaminant materials such as virgin polypropylene (PP) and teflon (PTFE). All sample containers, vials, and caps were soaked in ~10% (v/v) HNO<sub>3</sub> (70% v/v, Reagent grade, Mallinkrodt Baker, Phillipsburg, NJ) overnight then rinsed with Milli-Q (18-MΩ cm<sup>2</sup> deionized- distilled water) before soaking again for 2-4 hrs in 2.0% (v/v) HNO<sub>3</sub>, then sonicated for 30 min in a Ultrasonic bath (Branson, Danbury, CT) and finally rinsed again in Milli-Q water. Pipette tips were repeatedly rinsed prior to use with 2-5% (v/v) HNO<sub>3</sub> before use. Digestion vessels were cleaned with a more rigorous procedure that involved heating concentrated “Acid Digestion mix” (5:0.1:0.1 (v/v) of concentrated baseline nitric, hydrofluoric (50% v/v, Optima grade, Leicestershire, England), and perchloric (70% v/v, Ultrex II grade, Mallinkrodt Baker, Phillipsburg, NJ)) at 150°C overnight.

### **B2. Analysis of NIST 1640 SRM Trace Elements in Natural Water**

NIST 1640 SRM Trace Elements in Natural Water is an aqueous solution of naturally occurring elements in Rainwater at a 5% (v/v) nitric acid solution. The stock solution was

volumetrically transferred with an acid-rinsed virgin polypropylene pipette tip and diluted to the mark with 0.2 % (v/v) HNO<sub>3</sub> in a pre-cleaned polypropylene volumetric flask. Three mL aliquots were transferred to pre-cleaned polypropylene sample vials and analyzed by ICPMS. Blanks were prepared with Milli-Q water and acidified to 0.2 % (v/v) HNO<sub>3</sub>.

### **B3. Total dissolution of NIST Atmospheric Fine Particle SRM**

Eleven ~10-mg aliquots of a NIST interim urban atmospheric fine-particle SRM (iSRM) were weighed to five significant figures into a Teflon pressure vessel (CEM, Inc., Matthews, NC) using a 4-place analytical balance (Mettler-Toledo, Inc., Toledo Ohio, model AX105DR). Three mL of the Acid Digestion mix were added and the vessels sealed, and heated to a temperature of 150 °C for ~24 hours in a convection oven (Precision Economy Oven, Jouan, Winchester, VA).

The resulting clear solutions were heated to near dryness, and reconstituted with 0.2% HNO<sub>3</sub> [Pancras et al., 2005]. Separate aliquots were diluted 10- and 100-fold with 0.2% HNO<sub>3</sub> to pre-cleaned polypropylene vials and analyzed by ICPMS. Blanks were prepared with the same procedure using no SRM.

### **B4. Preparation of Test Slurries**

#### **B4.1. iSRM Test slurry**

The iSRM test slurry was prepared by sonicating 150 mg of the NIST SRM in 500 mL of Milli-Q water. Actual atmospheric slurry samples collected with SEAS-II contain few particles >2 µm. Therefore, a nitric acid pre-rinsed 5.0 µm-pore Teflon membrane filter

(Sterlitech, Kent, WA) in an acid-cleaned polycarbonate filtration apparatus (Sartorius, Sartorius, Goettingen, Germany) was used to remove particles larger than the pore size. Five filters were needed for this process. The filtrate was divided into two aliquots, and acidified to 0.2 and 2.0%, respectively, of high purity nitric acid.

#### **B4.2. Pooled SEAS sample slurry**

The SEAS slurry samples used in this study were taken from a study in Birmingham, AL and stored frozen, in their polypropylene collection vials. These were thawed, sonicated, and pooled directly to prepare the composite test slurry. Selected samples that were previously analyzed and shown to contain high concentrations (at minimum 5x method blank) of many elements were combined to produce ~150 mL of pooled slurry.

### **B5. Total Dissolution of Test slurry**

#### **B5.1. Blank filtrate for iSRM analysis**

Milli-Q water was filtered as described in section B4.1. Samples were evaporated to near dryness in a horizontal HEPA filtered, laminar flow, clean air hood. Three mL of Acid Digestion mix was added to the dried sample and heated at 150 overnight in a Teflon pressure vessel (CEM, Inc., Matthews, NC). The digested sample was evaporated to near dryness and reconstituted with 12 mL of 0.2% HNO<sub>3</sub>. Blanks were transferred to precleaned polypropylene vials, sonicated for 30 min, and analyzed.

## **B5.2. Test Slurries**

The procedure described in section B5.1. was performed on: (1) 12 mL (gravimetric) of iSRM test slurry per vessel and (2) 20mL (gravimetric) of pooled SEAS sample slurry per vessel.

## **B6. Direct ICPMS Analysis of Test Slurries**

Pre-cleaned polypropylene vials and caps were pre-weighed and filled with 3.5 mL aliquots of test slurries. The same was done with 3.5 mL of Milli-Q water. All samples were acidified with 10  $\mu\text{L}$  of  $\text{HNO}_3$  to bring the concentration to 0.2%  $\text{HNO}_3$  (v/v), sonicated(30-min), and analyzed by ICPMS.

## Appendix C.

Includes tables of the data used for the various plots shown in Figures.

**C1.** Table of Wind angles and speeds plotted in Figure 2.

<b>Time</b>	<b>Wind Angle degrees</b>	<b>Wind Speed m/s</b>
<b>6:00</b>	142	0.13
<b>6:30</b>	142	0.13
<b>7:00</b>	142	0.19
<b>7:30</b>	129	0.28
<b>8:00</b>	130	0.58
<b>8:30</b>	155	1.33
<b>9:00</b>	163	2.35
<b>9:30</b>	191	2.27
<b>10:00</b>	201	2.08
<b>10:30</b>	196	2.29
<b>11:00</b>	207	2.27
<b>11:30</b>	195	1.9
<b>12:00</b>	205	2.15
<b>12:30</b>	252	2.04
<b>13:00</b>	253	1.87
<b>13:30</b>	288	1.85
<b>14:00</b>	238	2.00
<b>14:30</b>	257	1.85
<b>15:00</b>	260	2.07
<b>15:30</b>	225	2.03
<b>16:00</b>	260	2.65
<b>16:30</b>	239	2.54
<b>17:00</b>	262	2.47
<b>17:30</b>	254	2.63
<b>18:00</b>	246	2.32
<b>18:30</b>	244	2.55
<b>19:00</b>	249	2.21
<b>19:30</b>	237	1.58
<b>20:00</b>	220	2.45
<b>20:30</b>	212	2.35

C2. Table of SO<sub>2</sub> and NH<sub>3</sub> concentrations and uncertainties in ppb plotted in Figure 5.

<b>Time</b>	<b>SO<sub>2</sub></b>		<b>NH<sub>3</sub></b>	
	<b>x</b>	<b>σ</b>	<b>x</b>	<b>σ</b>
<b>12:00</b>	0.70	0.718	2.18	0.17
<b>12:30</b>	5.03	0.794	2.13	0.17
<b>13:00</b>	5.10	0.709	1.83	0.16
<b>13:30</b>	10.64	0.965	2.41	0.17
<b>14:00</b>	11.50	3.098	2.33	0.17
<b>14:30</b>	30.90	2.568	1.82	0.16
<b>15:00</b>	28.67	0.239	1.60	0.16
<b>15:30</b>	32.64	1.166	1.53	0.16
<b>16:00</b>	31.47	0.382	1.42	0.15
<b>16:30</b>	39.60	1.958	1.37	0.15
<b>17:00</b>	37.90	0.993	1.28	0.15
<b>17:30</b>	30.87	1.968	1.32	0.15
<b>18:00</b>	31.13	1.267	1.48	0.15
<b>18:30</b>	39.10	4.295	1.39	0.15
<b>19:00</b>	41.30	5.357	1.25	0.15
<b>19:30</b>	12.67	6.367	1.34	0.15
<b>20:00</b>	4.00	1.282	5.09	0.23
<b>20:30</b>	4.67	0.094	6.43	0.25

**C3.** Table of PM<sub>2.5</sub> concentrations and uncertainties in ng/m<sup>3</sup> plotted in Figure 9.

<b>Time</b>	<b>PM<sub>2.5</sub></b>	
	<b>x</b>	<b>σ</b>
<b>12:00</b>	6682	400
<b>12:30</b>	8001	555
<b>13:00</b>	11103	522
<b>13:30</b>	10439	535
<b>14:00</b>	10693	499
<b>14:30</b>	9986	611
<b>15:00</b>	12212	678
<b>15:30</b>	13553	763
<b>16:00</b>	15266	740
<b>16:30</b>	14802	619
<b>17:00</b>	12374	557
<b>17:30</b>	11130	567
<b>18:00</b>	11333	577
<b>18:30</b>	11535	611
<b>19:00</b>	12217	568
<b>19:30</b>	11361	503
<b>20:00</b>	10051	489
<b>20:30</b>	9789	430

**C4.** Table of observed concentrations (hybrid dataset) and uncertainties and predicted concentrations in ng/m<sup>3</sup> for elements used in the Chemical Mass Balance (CMB) model plotted in Figure 10.

Time	Al			As			Cd			Cr			Cu			Fe			Mn									
	Observed	CMB pred.		Observed	CMB pred.		Observed	CMB pred.		Observed	CMB pred.		Observed	CMB pred.		Observed	CMB pred.		Observed	CMB pred.								
	x	σ	x	σ	x	σ	x	σ	x	σ	x	σ	x	σ	x	σ	x	σ	x	σ	x	σ						
12:00	75.2	1.2	58.8	5.8	0.23	0.04	0.21	0.05	0.034	0.00002	0.056	0.071	1.07	0.06	0.43	0.08	0.51	0.02	0.42	0.07	40.1	1.5	42.9	0.02	2.29	0.04	3.95	3.80
12:30	77.9	-	62.9	-	0.27	-	0.12	-	0.062	-	0.038	-	1.24	-	0.47	-	1.51	-	0.62	-	49.0	-	49.3	-	2.37	-	1.05	-
13:00	98.2	4.4	76.3	6.8	0.34	0.01	0.30	0.13	0.045	0.00002	0.073	1.524	1.20	0.04	1.10	0.20	1.44	0.06	1.30	0.21	55.8	2.5	62.2	2.4	1.99	0.14	2.55	4.73
13:30	97.5	2.9	87.2	7.6	0.54	0.06	0.50	0.17	0.017	0.00001	0.109	3.384	1.48	0.04	1.40	0.29	1.72	0.02	1.60	0.31	63.4	1.0	70.5	5.3	1.79	0.14	2.18	5.66
14:00	111.2	2.4	87.6	15.0	0.74	0.04	1.31	0.47	0.080	0.009	0.206	9.556	1.34	0.04	1.60	0.82	2.75	0.19	1.96	0.83	54.8	2.1	75.4	15.0	2.12	0.02	2.32	12.10
14:30	140.0	5.7	118.7	10.7	1.00	0.49	0.72	0.25	0.082	0.046	0.165	5.074	1.11	0.09	1.16	0.43	1.79	0.21	1.28	0.44	73.0	2.1	88.0	7.9	2.30	0.89	3.15	7.89
15:00	131.3	-	151.4	-	1.21	-	1.26	-	0.084	0.009	0.176	-	1.91	-	2.04	-	1.73	-	2.28	-	149.0	-	118.7	-	3.13	-	3.26	-
15:30	119.1	2.5	110.4	12.8	1.15	0.02	1.09	0.38	0.054	0.004	0.186	7.753	1.30	0.08	1.33	0.67	1.91	0.03	1.57	0.67	72.6	5.2	86.7	12.2	2.35	0.09	2.95	10.13
16:00	109.6	2.9	98.8	11.4	1.05	0.11	0.97	0.34	0.039	0.021	0.161	6.876	1.27	0.07	1.08	0.59	1.50	0.04	1.28	0.60	61.9	1.2	76.6	10.8	1.82	0.11	2.32	9.00
16:30	123.4	0.5	112.1	14.5	1.34	0.11	1.24	0.45	0.046	0.00002	0.196	8.999	1.52	0.07	1.13	0.77	1.45	0.13	1.33	0.78	67.9	2.6	85.9	14.1	1.92	0.11	2.52	11.52
17:00	123.3	10.2	106.8	8.9	1.49	0.11	1.48	0.11	0.044	0.00002	0.079	1.936	1.75	0.07	1.53	0.21	1.42	0.08	1.54	0.21	85.7	5.5	91.9	3.0	1.71	0.12	2.28	6.45
17:30	104.3	9.3	69.9	5.8	1.18	0.01	1.17	0.08	0.021	0.008	0.057	1.423	1.58	0.21	0.92	0.16	0.81	0.04	0.90	0.15	57.4	1.4	60.8	2.2	1.48	0.08	1.53	4.32
18:00	77.6	0.9	71.0	6.8	1.18	0.03	1.13	0.19	0.036	0.008	0.077	3.644	1.30	0.04	0.92	0.32	0.86	0.04	0.97	0.33	52.2	0.9	60.3	5.8	1.64	0.02	1.72	5.32
18:30	79.2	0.8	70.5	11.7	1.84	0.13	1.73	0.37	0.073	0.014	0.134	7.354	1.46	0.07	1.07	0.64	1.30	0.03	1.24	0.64	50.2	1.1	64.7	11.6	1.45	0.1	1.98	9.46
19:00	71.1	1.2	63.8	10.9	1.18	0.05	1.09	0.35	0.033	0.007	0.117	6.853	1.16	0.04	0.90	0.60	1.2	0.02	1.13	0.60	43.3	0.8	55.0	10.8	1.5	0.001	1.91	8.75
19:30	66.2	0.7	56.3	5.9	0.32	0.40	0.47	0.17	0.007	0.010	0.068	3.405	0.90	0.03	0.73	0.29	1.02	0.07	0.82	0.30	30.7	1.0	44.0	5.4	0.83	0.01	1.27	4.63
20:00	66.1	-	59.0	-	0.32	-	0.49	-	0.025	-	0.055	-	0.83	-	0.43	-	0.34	-	0.44	-	33.7	-	42.7	-	0.74	-	1.19	-
20:30	26.2	-	39.8	-	0.27	-	0.22	-	0.025	-	0.026	-	0.61	-	0.28	-	0.10	-	0.27	-	23.5	-	28.2	-	0.42	-	0.74	-

C4. continued from the previous page.

Time	Na			Ni			Pb			Se			V			Zn								
	Observed	CMB pred.	$\sigma$																					
12:00	349	5	352	35	2.96	0.06	2.71	0.39	1.11	0.00	1.48	0.07	0.10	0.03	0.02	0.05	4.10	0.20	2.03	0.07	3.44	0.94	0.91	0.11
12:30	355	-	357	-	8.77	-	10.45	-	2.42	-	5.05	-	0.35	-	0.03	-	11.15	0.18	7.52	-	8.17	-	2.62	-
13:00	317	3	317	30	4.41	0.00	6.20	2.39	3.08	0.02	4.26	1.33	0.84	0.40	1.08	2.06	5.86	0.47	4.27	1.13	5.36	0.34	3.13	2.39
13:30	289	6	289	27	1.51	0.07	2.21	5.26	3.83	0.02	4.13	2.92	0.88	0.09	2.36	4.57	2.56	0.16	1.32	2.47	4.65	1.41	4.66	5.26
14:00	308	5	308	28	1.60	0.50	0.92	15.02	5.30	0.01	5.45	8.34	1.47	0.31	6.69	13.00	2.29	0.09	0.25	7.06	3.88	0.15	6.89	15.02
14:30	303	4	303	28	1.36	0.85	1.41	7.86	5.46	0.72	4.96	4.36	1.05	0.40	3.51	6.84	2.41	0.00	0.94	3.70	3.36	0.23	6.42	7.86
15:00	298	4	298	-	1.11	-	1.12	-	5.62	-	4.54	-	1.48	-	6.38	-	2.53	0.21	0.46	-	5.94	-	5.38	-
15:30	329	9	329	30	1.37	0.10	2.53	12.17	4.94	0.01	5.38	6.76	1.52	0.06	5.43	10.54	3.46	0.10	1.61	5.73	5.50	0.23	6.27	12.17
16:00	354	3	354	33	1.58	0.13	2.44	10.80	4.19	0.08	4.68	6.00	1.60	0.31	4.82	9.35	4.04	0.03	1.61	5.08	5.09	0.28	5.38	10.80
16:30	368	8	368	34	1.54	0.10	1.43	14.15	3.82	0.02	4.91	7.86	2.23	0.17	6.31	12.25	3.86	0.19	0.90	6.66	7.45	1.48	6.12	14.15
17:00	421	18	421	41	1.59	0.03	3.74	3.02	3.40	0.01	3.92	1.68	2.02	0.35	1.37	2.62	3.98	0.06	2.77	1.43	4.94	0.22	3.61	3.02
17:30	408	5	408	40	1.22	0.09	2.84	2.24	2.19	0.01	2.59	1.24	1.15	0.20	1.02	1.93	3.73	0.63	2.17	1.06	3.40	0.88	2.23	2.23
18:00	438	12	438	42	2.09	0.01	2.63	5.76	1.83	0.01	2.38	3.20	1.43	0.19	2.58	4.97	3.75	0.14	1.91	2.71	3.25	0.29	1.92	5.76
18:30	458	13	458	43	1.66	0.03	3.40	11.62	2.54	0.02	3.60	6.45	2.73	0.16	5.19	10.04	5.49	0.06	2.38	5.46	4.76	0.19	3.15	11.62
19:00	405	11	405	38	1.5	0.05	3.91	10.83	2.0	0.13	3.21	6.01	1.37	0.01	4.83	9.36	5.48	0.18	2.63	5.09	4.59	5.16	2.40	10.83
19:30	246	5	246	23	0.90	0.09	0.41	5.37	0.44	0.00	1.53	2.98	0.06	0.14	2.40	4.64	2.15	0.12	0.18	2.53	2.95	0.09	1.78	5.37
20:00	283	-	283	-	0.64	-	0.56	-	0.40	-	0.72	-	0.36	-	2.47	-	2.17	0.18	0.42	-	0.81	-	0.61	-
20:30	127	-	127	-	0.34	-	0.15	-	0.16	-	0.34	-	0.10	-	1.14	-	0.67	0.01	0.13	-	1.28	-	0.34	-

**C5.** Table of CMB predicted source contributions in ng of total PM<sub>2.5</sub> / m<sup>3</sup> for the generic source-types used in the model plotted in Figure 11.

Time	Oil		Coal		GCR		Incinerator		Soil		Smoothed Soil		Sea Salt		Sand blasting	
	SCE	σ	SCE	σ	SCE	σ	SCE	σ	SCE	σ	SCE	σ	SCE	σ	SCE	σ
<b>12:00</b>	100	6	-	-	-	-	-	-	311	14	311	14	1137	115	71	15
<b>12:30</b>	409	10	-	-	-	-	-	-	327	7	327	7	1117	112	-	-
<b>13:00</b>	224	54	190	128	1.7	7.2	-	-	327	58	327	58	988	100	71	15
<b>13:30</b>	58	112	421	178	0.6	8.7	17.4	21.5	300	77	314	77	892	93	108	22
<b>14:00</b>	-	-	627	246	6.3	11.1	56.0	28.8	302	106	302	106	938	99	134	52
<b>14:30</b>	31	167	786	521	3.9	14.0	46.2	36.4	385	215	272	215	911	103	77	33
<b>15:00</b>	-	-	1144	417	-	-	18.6	53.7	368	180	242	180	866	97	157	49
<b>15:30</b>	71	257	974	381	0.8	15.6	25.2	48.9	212	160	212	160	975	110	95	48
<b>16:00</b>	73	228	864	353	0.2	13.9	21.4	43.3	193	148	193	148	1066	114	-	-
<b>16:30</b>	32	298	1132	429	-	-	26.2	56.9	163	180	163	180	1093	122	77	56
<b>17:00</b>	119	65	1283	485	-	-	7.9	64.3	132	208	132	208	1252	148	94	63
<b>17:30</b>	95	53	993	367	-	-	4.5	9.5	109	159	109	159	1241	132	58	49
<b>18:00</b>	86	123	1004	374	-	-	2.5	23.4	123	47	123	47	1334	145	58	49
<b>18:30</b>	112	245	929	162	0.1	8.2	6.8	46.6	79	104	79	104	1402	149	68	46
<b>19:00</b>	135	229	866	151	0.4	13.4	3.1	45.2	91	60	91	60	1232	132	61	43
<b>19:30</b>	-	-	430	174	0.1	7.1	5.8	20.1	135	74	135	74	764	80	56	19
<b>20:00</b>	13	109	443	173	-	-	-	-	147	73	147	73	887	91	24	22
<b>20:30</b>	-	-	204	74	-	-	0.2	9.7	136	35	136	35	397	41	16	9

**C6.** Table of elemental concentrations and uncertainties in  $\text{ng/m}^3$  in ambient air samples as determined by GFAAZ and ICPMS plotted in Figure 13.

Time	Al		As		Cr		Cu		Fe											
	GFAAZ x	ICPMS σ																		
12:00	63.7	1.2	75.2	1.2	0.14	0.04	0.23	0.04	1.08	0.02	0.65	0.02	0.80	0.07	0.51	0.02	40.1	1.4	145	0.6
12:30	73.9	0.3	77.9	0.3	0.10	0.08	0.27	0.08	1.25	0.05	0.40	0.05	1.54	0.1	1.51	0.03	49.0	0.3	65.9	0.2
13:00	71.7	4.4	98.2	4.4	0.97	0.01	0.34	0.01	1.19	0.07	0.68	0.07	1.68	0.14	1.44	0.06	55.8	2.4	82.9	7.2
13:30	80.4	2.9	97.5	2.9	0.28	0.06	0.54	0.06	1.48	0.08	0.53	0.08	2.12	0.01	1.72	0.02	63.4	0.7	78.8	1.0
14:00	75.8	2.4	111.2	2.4	0.45	0.04	0.74	0.04	1.34	0.00	0.35	0.00	3.28	0.07	2.75	0.19	54.8	1.9	77.6	0.2
14:30	109.4	0.6	64.9	0.6	0.64	0.10	0.50	0.10	1.10	0.02	0.34	0.02	2.10	0.05	1.07	0.07	73.0	2.0	49.5	1.0
15:00	89.2	2.1	131.3	2.1	0.79	0.04	1.21	0.04	1.91	0.005	0.64	0.005	2.14	0.1	1.73	0.01	349	6.2	644	2.3
15:30	89.1	2.5	119.1	2.5	0.93	0.02	1.15	0.02	1.32	0.10	0.41	0.10	2.18	0.05	1.91	0.03	72.6	5.2	117	2.9
16:00	84.0	2.9	109.6	2.9	0.83	0.11	1.05	0.11	1.27	0.05	0.51	0.05	1.99	0.06	1.50	0.04	61.9	1.1	84.1	0.3
16:30	102.3	0.5	123.4	0.5	1.18	0.11	1.34	0.11	1.51	0.02	0.61	0.02	1.80	0.01	1.45	0.13	67.9	2.5	93.2	0.2
17:00	96.8	10.2	123.3	10.2	1.21	0.11	1.49	0.11	1.76	0.04	1.02	0.04	1.62	0.13	1.42	0.08	85.7	5.4	94.9	0.2
17:30	71.0	9.3	104.3	9.3	0.98	0.01	1.18	0.01	1.56	0.01	0.63	0.01	1.10	0.12	0.81	0.04	57.4	1.2	82.8	1.2
18:00	64.8	0.9	77.6	0.9	0.98	0.03	1.18	0.03	1.32	0.09	0.41	0.09	1.17	0.04	0.86	0.04	52.2	0.6	61.2	1.2
18:30	63.6	0.8	79.2	0.8	1.57	0.13	1.84	0.13	1.44	0.00	0.77	0.00	1.45	0.12	1.30	0.03	50.2	0.9	63.0	2.2
19:00	51.4	1.2	71.1	1.2	1.16	0.05	1.18	0.05	1.14	0.04	0.34	0.04	1.0	0.03	6.44	0.02	43.3	0.4	53.8	1.7
19:30	43.0	0.7	66.2	0.7	0.32	0.06	0.55	0.06	0.92	0.06	1.26	0.06	0.39	0.06	1.02	0.07	30.7	0.8	62.8	0.4
20:00	36.0	1.7	66.1	1.7	0.21	0.06	0.55	0.06	0.83	0.04	0.33	0.04	0.42	0.1	0.34	0.06	33.7	1.0	55.1	0.8
20:30	134.5	3.0	26.2	3.0	0.27	0.004	0.26	0.004	0.60	0.02	0.36	0.02	0.27	0.1	-0.01	-0.03	23.6	0.2	28.0	1.1

C6. continued from the previous page.

Time	Mn			Ni			Pb			Se			Zn							
	GFAAZ	ICPMS	$\sigma$																	
12:00	1.52	0.02	2.29	0.04	2.21	0.21	2.96	0.06	1.07	0.28	1.11	0.001	0.28	0.13	-0.10	-0.14	5.33	0.07	2.00	0.07
12:30	1.61	0.03	2.37	0.33	5.90	0.1	8.77	0.19	1.82	0.3	2.42	0.02	0	0.14	0.35	0.13	8.02	0.09	8.25	0.06
13:00	1.40	0.02	1.99	0.14	3.35	0.38	4.41	0.002	2.68	0.22	3.08	0.02	0.81	0.30	0.84	0.40	5.86	0.14	4.84	0.16
13:30	1.12	0.10	1.79	0.14	1.64	0.22	1.51	0.07	3.56	0.75	3.83	0.02	0.96	0.26	0.88	0.09	5.12	0.09	2.49	0.58
14:00	1.17	0.10	2.12	0.02	0.99	0.26	1.60	0.50	4.26	0.69	5.30	0.01	1.34	0.40	1.47	0.31	3.94	0.10	3.82	0.17
14:30	1.42	0.12	1.11	0.09	1.39	0.26	0.46	0.04	4.72	0.30	2.82	0.002	1.05	0.32	0.75	0.14	3.86	0.08	1.56	0.07
15:00	2.10	0.15	3.13	0.21	1.27	0.6	1.11	0.07	5.37	0.9	5.62	0.13	1.39	0.08	1.48	0.24	6.55	0.06	2.20	0.56
15:30	1.59	0.02	2.35	0.09	1.11	0.17	1.37	0.10	3.88	0.48	4.94	0.01	1.86	0.36	1.52	0.06	5.40	0.11	5.86	0.47
16:00	1.36	0.03	1.82	0.11	1.07	0.33	1.58	0.13	3.29	0.75	4.19	0.08	1.69	0.30	1.60	0.31	5.17	0.16	4.76	0.68
16:30	1.40	0.04	1.92	0.11	1.17	0.12	1.54	0.10	3.15	0.66	3.82	0.02	2.40	0.26	2.23	0.17	8.27	0.12	5.18	0.39
17:00	1.41	0.07	1.71	0.12	1.00	0.34	1.59	0.03	2.50	0.45	3.40	0.01	2.27	0.12	2.02	0.35	5.72	0.17	4.61	0.08
17:30	0.84	0.09	1.48	0.08	1.03	0.38	1.22	0.09	1.67	0.41	2.19	0.01	1.40	0.12	1.15	0.20	4.11	0.19	2.05	0.39
18:00	1.12	0.05	1.64	0.02	1.66	0.09	2.09	0.01	1.73	0.23	1.83	0.01	1.48	0.02	1.43	0.19	3.73	0.22	2.80	0.23
18:30	1.15	0.09	1.45	0.10	1.39	0.09	1.66	0.03	2.40	0.22	2.54	0.02	2.62	0.06	2.73	0.16	4.83	0.16	4.68	0.21
19:00	0.9	0.06	1.45	0.00	1.2	0.09	2.55	0.05	1.5	0.43	2.55	0.13	1.23	0.21	1.37	0.01	4.31	0.09	136	50
19:30	0.13	0.10	0.83	0.01	0.43	0.16	0.90	0.09	0.41	0.29	0.44	0.003	0.63	0.19	0.06	0.14	-1.29	0.03	2.94	0.05
20:00	0.11	0.07	0.74	0.06	0.05	0.1	0.64	0.03	0.87	0.2	0.40	0.03	0.10	0.04	0.36	0.15	1.40	0.15	-0.69	-0.17
20:30	0.26	0.05	0.42	0.06	0.21	0.1	0.34	0.08	0.15	0.1	0.16	0.01	0.19	0.02	-0.02	-0.06	1.64	0.02	0.22	0.11

C6. continued from the previous page.

Time	Ag		Ba		Ca		Cd		K		Mg		Na		Sb		Sr		V		W	
	ICPMS	$\sigma$	ICPMS	$\sigma$	ICPMS	$\sigma$	ICPMS	$\sigma$	ICPMS	$\sigma$	ICPMS	$\sigma$	ICPMS	$\sigma$	ICPMS	$\sigma$	ICPMS	$\sigma$	ICPMS	$\sigma$	ICPMS	$\sigma$
12:00	-	-	3.18	0.11	239	11	0.03	NS	73.2	1.0	84.5	0.9	349	5	-	-	1.81	0.08	4.10	0.20	-	-
12:30	-	-	4.22	0.14	261	11	0.06	0.03	79.1	2.6	91.4	0.8	355	1	-	-	1.96	0.01	11.15	0.18	-	-
13:00	-	-	4.51	0.02	259	8	0.05	NS	57.8	6.6	78.4	1.5	317	3	-	-	1.74	0.12	5.86	0.47	-	-
13:30	0.030	0.004	3.67	0.17	227	7	0.02	NS	51.6	6.5	70.1	1.4	289	6	0.22	0.01	1.66	0.02	2.56	0.16	0.68	0.04
14:00	0.063	0.004	4.54	0.11	257	5	0.08	0.01	71.2	8.2	74.3	9.2	308	5	0.32	0.06	1.82	0.07	2.29	0.09	0.80	0.06
14:30	0.012	0.003	2.34	0.02	124	2	0.02	0.003	20.7	1.9	35.1	0.7	139	4	0.12	0.00	0.95	0.003	1.03	0.00	0.40	0.00
15:00	0.060	0.033	5.81	0.13	266	4	0.08	0.01	54.3	0.4	76.8	4.1	298	4	0.27	0.02	1.95	0.13	2.53	0.21	0.69	0.07
15:30	0.015	0.000	5.32	0.33	262	9	0.05	0.004	61.5	1.9	78.0	2.1	329	9	0.25	0.02	1.94	0.02	3.46	0.10	0.36	0.01
16:00	0.014	0.004	5.19	0.39	232	3	0.04	0.02	58.3	0.1	73.7	5.2	354	3	0.21	0.02	1.94	0.05	4.04	0.03	0.36	0.01
16:30	0.004	0.004	5.60	0.12	238	7	0.05	NS	59.6	0.9	71.7	3.1	368	8	0.27	0.02	2.04	0.12	3.86	0.19	0.27	0.05
17:00	0	NS	5.84	0.24	295	9	0.04	NS	69.9	0.2	76.1	0.3	421	18	0.33	0.09	1.92	0.19	3.98	0.06	0.24	0.004
17:30	0.012	0.008	4.94	0.08	211	1	0.02	0.01	45.0	2.1	68.6	1.3	408	5	0.26	0.02	1.70	0.17	3.73	0.63	0.27	0.01
18:00	0.004	0.004	4.67	0.15	177	12	0.04	0.01	61.4	3.5	64.8	1.0	438	12	0.19	0.02	1.38	0.06	3.75	0.14	0.19	0.01
18:30	0.007	NS	6.80	0.15	208	6	0.07	0.01	71.7	0.9	80.3	2.8	458	13	0.25	0.03	1.68	0.03	5.49	0.06	0.17	0.003
19:00	0	NS	5.91	0.17	405	24	0.03	0.01	421	53.6	81.7	0.6	641	11	0.47	0.02	1.53	0.12	5.48	0.18	0.16	0.05
19:30	-0.003	NS	1.75	0.10	123	1	0.01	0.01	65.4	2.5	44.6	2.1	246	5	0.14	0.01	0.58	0.03	2.15	0.12	0.16	0.01
20:00	0.006	0.006	2.79	0.18	102	2	0.02	0.02	51.0	4.6	51.3	1.4	283	2	0.13	0.03	0.62	0.04	2.17	0.18	0.15	0.05
20:30	0.004	0.004	0.91	0.03	52	3	0.02	0.004	17.0	1.9	28.7	0.03	127	1	0.07	0.01	0.32	0.04	0.67	0.01	0.10	0.01

NS - uncertainties < 0.001

C7. Table of  $X/Q^{MET}$ ,  $X/Q^{traj}$ , and  $X/Q^{iPDRM}$  values in ( $\cdot 10^{-8} \text{ s/m}^3$ ) plotted in Figures 14 and 15.

	Manatee			Big Bend			Gannon			Bartow									
	$X/Q^{MET}$	$X/Q^{traj}$	$X/Q^{iPDRM}$																
	100-m 500-m Total			100-m 500-m Total			100-m 500-m Total			100-m 500-m Total									
12:00	0.58	-	0.52	0.34	0.23	0	0	0	0	0	0	0	0	0	0	0			
12:30	0.45	-	1.17	1.17	0.33	0.09	0.11	0.20	0.37	0	0	0	0	0	0	0			
13:00	0	-	0.23	0.23	2.57	0.97	0.47	1.45	3.01	0.01	0	0	0	0	0	0			
13:30	0	-	0.01	0.01	1.21	2.31	1.16	3.51	7.02	0.25	0	0	0	0.02	0	0			
14:00	0	-	0	0	0.15	0.57	1.72	2.30	4.74	1.76	0.49	0.00	0.49	0.48	0.51	0	0		
14:30	0	-	0	0	0	0.07	1.21	1.28	2.54	1.85	2.28	0.02	2.30	2.51	1.14	0	0		
15:00	0	-	0	0	0	0	0.60	0.60	1.09	1.62	2.45	0.11	2.56	2.49	0.96	0	0		
15:30	0	-	0	0	0	0	0.15	0.15	0.28	1.29	2.34	0.36	2.70	2.87	0.71	0.49	0.01	0.50	0.26
16:00	0	-	0	0	0.01	0	0.04	0.04	0.07	3.28	2.88	0.93	3.81	2.76	1.78	0.72	0.02	0.74	0.42
16:30	0	-	0	0	0	0	0.01	0.01	0.02	3.38	3.00	1.88	4.88	3.83	2.23	1.66	0.04	1.70	0.30
17:00	0	-	0	0	0	0	0.02	0.02	0.04	3.67	2.70	1.01	3.71	3.63	2.11	2.13	0.16	2.29	0.34
17:30	0	-	0	0	0.01	0	0.05	0.05	0.09	3.49	2.88	0.36	3.24	2.90	1.64	2.27	0.15	2.42	0.36
18:00	0	-	0	0	0	0	0.35	0.35	0.63	3.16	3.39	0.07	3.46	2.47	2.26	2.26	0.11	2.37	0.49
18:30	0	-	0	0	0	0	0.15	0.15	0.27	4.36	3.72	0.29	4.01	3.38	3.17	2.50	0.06	2.56	0.56
19:00	0	-	0	0	0	0	0.02	0.02	0.04	4.15	3.25	1.19	4.44	3.58	3.25	2.13	0.03	2.16	0.50
19:30	0	-	0	0	0	0	0	0	0	1.14	1.84	0.37	2.21	1.08	0.16	3.50	0	3.50	0.34
20:00	0	-	0	0	0	0	0	0	0	0.57	0	0.01	0.01	0.001	0.26	0.84	0	0.84	0.35
20:30	0	-	0	0	0	0	0	0	0	0.01	0	0	0	0	0	0.02	0	0.02	0.02

C7. continued from the previous page.

	<b>Cargill</b>		<b>Gulf Coast Recyc.</b>		<b>McKay</b>		<b>PCRR</b>		<b>Shipyard</b>		<b>Soil</b>		<b>Sea Salt</b>	
	$X/Q_{MET}$	$X/Q_{traj}$	$X/Q_{MET}$	$X/Q_{traj}$	$X/Q_{traj}$	$X/Q_{traj}$	$X/Q_{traj}$	$X/Q_{traj}$	$X/Q_{traj}$	$X/Q_{traj}$	$SC_{SC^{iPDRM}}$	$SC_{SC^{iPDRM}}$	$SC_{SC^{iPDRM}}$	$SC_{SC^{iPDRM}}$
<b>12:00</b>	0.01	0	0	0	0	0	0	0	0	0	31.1	35.3	113.7	100.6
<b>12:30</b>	0.02	0	0	0	0	0	0	0	0	0	32.7	36.4	111.7	104.7
<b>13:00</b>	0.91	0.35	0	0	0	0	0	0	0	0	32.7	36.8	98.8	89.9
<b>13:30</b>	4.30	2.72	0	0.01	0.001	0	0	0	0	0	31.4	26.8	89.2	77.2
<b>14:00</b>	4.18	4.02	0.14	5.64	1.43	0.38	0.37	0	0.27	0.27	30.2	25.9	93.8	99.4
<b>14:30</b>	0.16	2.41	5.18	4.20	2.31	3.76	0.24	0	0.96	0.63	27.2	23.1	91.1	77.9
<b>15:00</b>	0.14	0.67	5.54	5.60	2.22	3.98	0.91	0	8.18	3.17	24.2	22.9	86.6	91.1
<b>15:30</b>	0.08	0.52	6.40	2.16	0.94	3.74	1.56	0	7.25	1.32	21.2	22.4	97.5	96.6
<b>16:00</b>	1.91	2.57	0.93	1.86	0.86	1.38	1.17	0	6.59	1.07	19.3	19.4	106.6	99.2
<b>16:30</b>	0.71	1.26	2.36	1.62	0.11	2.37	1.85	0.23	3.32	0.91	16.3	18.5	109.3	103.6
<b>17:00</b>	1.61	2.43	1.00	2.04	0.51	2.25	0.91	1.15	2.87	1.64	13.2	15.1	125.2	120.3
<b>17:30</b>	2.60	0.18	0.42	1.42	0.39	1.76	0.11	2.33	2.25	0.85	10.9	12.5	124.1	109.7
<b>18:00</b>	0.22	0.31	4.01	3.03	0.15	2.60	0.15	2.44	5.19	0.90	12.3	10.5	133.4	113.9
<b>18:30</b>	0.46	0.08	2.01	0.50	0.22	0.79	0.60	1.67	1.92	0.33	7.9	6.7	140.2	159.5
<b>19:00</b>	0.33	0.71	2.84	0.17	0.11	0.38	0.29	1.20	2.81	0.35	9.1	7.7	123.2	126.4
<b>19:30</b>	10.15	1.60	0	0.01	0.001	0.01	0.001	0.68	0.44	0.23	13.5	15.5	76.4	65.5
<b>20:00</b>	3.71	25.5	0	0	0	0	0	0.69	0	0	14.7	16.8	88.7	88.9
<b>20:30</b>	5.28	38.0	0	0	0	0	0	0	0	0	13.6	11.6	39.7	38.2

**C8.** Table of observed concentrations (hybrid dataset) and uncertainties and predicted concentrations in  $\mu\text{g}/\text{m}^3$  for  $\text{SO}_2$  and  $\text{NH}_3$  and in  $\text{ng}/\text{m}^3$  for elements plotted in Figure 17.

	$\text{SO}_2$ ( $\mu\text{g}/\text{m}^3$ )			$\text{NH}_3$ ( $\mu\text{g}/\text{m}^3$ )			$\text{Ag}$ ( $\text{ng}/\text{m}^3$ )			$\text{Al}$ ( $\text{ng}/\text{m}^3$ )			$\text{As}$ ( $\text{ng}/\text{m}^3$ )			$\text{Ba}$ ( $\text{ng}/\text{m}^3$ )			$\text{Ca}$ ( $\text{ng}/\text{m}^3$ )		
	Obs.	Pred.	$\sigma$	Obs.	Pred.	$\sigma$	Obs.	Pred.	$\sigma$	Obs.	Pred.	$\sigma$	Obs.	Pred.	$\sigma$	Obs.	Pred.	$\sigma$	Obs.	Pred.	$\sigma$
<b>12:00</b>	1.8	3.6	1.8	5.6	0.4	5.1	-	-	-	75.2	1.2	67.4	0.23	0.04	0.31	3.18	0.11	2.65	239	11	182
<b>12:30</b>	12.9	11.8	2.0	5.5	0.4	5.3	-	-	-	77.9	0.3	75.2	0.27	0.08	0.35	4.22	0.14	4.36	261	11	214
<b>13:00</b>	13.1	14.7	1.8	4.7	0.4	5.8	-	-	-	98.2	4.4	91.6	0.34	0.01	0.40	4.51	0.02	4.07	259	8	241
<b>13:30</b>	27.3	24.2	2.5	6.2	0.4	5.7	-	-	-	97.5	2.9	99.9	0.54	0.06	0.51	3.67	0.17	4.26	227	7	251
<b>14:00</b>	29.3	31.2	7.9	5.9	0.4	5.9	0.058	0.005	0.035	111.2	2.4	110.9	0.74	0.04	0.72	4.54	0.11	4.13	257	5	236
<b>14:30</b>	78.9	78.7	6.6	4.6	0.4	5.0	0.057	0.004	0.056	140.0	5.7	140.8	1.00	0.49	1.08	5.18	0.02	5.75	262	2	269
<b>15:00</b>	73.1	72.9	0.6	4.1	0.4	4.1	0.056	0.033	0.054	131.3	2.1	135.3	1.21	0.04	1.17	5.81	0.13	5.15	266	4	253
<b>15:30</b>	83.3	81.6	3.0	3.9	0.4	4.0	0.011	0.010	0.023	119.1	2.5	116.7	1.15	0.02	1.21	5.32	0.33	5.42	262	9	249
<b>16:00</b>	80.3	80.4	1.0	3.6	0.4	4.4	0.010	0.005	0.021	109.6	2.9	107.4	1.05	0.11	1.19	5.19	0.39	5.23	232	3	229
<b>16:30</b>	101.1	106.2	5.0	3.5	0.4	3.9	-0.001	0.005	0.003	123.4	0.5	116.2	1.34	0.11	1.41	5.60	0.12	6.50	238	7	269
<b>17:00</b>	97.0	102.2	2.5	3.3	0.4	3.9	-0.0001	0.010	0.013	123.3	10.2	113.6	1.49	0.11	1.41	5.84	0.24	6.25	295	9	252
<b>17:30</b>	79.1	82.5	5.0	3.4	0.4	2.5	0.008	0.009	0.010	104.3	9.3	89.8	1.18	0.01	1.15	4.94	0.08	5.08	211	1	203
<b>18:00</b>	80.0	74.1	3.3	3.8	0.4	2.3	-0.0002	0.005	0.004	77.6	0.9	79.1	1.18	0.03	1.11	4.67	0.15	4.72	177	12	187
<b>18:30</b>	100.8	97.7	11.1	3.6	0.4	1.8	0.003	0.010	0.006	79.2	0.8	87.3	1.84	0.13	1.46	6.80	0.15	5.85	208	6	209
<b>19:00</b>	106.5	101.5	13.8	3.2	0.4	2.1	-0.0001	0.010	0.003	71.1	1.2	89.9	1.18	0.05	1.36	5.91	0.17	5.91	187	24	212
<b>19:30</b>	32.7	33.2	16.5	3.5	0.4	3.2	-0.0001	0.010	0.0001	66.2	0.7	52.6	0.32	0.40	0.54	1.75	0.10	2.57	123	1	128
<b>20:00</b>	10.4	12.3	3.3	13.2	0.6	14.1	0.001	0.006	0.001	66.1	1.7	49.5	0.32	0.40	0.36	2.79	0.18	2.16	102	2	119
<b>20:30</b>	12.1	10.3	0.2	16.7	0.7	15.9	0.000	0.005	0.001	26.2	3.0	42.5	0.27	0.39	0.13	0.91	0.03	1.79	52	3	93

C8. continued from the previous page.

	Cd (ng/m <sup>3</sup> )		Cr (ng/m <sup>3</sup> )		Cu (ng/m <sup>3</sup> )		Fe (ng/m <sup>3</sup> )		Mg (ng/m <sup>3</sup> )		Mn (ng/m <sup>3</sup> )		Na (ng/m <sup>3</sup> )								
	X	σ	Obs.	Pred.	X	σ	Obs.	Pred.	X	σ	Obs.	Pred.	X	σ	Obs.	Pred.					
<b>12:00</b>	0.034	NS	0.033	1.07	0.06	1.11	0.51	0.02	0.66	40.1	1.5	42.0	84.5	0.9	58.0	1.04	0.02	0.49	349	5	317
<b>12:30</b>	0.062	0.035	0.078	1.24	0.04	1.24	1.51	0.03	1.64	49.0	0.8	47.0	91.4	0.8	82.5	1.13	0.03	1.31	355	1	339
<b>13:00</b>	0.045	NS	0.040	1.20	0.04	1.45	1.44	0.06	1.68	55.8	2.5	57.0	78.4	1.5	75.4	0.92	0.02	0.89	317	3	298
<b>13:30</b>	0.017	NS	0.013	1.48	0.04	1.49	1.72	0.02	2.29	63.4	1.0	61.6	70.1	1.4	77.0	0.64	0.10	0.76	289	6	271
<b>14:00</b>	0.080	0.009	0.071	1.34	0.04	1.42	2.75	0.19	1.85	54.8	2.1	62.9	74.3	9.2	75.2	0.69	0.10	0.99	308	5	336
<b>14:30</b>	0.082	0.046	0.103	1.11	0.09	1.55	1.79	0.21	1.58	73.0	2.1	75.0	75.6	0.7	71.1	0.94	0.12	1.17	303	4	287
<b>15:00</b>	0.084	0.009	0.101	1.91	0.05	2.01	1.73	0.01	2.38	149	6.3	121	76.8	4.1	71.5	1.62	0.15	1.40	298	4	321
<b>15:30</b>	0.054	0.004	0.062	1.30	0.08	1.65	1.91	0.03	1.44	72.6	5.2	80.5	78.0	2.1	70.3	1.11	0.02	1.10	329	9	339
<b>16:00</b>	0.039	0.021	0.064	1.27	0.07	1.55	1.50	0.04	1.30	61.9	1.2	70.4	73.7	5.2	69.1	0.88	0.03	0.98	354	3	346
<b>16:30</b>	0.046	NS	0.034	1.52	0.07	1.59	1.45	0.13	1.31	67.9	2.6	73.2	71.7	3.1	76.7	0.92	0.04	1.06	368	8	370
<b>17:00</b>	0.044	NS	0.052	1.75	0.07	1.67	1.42	0.08	1.64	85.7	5.5	84.0	76.1	0.3	81.2	0.93	0.07	1.02	421	18	419
<b>17:30</b>	0.021	0.008	0.044	1.58	0.21	1.26	0.81	0.04	1.14	57.4	1.4	57.8	68.6	1.3	69.7	0.57	0.09	0.66	408	5	376
<b>18:00</b>	0.036	0.008	0.039	1.30	0.04	1.25	0.86	0.04	1.32	52.2	0.9	54.9	64.8	1.0	71.2	0.64	0.05	0.63	438	12	385
<b>18:30</b>	0.073	0.014	0.050	1.46	0.07	1.13	1.30	0.03	1.15	50.2	1.1	44.3	80.3	2.8	89.3	0.67	0.09	0.74	458	13	533
<b>19:00</b>	0.033	0.007	0.041	1.16	0.04	1.16	1.23	0.02	1.04	43.3	0.8	46.6	71.4	3.0	78.5	0.38	0.06	0.67	405	11	435
<b>19:30</b>	0.007	0.010	0.021	0.90	0.03	0.88	1.02	0.07	0.51	30.7	1.0	32.5	44.6	2.1	40.0	0.13	0.10	0.27	246	5	218
<b>20:00</b>	0.025	0.017	0.035	0.83	0.06	1.02	0.34	0.06	0.37	33.7	1.1	29.6	51.3	1.4	41.5	0.11	0.07	0.42	283	2	283
<b>20:30</b>	0.025	0.004	0.021	0.61	0.02	0.79	0.10	0.03	0.17	23.5	0.4	25.5	28.7	0.03	20.2	0.26	0.05	0.42	127	1	129

NS - uncertainties < 0.001

C8. continued from the previous page.

	Ni (ng/m <sup>3</sup> )		Pb (ng/m <sup>3</sup> )		Sb (ng/m <sup>3</sup> )		Se (ng/m <sup>3</sup> )		Sr (ng/m <sup>3</sup> )		V (ng/m <sup>3</sup> )		W (ng/m <sup>3</sup> )		Zn (ng/m <sup>3</sup> )									
	Obs.	Pred.	Obs.	Pred.	Obs.	Pred.	Obs.	Pred.																
12:00	2.96	0.06	2.99	1.11	0.00	0.86	-	-	-	-	-	-	-	-	-	-	2.38	0.41	2.41					
12:30	8.77	0.19	8.71	2.42	0.02	2.69	-	-	-	-	-	-	-	-	-	-	6.85	0.41	6.88					
13:00	4.41	0.00	4.50	3.08	0.02	2.70	-	-	-	-	-	-	-	-	-	-	4.07	0.45	3.99					
13:30	1.51	0.07	1.75	3.83	0.02	3.75	-	-	-	-	-	-	-	-	-	-	2.52	0.77	2.39					
14:00	1.60	0.50	1.31	5.30	0.01	5.35	0.28	0.07	0.15	1.47	0.31	1.24	1.82	0.07	1.92	2.29	0.09	2.27	0.70	0.08	0.46	2.58	0.45	2.67
14:30	1.36	0.85	1.08	5.46	0.72	5.39	0.26	0.04	0.27	1.05	0.40	1.57	1.89	0.00	2.17	2.41	0.00	2.55	0.65	0.05	0.70	2.13	0.41	2.13
15:00	1.11	0.07	1.22	5.62	0.13	6.09	0.23	0.04	0.28	1.48	0.24	1.45	1.95	0.13	2.11	2.53	0.21	2.26	0.59	0.09	0.68	3.08	0.69	3.31
15:30	1.37	0.10	1.33	4.94	0.01	4.90	0.22	0.04	0.23	1.52	0.06	1.65	1.94	0.02	2.06	3.46	0.10	3.38	0.26	0.05	0.32	4.32	0.63	4.65
16:00	1.58	0.13	1.60	4.19	0.08	4.11	0.18	0.04	0.22	1.60	0.31	1.56	1.94	0.05	1.83	4.04	0.03	3.98	0.26	0.05	0.29	3.66	0.80	3.77
16:30	1.54	0.10	1.39	3.82	0.02	4.16	0.23	0.04	0.22	2.23	0.17	2.04	2.04	0.12	2.14	3.86	0.19	4.01	0.17	0.07	0.07	5.42	0.57	5.55
17:00	1.59	0.03	1.60	3.40	0.01	3.54	0.29	0.09	0.24	2.02	0.35	1.84	1.92	0.19	1.91	3.98	0.06	4.17	0.14	0.05	0.18	3.86	0.44	3.82
17:30	1.22	0.09	1.41	2.19	0.01	2.17	0.23	0.04	0.19	1.15	0.20	1.42	1.70	0.17	1.49	3.73	0.63	3.82	0.17	0.05	0.14	1.76	0.59	2.14
18:00	2.09	0.01	1.81	1.83	0.01	2.26	0.15	0.04	0.17	1.43	0.19	1.41	1.38	0.06	1.35	3.75	0.14	4.32	0.09	0.05	0.07	1.93	0.52	2.35
18:30	1.66	0.03	1.87	2.54	0.02	2.81	0.22	0.04	0.20	2.73	0.16	1.85	1.68	0.03	1.49	5.49	0.06	5.23	0.07	0.05	0.08	3.43	0.48	3.23
19:00	1.47	0.05	1.69	2.01	0.13	2.10	0.19	0.23	0.20	1.37	0.01	1.76	1.40	0.12	1.51	5.48	0.18	4.80	0.06	0.07	0.05	2.94	0.45	2.69
19:30	0.90	0.09	1.00	0.44	0.00	0.76	0.11	0.04	0.09	0.06	0.14	0.62	0.58	0.03	0.92	2.15	0.12	2.50	0.06	0.05	0.04	1.72	0.82	0.97
20:00	0.64	0.03	0.94	0.40	0.03	0.55	0.10	0.05	0.11	0.36	0.15	0.25	0.62	0.04	1.00	2.17	0.18	2.32	0.05	0.07	0.04	0.81	0.46	1.16
20:30	0.34	0.08	0.15	0.16	0.01	0.02	0.03	0.04	0.10	0.10	0.03	0.07	0.32	0.04	0.85	0.67	0.01	0.55	0.001	0.05	0.03	0.82	0.41	0.87

C9. Table of Abundance values in g element / g Total PM<sub>2.5</sub> plotted in Figure 18.

	Coal				Oil				Incinerator				
	Literature		iPDRM		Literature		iPDRM		Literature		iPDRM		
	Ab	σ	Wet Scrubber	Ab	σ	Manatee Bartow	Manatee Bartow	Ab	σ	McKay	PCRR		
Ag	0.0004	0.0004	0.0002	0.0002	0.0001	0.0002	-	-	0.0002	0.0001	0	2E-06	
Al	0.25	0.12	0.07	-	0.03	0.04	0.10	0.10	0.03	0.02	0.04	0.027	0.018
As	0.0009	0.0003	0.0009	0.0002	0.0005	0.002	0.003	0.003	0.0003	0.0002	0.0043	0.005	0.006
Ba	5E-03	0.005	0.011	0.01	0.002	0.003	-	-	0.006	0.003	0.01	0.0004	0.001
Ca	0.08	0.04	0.09	0.05	0.08	0.09	-	-	0.05	0.03	0.12	0.004	0.053
Cd	0.0002	0.009	5E-05	0.002	3E-06	2E-06	0	0	0.0001	0.0001	0.0003	0.0002	0.0005
Cr	0.0009	0.009	0.0001	0.0004	0.0004	0.002	0.003	0.003	0.0015	0.0007	0.002	0.0004	0.001
Cu	0.0004	0.0002	0.0002	7E-05	0.001	0.0003	0.002	0.002	0.002	0.0008	0.001	0.0005	0.0004
Fe	0.17	0.17	0.05	0.02	0.02	0.10	0.10	0.026	0.026	0.021	0.07	0.013	0.012
Mg	0.05	0.02	0.03	0.02	0.03	0.02	-	-	-	-	0.12	0.17	0.006
Mn	0.001	-	0.001	0.0004	0.0005	0.0002	0.002	0.003	0.001	0.001	0.002	0.005	0.009
Na	0.04	0.01	0.03	0.02	0.02	0.03	-	-	0.04	0.01	0.04	0.01	0.055
Ni	0.0009	0.0002	0.0002	0.0001	0.001	0.0002	0.005	0.002	0.05	0.025	0.01	0.001	9E-06
Pb	0.001	0.001	0.002	0.001	0.003	0.0001	0.005	0.0006	0.015	0.004	0.002	0.010	0.127
Sb	0.0001	0.0001	0.0001	0.003	-	0.0001	-	-	0.0006	0.002	-	0.0007	0.007
Se	0.0003	0.0003	0.005	0.004	0.001	0.001	0.002	0.003	0.0001	0.0001	0.001	0.001	0.005
Sr	0.006	0.01	0.003	0.001	0.001	0.001	-	-	0.001	0.0001	-	0.001	0.04
V	0.001	0.001	0.0002	0.002	0.001	0.001	-	-	0.05	0.006	-	0.04	0.002
W	-	-	-	-	-	-	5E-07	-	-	-	-	-	0
Zn	0.001	0.007	0.001	0.0004	0.002	0.0005	0.008	0.006	0.026	0.020	0.01	0.005	0.16

\* -Electrostatic Precipitator; † -Wet Scrubber

C9. continued from the previous page.

	Lead Recycling				Phosphate Fertilizer Plant				Steel Sandblast			Soil			Sea Salt			
	Literature		iPDRM		Literature		iPDRM		Lit.		Literature		iPDRM		Literature		iPDRM	
	Ab	$\sigma$	GCR	Park	Ab	$\sigma$	Cargill	Park	Ab	Ab	Ship yard	Agr. Ab	Ind. Ab	Soil	Ab	$\sigma$	Sea Salt	
Ag	0.0005	0.0005	-	0.001	-	-	0	-	-	0	-	-	-	0	-	-	0	
Al	0.05	0.03	0.34	0.65	0.03	0.01	0.204	0.13	0.013	0.02	0.18	0.08	0.18	-	-	-	0.001	
As	0.010	0.006	0.002	0.004	0.0002	0.000	0.001	0.0001	0.0002	0.0002	0	3E-05	0	-	-	-	0.0003	
Ba	0.01	0.02	-	0.001	0.03	-	-	0.007	-	0	0.002	0.002	0.004	-	-	-	0.0002	
Ca	0.01	0.01	-	0.003	0.21	0.24	-	0.22	0.014	0.02	0.05	0.37	0.43	0.01	0.001	0.02	0.02	
Cd	0.005	0.010	-	0.002	0.0001	0.0001	-	0.0001	-	-	-	-	-	-	-	-	0	
Cr	0.0004	0.002	0.006	0.0001	0.001	0.002	0.007	0.003	0.010	0.0017	0.0005	0.002	0.003	-	-	-	0	
Cu	0.0035	0.004	0.008	0.0006	0.0004	0.0001	0.007	0.001	0.012	0.003	0.0002	0.0005	0.0002	-	-	-	2E-05	
Fe	0.06	0.09	0.31	0.07	0.05	0.04	0.27	0.07	0.111	0.14	0.12	0.07	0.12	-	-	-	0	
Mg	0.01	0.01	-	0.002	0.001	0.00	-	0.02	0.012	0.01	0.002	0.02	0.04	0.03	0.003	0.003	0.03	
Mn	0.001	0.001	0.006	0.010	0.002	0.002	0.002	0.002	0.002	0.001	0.003	0.007	0.0002	-	-	-	0	
Na	0.03	0.02	-	0	0.004	0.02	-	0.06	0.014	0.002	0.00	0.01	0.02	0.31	0.03	0.31	0.31	
Ni	0.001	0.000	0.004	0.001	0.0005	0.0003	0.002	0.001	0.006	0.001	0.0002	0.0001	0.0001	-	-	-	0	
Pb	0.60	0.15	0.02	0.08	0.001	0.0003	0.008	-	0.010	0.001	0.0002	0.0005	2E-05	-	-	-	0	
Sb	0.04	0.03	-	0.004	0.002	-	-	0.001	-	-	-	-	8E-05	-	-	-	0	
Se	0.001	0.001	0.002	0.001	0.0001	-	0.002	-	-	7E-07	-	-	-	-	-	-	0.0001	
Sr	0.001	0.0004	-	0.008	0.003	0.004	-	0.003	-	3E-05	0.0006	0.0009	0.003	-	-	-	0	
V	0.0001	0.0001	-	2E-05	0.002	0.002	-	0.001	0.0001	0.0001	0.0006	0.0005	5E-04	-	-	-	0.0006	
W	-	-	-	0.02	-	-	-	-	-	-	-	-	0.0002	-	-	-	0	
Zn	0.003	0.002	0.023	1E-05	0.003	0.001	0.014	0.005	0.008	0.0004	0.0004	0.003	0.0004	-	-	-	0	

**C10.** Table of observed and predicted Pb concentrations in ng/m<sup>3</sup> from Park's model and the iPDRM from major contributing sources. Plotted in Figure 19.

	Observed Pb				Predicted Pb (Park)			Predicted Pb (iPDRM)						
	GFAAZ x	σ	ICPMS x	σ	Total	Big Bend	Gannon	GCR	Total	Big Bend	Gannon	GCR	McKay	PCRR
<b>12:00</b>	1.07	0.28	1.11	0.001	5.18	0.27	0	0	0.86	0	0	0	0	0
<b>12:30</b>	1.82	0.32	2.42	0.02	4.28	0.38	0	0	2.69	0.19	0	0	0	0
<b>13:00</b>	2.68	0.22	3.08	0.02	4.51	2.96	0.002	0	2.70	1.61	0	0	0	0
<b>13:30</b>	3.56	0.75	3.83	0.02	2.89	1.40	0.06	0.002	3.75	3.74	0	0.001	0	0
<b>14:00</b>	4.26	0.69	5.30	0.01	2.12	0.18	0.45	0.08	5.35	2.52	0.03	2.10	0.66	0
<b>14:30</b>	4.72	0.30	2.82	0.00	3.35	0	0.47	2.97	5.39	1.36	0.13	3.38	0.43	0
<b>15:00</b>	5.37	0.88	5.62	0.13	3.34	0	0.41	3.17	6.09	0.58	0.13	3.26	1.62	0
<b>15:30</b>	3.88	0.48	4.94	0.01	3.46	0	0.33	3.67	4.90	0.15	0.15	1.37	2.77	0
<b>16:00</b>	3.29	0.75	4.19	0.08	2.87	0.01	0.84	0.53	4.11	0.04	0.15	1.27	2.08	0
<b>16:30</b>	3.15	0.66	3.82	0.02	3.32	0.001	0.86	1.35	4.16	0.01	0.20	0.16	3.28	0.08
<b>17:00</b>	2.50	0.45	3.40	0.01	3.10	0.01	0.94	0.57	3.54	0.02	0.19	0.75	1.62	0.37
<b>17:30</b>	1.67	0.41	2.19	0.01	2.90	0.01	0.89	0.24	2.17	0.05	0.15	0.58	0.19	0.71
<b>18:00</b>	1.73	0.23	1.83	0.01	3.76	0	0.81	2.30	2.26	0.34	0.13	0.22	0.27	0.70
<b>18:30</b>	2.40	0.22	2.54	0.02	3.79	0	1.11	1.15	2.81	0.14	0.18	0.33	1.07	0.51
<b>19:00</b>	1.5	0.43	2.55	0.13	3.97	0	1.06	1.63	2.10	0.02	0.19	0.16	0.52	0.68
<b>19:30</b>	0.41	0.29	0.44	0.00	2.32	0.002	0.29	0.001	0.76	0	0.06	0.001	0.002	0.34
<b>20:00</b>	0.87	0.15	0.40	0.03	0.95	0	0.15	0	0.55	0	0	0	0	0.21
<b>20:30</b>	0.15	0.08	0.16	0.01	0.82	0	0.002	0	0.02	0	0	0	0	0

**C11.** Table of observed and predicted Zn concentrations in ng/m<sup>3</sup> from Park's model and the iPDRM from major contributing sources. Plotted in Figure 20.

	Observed Zn				Predicted Zn (Park)				Predicted Zn (iPDRM)						
	GFAAZ x	$\sigma$	ICPMS x	$\sigma$	Total	Man- atee	Big Bend	Gan- non	GCR	Total	Man- atee	Big Bend	Gan- non	Mc Kay	PCRR
<b>12:00</b>	5.33	0.07	2.00	0.07	5.18	4.78	0.40	0	0	2.41	2.27	0.01	0	0	0
<b>12:30</b>	8.02	0.09	8.25	0.06	4.28	3.72	0.56	0	0	6.88	6.62	0.12	0	0	0
<b>13:00</b>	5.86	0.14	4.84	0.16	4.51	0	4.36	0.004	0	3.99	2.87	0.95	0	0	0
<b>13:30</b>	5.12	0.09	2.49	0.58	2.89	0	2.06	0.16	0.002	2.39	0	2.21	0	0	0
<b>14:00</b>	3.94	0.10	3.82	0.17	2.12	0	0.26	1.15	0.06	2.67	0	1.49	0.11	0.85	0
<b>14:30</b>	3.86	0.08	1.56	0.07	3.35	0	0	1.21	2.10	2.13	0	0.80	0.59	0.55	0
<b>15:00</b>	6.55	0.06	2.20	0.56	3.34	0	0	1.06	2.24	3.31	0	0.34	0.58	2.10	0
<b>15:30</b>	5.40	0.11	5.86	0.47	3.46	0	0	0.84	2.59	4.65	0	0.09	0.67	3.60	0
<b>16:00</b>	5.17	0.16	4.76	0.68	2.87	0	0.02	2.14	0.38	3.77	0	0.02	0.65	2.70	0
<b>16:30</b>	8.27	0.12	5.18	0.39	3.32	0	0	2.21	0.95	5.55	0	0.01	0.90	4.26	0.10
<b>17:00</b>	5.72	0.17	4.61	0.08	3.10	0	0.01	2.40	0.40	3.82	0	0.01	0.85	2.10	0.47
<b>17:30</b>	4.11	0.19	2.05	0.39	2.90	0	0.01	2.28	0.17	2.14	0	0.03	0.68	0.25	0.91
<b>18:00</b>	3.73	0.22	2.80	0.23	3.76	0	0	2.06	1.62	2.35	0	0.20	0.58	0.34	0.89
<b>18:30</b>	4.83	0.16	4.68	0.21	3.79	0	0	2.85	0.81	3.23	0	0.09	0.79	1.39	0.65
<b>19:00</b>	4.31	0.09	1.36	50	3.97	0	0	2.71	1.15	2.69	0	0.01	0.84	0.67	0.86
<b>19:30</b>	-1.29	0.03	2.94	0.05	2.32	0	0	0.74	0.001	0.97	0	0	0.25	0.002	0.44
<b>20:00</b>	1.40	0.15	-0.69	-0.17	0.95	0	0	0.37	0	1.16	0	0	0	0	0.26
<b>20:30</b>	1.64	0.02	0.22	0.11	0.82	0	0	0.004	0	0.87	0	0	0	0	0

## Glossary

**$\chi/Q$** : Gaussian plume modeled dispersion factors ( $s/m^3$ )

**$\chi/Q^{iPDRM}$** : iPDRM solutions to Gaussian plume modeled dispersion factors ( $s/m^3$ )

**$\chi/Q^{MET}$** : Gaussian plume modeled dispersion factors ( $s/m^3$ ) with input parameters as calculated by Park

**$\chi/Q^{pPDRM}$** : Park PDRM solutions to Gaussian plume modeled dispersion factors ( $s/m^3$ )

**$\chi/Q^{traj}$** : Gaussian plume modeled dispersion factors ( $s/m^3$ ) with input parameters as calculated by trajectory analysis

**ABL**: Atmospheric Boundary Layer

**BRACE**: Bay Regional Atmospheric Chemistry Experiment

**CALMET**: California Meteorological Model

**CC**: Correlation Coefficient

**CEM**: Continuous Emissions Monitor

**CFPP**: Coal-fired Power Plant

**CMB**: Chemical Mass Balance

**EPA**: United States Environmental Protection Agency

**ESP**: Electrostatic Precipitators

**FA**: Factor Analysis

**Fa2**: Statistical Analysis Tool: The fraction of predictions within a factor of 2 of the observed concentration value

**FDEP**: Florida Department of Environmental Protection

**GFAAZ**: Graphite Furnace Atomic Absorption Spectrometer with Zeeman Correction

**GPM**: Gaussian Plume Model

**HCRR:** Hillsborough County Refuse Recovery (Local Incinerator)

**ICPMS:** Inductively Coupled Plasma Mass Spectrometry

**INAA:** Instrumental Neutron Activation Analysis

**iPDRM:** improved Pseudo-Deterministic Receptor Model

**LB:** Lower bounds

**MAGE:** Statistical Analysis Tool: Mean Absolute Gross Error

**MB:** Statistical Analysis Tool: Mean Bias

**MFB:** Statistical Analysis Tool: Mean Fractional Bias

**MLR:** Multiple Linear Regression

**MNB:** Statistical Analysis Tool: Mean Normalized Bias

**MNGE:** Statistical Analysis Tool: Mean Normalized Gross Error

**NEI:** National Emission Inventory

**NET:** National Emission Trends (precursor to NEI)

**NMSE:** Statistical Analysis Tool: Normalized Mean Square Error

**NOAA:** National Oceanic and Atmospheric Administration

**OFPP:** Oil-fired Power Plant

**PCA:** Principle Component Analysis

**PCRR:** Pinellas County Refuse Recovery (Local Incinerator)

**PDRM:** Pseudo-Deterministic Receptor Model

**PM:** Particulate matter

**PM<sub>2.5</sub>:** Particulate matter with an aerodynamic diameter < 2.5  $\mu\text{m}$

**PMF:** Positive Matrix Factorization

**pPDRM:** Pseudo-Deterministic Receptor Model used by Park

**RMSE:** Statistical Analysis Tool: Root Mean Square Error

**SCE:** Source Contribution Estimate

**SEAS:** Semi-continuous Elements in Aerosol Sampler

**SPECIATE:** EPA database of source profiles

**TSP:** Total suspended particle concentrations

**UB:** Upper bounds

**WS:** Wet Scrubber

## Bibliography

- Beychok, M. R. (2005), Fundamentals of Stack Gas Dispersion. 4<sup>th</sup> ed.
- Binkowski, F. S. (1979), A simple semi-empirical theory for turbulence in the atmospheric surface layer, *Atmos. Environ.*, 13, 247–253.
- Briggs, G. A. (1969), Plume rise, Crit. Rev. Ser. T/D 25075, U.S. At. Energy Comm., Washington, D. C. (Available from Natl. Tech. Inf. Serv., Springfield, Va.)
- Briggs, G. A. (1971), Some recent analyses of plume rise observations, in Proceedings of the Second International Clean Air Congress, edited by H. M. Englund and W. T. Beery, pp. 1029– 1032, Elsevier, New York.
- Briggs, G. A. (1974), Diffusion estimation for small emissions, in Environmental Research Laboratories Air Resources Atmospheric Turbulence and Diffusion Laboratory 1973 Annual Report, USAEC Rep. ATDL-106, NOAA, Washington, D. C.
- Coles, David G., Ragaini, Richard C., Ondov, John M. (1979) Chemical Studies of Stack Fly Ash from a Coal-Fired Power Plant. *Environ. Sci. & Tech.* 13. 455-459.
- Cooper, D. W. (1982), Receptor-oriented source-receptor analysis, paper presented at Specialty Conference on Receptor Models Applied to Contemporary Pollution Problems, Northeast Atl. Int. Sect. of the Air Pollut. Control Assoc., Danvers, Mass., 17–20 Oct.
- Draxler, R. R. (1976), Determination of atmospheric diffusion parameters, *Atmos. Environ.*, 10, 99–105.
- Gifford, F. A. (1961), Use of routine meteorological observations for estimating, atmospheric dispersion, *Nucl. Safety*, 2, 47–51.
- Greenberg, R. R., Gordon, G.E., Zoller, W.H., Jacko, R.B., Neuendorf, D.W., Yost, Y.J. (1978) Composition of Particles Emitted from the Nicosia Municipal Incinerator. *Environ. Sci. & Tech.*, 12, 1329-1332.
- Google Earth, 2007. Google Earth, <http://earth.google.com>, October, 2007.
- Gordon, G. E. (1988), Receptor models, *Environ. Sci. Technol.*, 22, 1132–1142.
- Han., M., (1992), Receptor modeling of airborne pollutants in the State of Maryland, Ph.D. Thesis, University of Maryland.
- Haupt, S. E. (2005) A Demonstration of coupled receptor/dispersion modeling with a genetic algorithm. *Atmos. Environ.*, 39, 7181-7189.

- Henry, R. C. (1987), Current factor analysis models are ill-posed, *Atmos. Environ.*, 21, 1815–1820.
- Henry, R. C. (2000), UNMIX theory and applications, in *Final Report of Workshop on UNMIX and PMF as Applied to PM2.5*, Publ. EPA/600/A-00/48, edited by R. D. Willis, pp. 4 –6, U.S. Environ. Prot. Agency, Washington, D. C.
- Henry, R. C., and G. A. Norris (2002), EPA UNMIX 2.3 User Guide, Natl. Exposure Res. Lab., U.S. Environ. Prot. Agency, Research Triangle Park, N. C.
- Irwin, J. S. (1979), Scheme for estimating dispersion parameters as a function of release height, *Publ. EPA-600/4-79-062*, U.S. Environ. Prot. Agency, Washington, D. C.
- Joseph, J. (1988) The Chemical Characterization of Airborne Particles Released by Three West Virginia Coal-Fired Power Plants for Receptor Model Studies. Masters Thesis. University of Maryland.
- Kidwell, C. B., and J. M. Ondov (2001), Development and evaluation of a prototype system for collecting sub-hourly ambient aerosol for chemical analysis, *Aerosol Sci. Technol.*, 35, 596–601.
- Kidwell, C. B., and J. M. Ondov (2004), Elemental analysis of sub-hourly ambient aerosol collections, *Aerosol Sci. Technol.*, 38, 205– 218.
- Kumar, A., J. Luo, and G. Bennett (1993), Statistical evaluation of lower flammability distance (LFD) using four hazardous release models, *Process Safety Prog.*, 12, 1–11.
- Kumar, A., N. K. Bellam, and A. Sud (1999), Performance of an industrial source complex model: Predicting long-term concentrations in an urban area, *Environ. Prog.*, 18, 93– 100.
- Lioy, P. J., M. P. Zelenka, M. D. Cheng, N. M. Reiss, and W. E. Wilson (1989), The effect of sampling duration on the ability to resolve source types using factor analysis, *Atmos. Environ.*, 23, 239– 254.
- MatWeb, (2009), Material Property Data, <http://www.matweb.com/>, May, 2009.
- McElroy, J.L., Pooler, F., (1968), The St. Louis Dispersion Study, Volume II-Analysis, U.S. EPA Publication AP-53.
- McElroy, J.L., (1969), A Comparative Study of Urban and Rural Dispersion, *J. Appl. Meteor.*, 8, 19.
- Mroz, E. J., (1976), The Study of the Elemental Composition of Particulate Emissions from an Oil-Fired Power Plant. Ph.D. Thesis, University of Maryland.

- Nelms, S.M., (2005), *Inductively Coupled Plasma Mass Spectrometry Handbook*, Oxford, Boca Raton, FL.
- Ondov, J. M., R. C. Ragaini, and A. H. Biermann (1979), Elemental emissions from a coal-fired power plant: Comparison of a Venturi wet scrubber system with a cold-side electrostatic precipitator, *Environ. Sci. Technol.*, *13*, 598–607.
- Ondov, J. M., C. E. Choquette, W. H. Zoller, G. E. Gordon, A. H. Biermann, and R. E. Heft (1989), Atmospheric behavior of trace elements on particles emitted from a coal-fired power plant, *Atmos. Environ.*, *23*, 2193– 2204.
- Ondov, J. M., W. R. Kelly, J. Z. Holland, Z. Lin, and S. A. Wight (1992), Tracing fly ash emitted from a coal-fired power plant with enriched rare earth isotopes, *Atmos. Environ., Part B*, *26*, 453– 462.
- Ondov, J.M., Wexler, A.S. (1998), Where Do Particulate Toxins Reside? An Improved Paradigm for the Structure and Dynamics of the Urban Mid-Atlantic Aerosol, *Environ. Sci. Technol.*, *32*, 2547-2555.
- Ondov, J. M., J. P. Pancras, S. Gazula, M. Yu, J. Turner, A. Robinson, S. Pandis, N. D. Poor, and R. K. Stevens (2003), Highly time-resolved measurements of elemental composition at the Baltimore, St. Louis, Pittsburgh, and Tampa Supersites using the UM high-frequency aerosol slurry sampler: Unprecedented resolution of the sources of primary atmospheric aerosol, paper presented at 2003 PM AAAR Meeting, Am. Assoc. for Aerosol Res., Pittsburgh, Pa., 31 March to 4 April.
- Paatero, P. (1997), Least square formulation of robust non-negative factor analysis, *Chemom. Intel. Lab. Syst.*, *37*, 23– 35.
- Paatero, P. (1999), The multilinear engine: A table-driven, least squares program for solving multilinear problems, including the n-way parallel factor analysis model, *J. Comput. Graph. Stat.*, *8*, 854–888.
- Pancras, J.P., Ondov, J.M., Zeisler, R. (2005), Multi-element electrothermal AAS determination of 11 marker elements in fine ambient aerosol slurry samples collected with SEAS-II. *Anal. Chim. Acta*, *538*, 303-12.
- Pancras, J. P., Ondov, J. M., Poor, N., Landis, M. S., Stevens, R. K. (2006) Identification of sources and estimation of emission profiles from highly time-resolved pollutant measurements in Tampa, FL, *Atmos. Environ.*, *40*, 467-81.
- Panofsky, H. A., Blackadar, A. K., McVehil, G. E., (1960), The diabatic wind profile, *Q. J. R. Meteorol. Soc.*, *86*, 390– 398.

- Park, S.S., Pancras, J.P., Ondov, J., Poor, N., (2005(a)), A New Pseudo-Deterministic Multivariate Receptor Model for Accurate Individual Source Apportionment Using Highly Resolved Ambient Concentration Measurements, *J. of Geophys. Res.*, *110*, D078S15.
- Park, S.S., Pancras, J.P., Ondov, J.M., Robinson, Allen. (2005(b)). Application of the Pseudo-Deterministic Receptor Model to resolve Power Plant Influences on Air Quality in Pittsburgh, *Aero. Sci. & Tech.*, *40*, 883-897.
- Pasquill, F. (1961), The estimation of the dispersion of windborne material, *Meteorol. Mag.*, *90*, 33– 49.
- Poor, N., Pribble, R. and Greening, H. (2001), Direct wet and dry deposition of ammonium, nitric acid, ammonium and nitrate to the Tampa Bay Estuary, FL, USA, *Atmos. Environ.* *35*, 3947–3955.
- Poor, N., Amalfilano, C., Ondov, J.M, Pancras, J.P., Gazula, S., Dasgupta, P., Al-Horr, R., (2003), Real-time monitoring of gases and aerosols reveals source contributions, paper presented at NARSTO Workshop on Innovative Methods for Emission-Inventory Development and Evaluation, NARSTO, Austin, Tex., 14– 17 Oct.
- Rheingrover, S. W., Gordon, G.E., (1988), Wind-trajectory method for determining compositions of particles from major air pollution sources, *Aerosol Sci. Technol.*, *8*, 29– 61.
- Scire, J. S., R. R. Francoise, M. E. Fernau, and R. J. Yamartino (2000), *A User's Guide for the CALMET Meteorological Model (Version 5)*, Earth Tech, Inc., Concord, Mass.
- Seinfeld, J. H., Pandis, S. N., (1998), *Atmospheric Chemistry and Physics*, John Wiley & Sons, New York.
- Shum, Y. S., Loveland, W.D., Hewson, E.W., (1975), The use of artificial activable trace elements to monitor pollutant source strengths and dispersal patterns. *JAPCA*.
- Tanaka, S. Yashushi, N. Sato, N. Fukasawa, T., Santosa, S.J., Yamanaka, K., Ootoshi, T. (1998), Rapid and simultaneous multi-element analysis of atmospheric particulate matter using inductively coupled plasma mass spectrometry with laser ablation sample introduction. *J. of Anal. Atom. Spectrom.*, *13*, 135-140.
- Taylor, H.E., (2001), *Inductively Coupled Plasma-Mass Spectrometry*, Academic Press, New York.
- Thurston, G. D., and J. D. Spengler (1985), A quantitative assessment of source contributions to inhalable particulate matter pollution in metropolitan Boston, *Atmos. Environ.*, *19*, 9 – 25.

- U.S. Environmental Protection Agency (U.S. EPA) (1980), Guidelines on air quality models, *OAQPS Guideline Ser.*, Research Triangle Park, N. C.
- U.S. Environmental Protection Agency (U.S. EPA) (1995), User's Guide for the Industrial Source Complex (ISC3) Dispersion Models, vol. II, *Description of Model Algorithms*, Research Triangle Park, N. C.
- U.S. Environmental Protection Agency (U.S. EPA) (2006), Documentation for the Final 2002 Point Source National Emissions Inventory, Emission Inventory and Analysis Group, Air Quality and Analysis Division, Research Triangle Park, N. C.
- U.S. Environmental Protection Agency (U.S. EPA) (2006), SPECIATE 4.0: Speciation Database Development Documentation Final Report, Office of Research and Development, Research Triangle Park, N. C.
- U.S. Environmental Protection Agency (U.S. EPA) (2009), Clean Air Markets: Data and Maps, Continuous Emissions Monitor (CEM) database, <http://camddataandmaps.epa.gov/gdm/index.cfm?fuseaction=emissions.wizard>, Clean Air Markets Division, Washington, D.C.
- U.S. Department of Agriculture Agricultural Research Service (U.S.D.A.-A.R.S), (2007), National Program 203 Air Quality Accomplishment Report, 2002-2007, Washington, D.C.
- Warneck, P., (1988), *Chemistry of the Natural Atmosphere*, Academic Press, New York.
- Weitkamp, E.A., Lipsky, E.M., Pancras, J.P., Ondov, J.M., Polidori, A., Turpin, B.J., Robinson, A.L. (2005), Fine Particle Emission Profile for a Large Coke Production Facility Based on Highly Time- Resolved Fence Line Measurements, *Atmos. Environ.*, 39, 6719–6733.
- Wittig, A. E., Allen, D. T., (2008), Improvement of the Chemical Mass Balance model for apportioning-sources of non-methane hydrocarbons using composite aged source profiles. *Atmos. Environ.*, 42, 1319-1337.
- Yamartino, R. J. (1982), Formulation and application of a hybrid receptor model, paper presented at Specialty Conference on Receptor Models Applied to Contemporary Pollution Problems, Northeast Atl. Int. Sect. of the Air Pollut. Control Assoc., Danvers, Mass., 17–20 Oct.